

Reaction Mechanism Analysis of Si Electrodeposition Process in Ionic Liquids

イオン液体を用いた Si 電解析出プロセス
における反応機構の解析

February, 2018

Waseda University

Graduate School of Advanced Science and Engineering

Department of Advanced Science and Engineering

Research on Applied Chemistry A

Yasuhiro TSUYUKI

露木 康博

Contents

Chapter 1:

General Introduction

1.1 Ionic Liquids	2
1.1.1 Characteristics of ionic liquids	2
1.1.2 Application of ionic liquids	6
1.2 The Demand of Si	9
1.2.1 Si-based solar cells	11
1.2.2 Fabrication process of Si thin film solar cells	13
1.3 The Electrodeposition of Si	14
1.4 Strategy of This Study	19
References	21

Chapter 2:

Overall Reaction Mechanism Analysis of Si Electrodeposition in Ionic Liquids

2.1 Introduction	28
2.2 Experimental	29
2.3 Results and Discussion	33
Conclusions	53
References	54

Chapter 3:

Analysis of Cathodic Reaction Process of SiCl₄ in Ionic Liquids

3.1 Introduction	56
3.2 Experimental	57
3.3 Results and Discussion	60
3.3.1 Analysis of reduction steps during the electrodeposition	60

3.3.2 Analysis of the intermediate state during the electrodeposition	62
3.3.3 Analysis of the pathway of the intermediate state formation	73
Conclusions	84
References	85

***Chapter 4:
Overall Reaction Mechanism Analysis of Si Electrodeposition in
Ionic Liquids***

4.1 Introduction	88
4.2 Experimental	90
4.3 Results and Discussion	92
4.3.1 Analysis of the effect of electrodeposition conditions on as-deposited films	92
4.3.2 Analysis of the reduction mechanism of SiCl ₄	105
Conclusions	111
References	112

***Chapter 5:
Study for The Fabrication of Si Thin Film Solar Cell Devices***

5.1 Introduction	116
5.2 Experimental	117
5.3 Results and Discussion	120
5.3.1 The control of film structure	120
5.3.2 Doping on the electrodeposited films	133
Conclusions	142
References	143

<i>Chapter 6: General Conclusions</i>	145
--	-----

<i>List of Achievements</i>	151
<i>Acknowledgement</i>	157

Chapter 1:

General Introduction

1.1 Ionic Liquids

1.1.1 Characteristics of Ionic Liquids

The liquids which are the materials made from ions and synthesized at low temperatures are called as “Ionic Liquids”. In recent, ionic liquids have gain much attentions in all over the world, starting from the question that why they have low melting points to the behavior of their unique properties which usual liquids can not have. The one of the most noteworthy characteristic of ionic liquids for researchers who would like to use might be non-volatile liquids. Liquids can not avoid being evaporated, however, some of ionic liquids can exist in stable in the air, have no vapor pressure, dissolve several materials, and have large ionic conductivity. Therefore, it has been expected to apply them to several science fields [1].

Many of them consist of organic ions and complex ions. Researchers have been attracted this point because they can design them, and try to find several physical properties and functions. Moreover, a suitable liquid can be synthesized by changing the cation and anion pair. As you can see, the applied filed of ionic liquids are in a very wide range.

It seems that ionic liquids have been started to be used in the nineteenth centuries. Researchers engaging in the electrochemistry have focused on them as the solvent of molten salt which can transfer the electron at low temperatures. However, the problem was not stable to the air and water. For this problem, Wilkers et al. [2] has successfully to synthesize the ionic liquids using BF_4^- which was stable to the air and water. Following this report, ionic liquids have been focus on as reaction and separation fields which was non-volatility, non-flammability and thermal stability as well as the electrolyte [3, 4]. Then, they have gained much attention in the electrochemistry [5-13]. Other application will be described later. The detail of the background should be referred with the Wilkes' review on 2002 [14]. As recent ionic liquids, it is defined the salts which have a melting point lower than 100 °C [14-16].

As described above, ionic liquids are consisted from cation and anion. The typical cations are imidazolium-based, pyrrolidinium-based, pyridinium-based, piperidinium-

based, ammonium-based, or phosphonium-based one. The typical anions are halogen ions (Cl^- , Br^- , I^-), tetrafluoroborate (BF_4^-), hexafluorophosphate (PF_6^-), bis(trifluoromethanesulfonyl)amide ($[\text{NTf}_2]^-$) [17-19]. The typical structures are shown in Fig. 1.1.

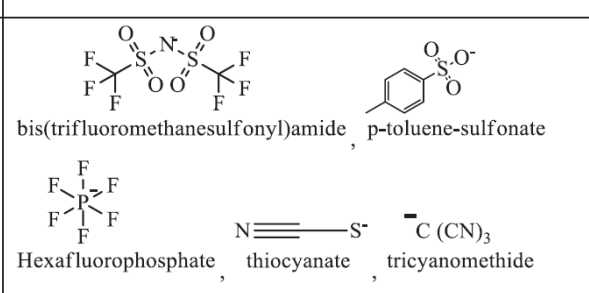
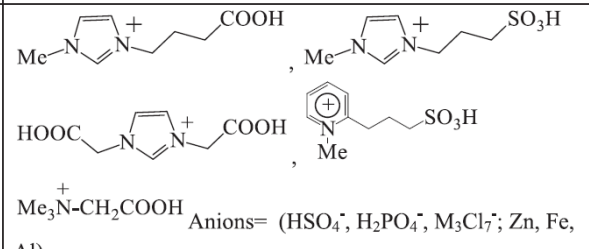
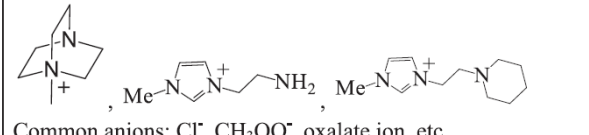
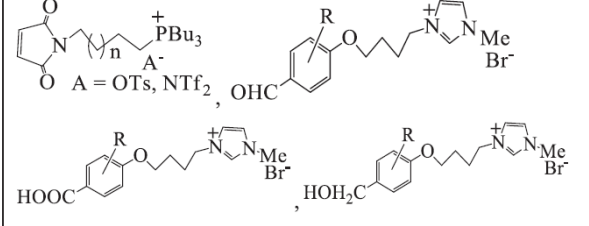
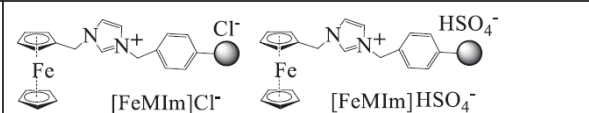
SN	Types of ionic liquids (Classes)	Some typical examples	Remark
1	Neutral ionic liquids	 <p>bis(trifluoromethanesulfonyl)amide, p-toluene-sulfonate</p> <p>Hexafluorophosphate, thiocyanate, tricyanomethide</p>	Anions are associated with cations with weak electrostatic interaction, low melting point, low viscosity, used as inert solvent, good thermal and electrochemical stability
2	Acidic ionic liquids	 <p>Me⁺N-CH₂COOH Anions= (HSO_4^-, H_2PO_4^-, M_3Cl_7^-; Zn, Fe, Al)</p>	ionic liquids with acidic cations or acidic anion, enhanced solubility in water, possess good catalytic efficiency
3	Basic ionic liquids	 <p>Common anions: Cl^-, CH_3OO^-, oxalate ion, etc.</p>	These ionic liquids are basic in nature due to presence of one or more amine group (1° , 2° or 3° amine)
4	Functionalized ionic liquids	 <p>A = OTs, NTf_2^-, OHC</p>	Ionic liquids that has a covalently bound functional group on the cation and/or anion
5	Supported Ionic Liquids	 <p>[FeMIm]Cl^-, [FeMIm]HSO_4^-</p>	

Fig. 1.1 The classification of the typical structure of ionic liquids [17] (Copyright 2017 by J. Mol. Liq. Reproduced with permission of J. Mol. Liq. by Copyright Clearance Center's RightsLink® service)

The main characteristics of ionic liquids are following, while it should be noted that all ionic liquids have all following characteristics, and the degree of these characteristics changes depending on the constitution of cation and anion.

- Non-flammability
- High thermal stability
- High electrochemical stability
- High ionic conductivity
- Easily design of their properties and functions

Here, for considering the application to the electrochemistry, the characteristic of the electrochemistry which means a wide electrochemical window is described. Ionic liquids can have high electrochemical windows of 3 ~ 6 V, while some ionic liquids have that of around 2 V [20-21], because they are mostly composed from low reactive ions. It should be noted that the potential range becomes lower with the addition of some molecules such as precursors [22-23]. Lane [24] has reviewed the mechanism of the decomposition of cations and classified their stabilities (Fig. 1.2).

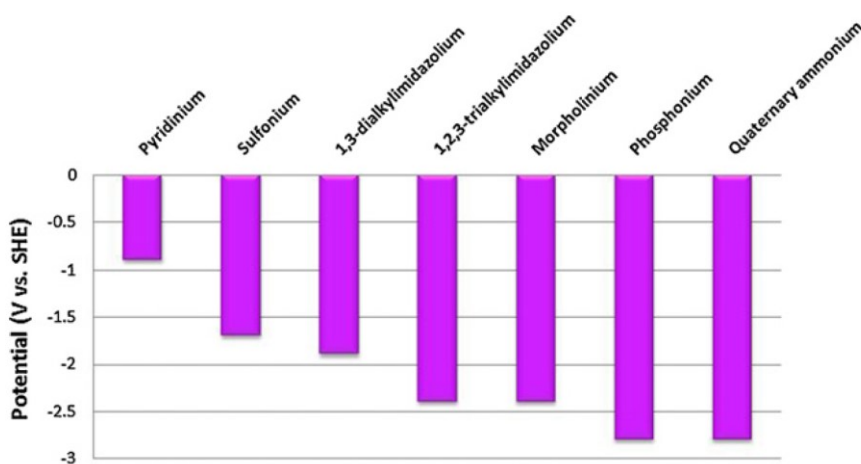


Fig. 1.2 The estimated cathodic stability of main types of cations [24] (Copyright 2012 by Electrochim. Acta. Reproduced with permission of Electrochim. Acta by Copyright Clearance Center's RightsLink® service)

The anodic stabilities of main types of anions have also been reported as follows: $[\text{TFSA}]^- > [\text{FAP}]^- > [\text{TfO}]^- > [\text{DCA}]^- > [\text{TFA}]^-$, in which it means that $[\text{TFSA}]^-$ has high stability [25]. It should be noted that their viscosity would occasionally be challenging for the application, while there are several good characteristics. In basic, the viscosity of ionic liquids is higher than water, and some ionic liquids have several hundred times than water at room temperature [26]. For example, the ionic liquid of 1-Butyl-3-methylimidazolium nonafluorobutanesulfonate has 323 cP [26]. The viscosity of other ionic liquids can be referred the report by Hagiwara et al. [26]. Therefore, it is necessary to choose the ionic liquids which have low viscosity, and/or decrease the viscosity with the increase of the temperature [27-28] in order to overcome these challenging points of ionic liquids.

1.1.2 Application of Ionic Liquids

Ionic liquids are applied for a wide range fields owing to their unique characteristics described in previous section, such as the synthesis of nanomaterials, biochemical, batteries, electrodeposition of metals and semiconductors, capacitors, dye-sensitized solar cells and so on. The examples of application fields are shown in Fig. 1.3. Here, the application in the electrodeposition will be focused on as following.

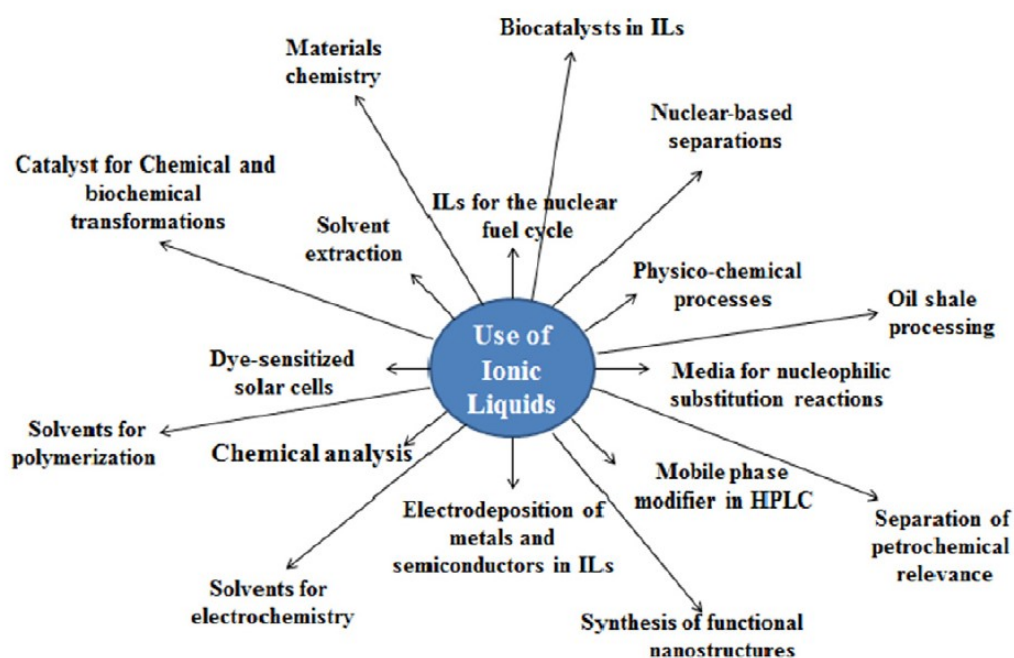


Fig. 1.3 The examples of the applications of ionic liquids [17] (Copyright 2017 by J. Mol. Liq. Reproduced with permission of J. Mol. Liq. by Copyright Clearance Center's RightsLink® service)

The application of ionic liquids to the electrodeposition

The one of the promising application field is the electrodeposition of reactive metals and semiconductors [29]. The characteristics of ionic liquids especially the wide electrochemical windows can help to electrodeposit metals and semiconductors. These studies seem to have started been from the Hall-Heroult process which is the commercialization of the Al electrodeposition [1]. The electrodeposition using ionic liquids would also be helpful for the metals which can be electrodeposited in aqueous solvents because they do not produce the hydrogen evolution during the electrodeposition, which prevent the hydrogen embrittlement, owing to their aprotic properties. Figure 1.4 shows the elements which can and can not be electrodeposited in aqueous solvents [30].

1A 1 H 1.00794 Hydrogen	2A																3A 4A 5A 6A 7A 8A 2 He 4.002602 Helium																																																																																																																																																																																																																
3 Li 6.941 Lithium	4 Be 9.012182 Beryllium																	5 B 10.811 Boron	6 C 12.0107 Carbon	7 N 14.0067 Nitrogen	8 O 15.9994 Oxygen	9 F 18.9984032 Fluorine	10 Ne 20.1797 Neon																																																																																																																																																																																																										
11 Na 22.989769 Sodium	12 Mg 24.3050 Magnesium																	13 Al 26.9815386 Aluminum	14 Si 28.0855 Silicon	15 P 30.973762 Phosphorus	16 S 32.065 Sulfur	17 Cl 35.453 Chlorine	18 Ar 39.948 Argon																																																																																																																																																																																																										
19 K 39.0983 Potassium	20 Ca 40.078 Calcium	21 Sc 44.955912 Scandium	22 Ti 47.887 Titanium	23 V 50.9415 Vanadium	24 Cr 51.9961 Chromium	25 Mn 54.938045 Manganese	26 Fe 55.845 Iron	27 Co 58.933195 Cobalt	28 Ni 58.6934 Nickel	29 Cu 63.546 Copper	30 Zn 65.38 Zinc	31 Ga 69.723 Gallium	32 Ge 72.63 Germanium	33 As 74.92160 Arsenic	34 Se 78.96 Selenium	35 Br 79.904 Bromine	36 Kr 83.798 Krypton																																																																																																																																																																																																																
37 Rb 85.4678 Rubidium	38 Sr 87.62 Strontium	39 Y 88.90585 Yttrium	40 Zr 91.224 Zirconium	41 Nb 92.90638 Niobium	42 Mo 95.94 Molybdenum	43 Tc [98] Technetium	44 Ru 101.07 Ruthenium	45 Rh 102.90550 Rhodium	46 Pd 106.42 Palladium	47 Ag 107.8682 Silver	48 Cd 112.411 Cadmium	49 In 114.818 Indium	50 Sn 118.710 Tin	51 Sb 121.760 Antimony	52 Te 127.60 Tellurium	53 I 126.90447 Iodine	54 Xe 131.293 Xenon																																																																																																																																																																																																																
55 Cs 132.9054519 Cesium	56 Ba 137.327 Barium	57 La 138.90547 Lanthanum	58 Ce 140.116 Cerium	59 Pr 140.90765 Praseodymium	60 Nd 144.242 Neodymium	61 Pm [145] Promethium	62 Sm 150.36 Samarium	63 Eu 151.964 Europium	64 Gd 157.25 Gadolinium	65 Tb 158.92535 Terbium	66 Dy 162.500 Dysprosium	67 Ho 164.93032 Holmium	68 Er 167.259 Erbium	69 Tm 168.93421 Thulium	70 Yb 173.054 Ytterbium	71 Lu 174.9668 Lutetium																																																																																																																																																																																																																	
87 Fr [223] Francium	88 Ra [226] Radium	89 Ac [227] Actinium	90 Th 232.03806 Thorium	91 Pa 231.03688 Protactinium	92 U 238.02891 Uranium	93 Np [237] Neptunium	94 Pu [244] Plutonium	95 Am [243] Americium	96 Cm [247] Curium	97 Bk [247] Berkelium	98 Cf [251] Californium	99 Es [252] Einsteinium	100 Fm [257] Fermium	101 Md [258] Mendelevium	102 No [259] Nobelium	103 Lr [262] Lawrencium																																																																																																																																																																																																																	
		Lanthanides																Actinides																																																																																																																																																																																																															
		58 Ce 140.116 Cerium																59 Pr 140.90765 Praseodymium																60 Nd 144.242 Neodymium																61 Pm [145] Promethium																62 Sm 150.36 Samarium																63 Eu 151.964 Europium																64 Gd 157.25 Gadolinium																65 Tb 158.92535 Terbium																66 Dy 162.500 Dysprosium																67 Ho 164.93032 Holmium																68 Er 167.259 Erbium																69 Tm 168.93421 Thulium																70 Yb 173.054 Ytterbium																71 Lu 174.9668 Lutetium															
		90 Th 232.03806 Thorium																91 Pa 231.03688 Protactinium																92 U 238.02891 Uranium																93 Np [237] Neptunium																94 Pu [244] Plutonium																95 Am [243] Americium																96 Cm [247] Curium																97 Bk [247] Berkelium																98 Cf [251] Californium																99 Es [252] Einsteinium																100 Fm [257] Fermium																101 Md [258] Mendelevium																102 No [259] Nobelium																103 Lr [262] Lawrencium															

Metals that can be electrodeposited from aqueous solution
 Semiconductor
 Refractory metals (broadly defined)
 Refractory metals (narrowly defined)

Fig. 1.4 The table of elements which can be electrodeposited in aqueous solvents, in which the elements which can not be electrodeposited in aqueous solvents are also shown. [31] (Copyright 2015 by Solid State Mater. Sci. Reproduced with permission of Solid State Mater. Sci. by Copyright Clearance Center's RightsLink® service)

In those electrodeposition, it has been reported that ionic liquids based on trifluoromethanesulfonate (CF_3SO_3^-), bis (trifluoromethanesulfonyl) amide $[(\text{CF}_3\text{SO}_2)_2\text{N}^-]$, and tris (trifluoromethanesulfonyl) methide $[(\text{CF}_3\text{SO}_2)_3\text{C}^-]$, which are the hydrophobic anions, should be used to be stable in the air [32, 33]. Based on these background, the electrodeposition of less reactive metals has been conducted: Zn [34-36], Cu [37-40], Ag [41-44], Pt [45,46] etc.

In the electrodeposition of reactive metals and semiconductor, air- and water-stable ionic liquids have also been used: Al [47-50], Li [51, 52], Ta [53-57], Ge [58-60], Si etc. The study of the Si electrodeposition will be described later.

1.2 The Demand of Si

Si is one of the key material in industry such as semiconductor electric devices, solar cells, MEMS, Li ion batteries [61, 62], etc. Especially, in considering the sustainable energy in the future, the demand of Si for solar cells will continuously increase (Fig. 1.5). It has been considered that the CO₂ emission cause the global warming, and it is prospected that the amount of the CO₂ emission in 2030 will increase with the development of the industries in China and India [63]. In recent, United Nations Framework Convention on Climate Change, COP21 was held in Paris, in which it has been decided to suppress the temperature increase within 2 °C for creating the low-carbon society not depending on the fossil fuels [64]. For this, the photovoltaic (PV) power generation has been attracted as one of the renewable energy. It is no doubt that several countries will pay attention to the enlargement of the solar cell industry. It is predicted that this market will increase to 45 ~ 55 GW per a year in 2020 [65]. In Japan, the New Energy and Industrial Technology Development Organization also showed us the road map for developing the solar cells by 2050 as called “PV2030+” (Fig. 1.6) [66], in which the road map to fabricate the solar cells with the cost less than 7 JPY/kWh is described.

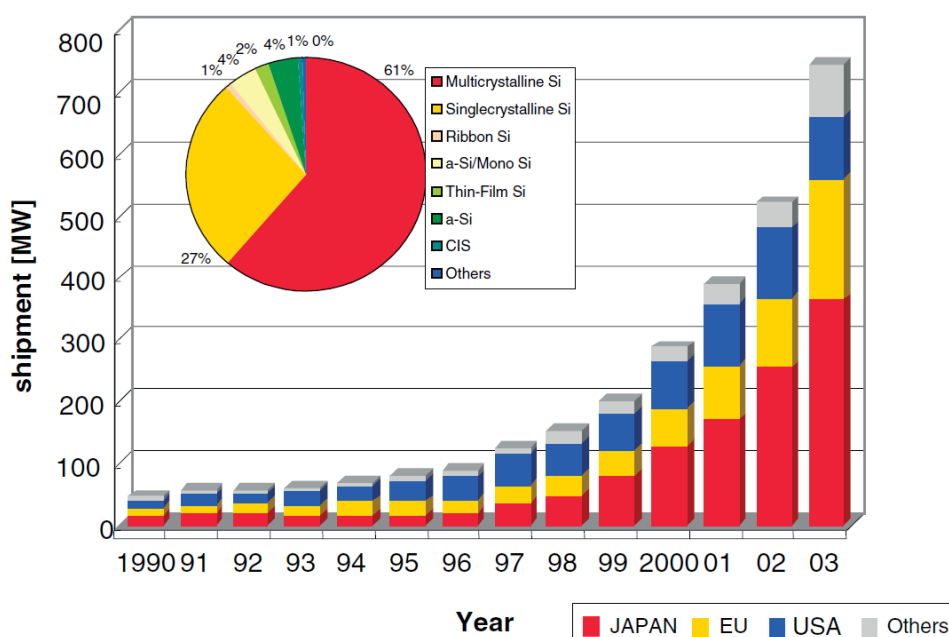


Fig. 1.5 The shipment of solar cell in the world [67] (Copyright 2005 by Progress in Photovoltaics. Reproduced with permission of Progress in Photovoltaics by Copyright Clearance Center’s RightsLink® service)

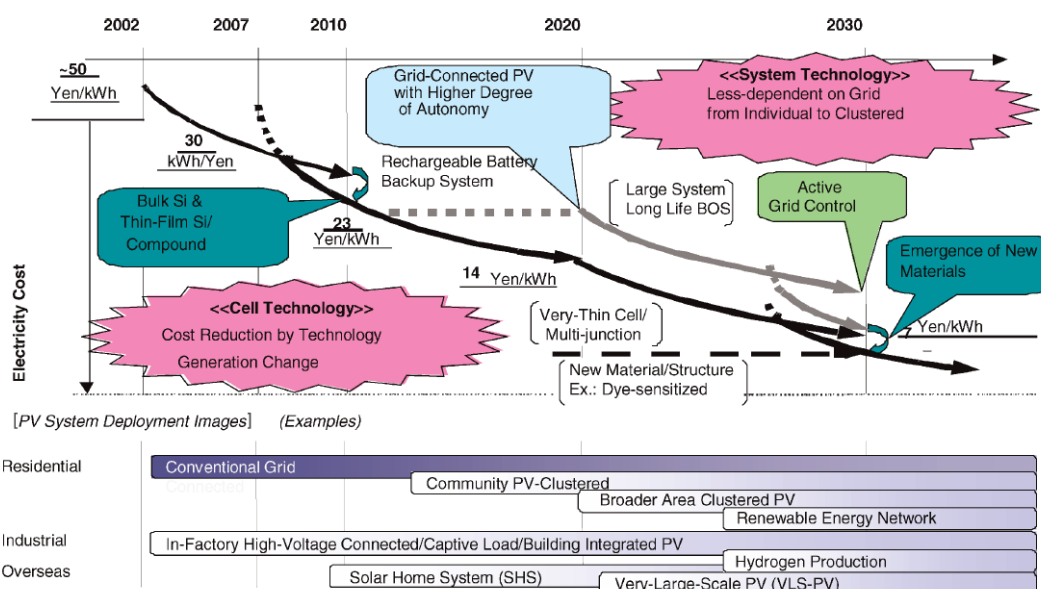


Fig. 1.6 The roadmap of PV 2030+ [67] (Copyright 2005 by Progress in Photovoltaics. Reproduced with permission of Progress in Photovoltaics by Copyright Clearance Center’s RightsLink® service)

1.2.1 Si-based solar cells

Among the various types of solar energy conversion, Si-based solar cells are attractive because the technology and its stability have been reliably established over many years [68-71], especially the crystalline Si solar cells are the dominant in the solar cell industry [67], which can achieve the conversion efficiency over 25 % [68-74]. In the crystalline Si-based solar cells, high purity Si (6 ~ 7N) with semiconductor characteristic is used. As the fabrication process of the crystalline Si and solar cells, the following process [75] are widely used; metallurgical grade Si (MG-Si) was fabricated from silica stones, quartz sand, and diatomaceous earth with wood, charcoal, and coal. These MG-Si will be gasified to silane gases such as SiHCl_3 and SiH_4 by the reaction of MG-Si with H_2 and SiCl_4 to fabricate 11N Si. Then off-grade Si or scrap Si are used as solar grade Si (SG-Si). For the fabrication of single-crystal or poly-crystalline Si, the Czochralski (CZ) method or the floating-zone (FZ) method are conducted. To fabricate the solar cell structure, several treatments such as doping are performed. The simplified procedure is described in Fig. 1.7 by the author.

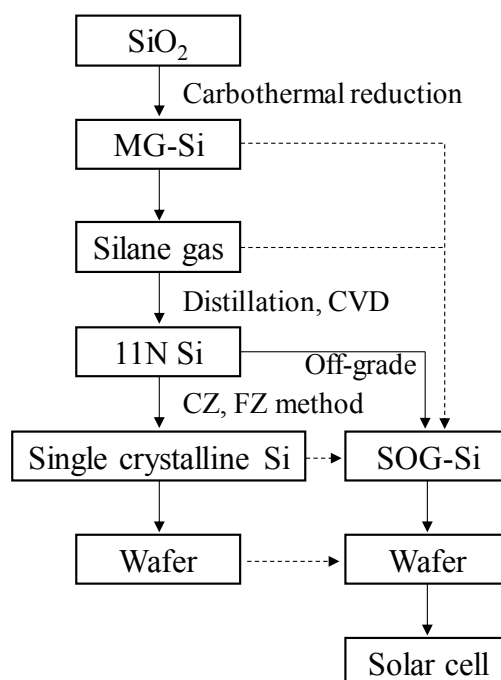


Fig. 1.7 The conventional process to fabricate the crystalline Si and solar cell

As described above, the conversion efficiency of crystalline Si solar cells is higher than other Si-based one, while there are challenging to fabricate them with low cost and saving the resources. In considering the future as described above, the solar cells with high efficiency will be necessary fabricated by low cost. For this, Si thin film solar cells, which can save the Si source, has been attracted. The thickness of Si layer in thin film solar cells are thinner than crystalline Si solar cells by 1/100. The conversion efficiency is not higher than crystalline one (7 ~ 10 %), while there are some characteristics such as the small temperature dependence of the conversion efficiency. In the Si thin film solar cells, amorphous Si and/or microcrystalline Si are used, in which several ~ several tens % H are incorporated. Thus, they are sometimes called as hydrogenated amorphous silicon or hydrogenated microcrystalline Si.

To develop the Si thin film solar cells, it has been researching to obtain the high efficiency. A relatively high efficiency by applying nanostructure to the thin films has been reported, and then the Si thin film solar cells with nanostructure have been attracted

as a next-generation solar cells [76-84]. For example, M. A. Green [76] has reported that the conversion efficiency over 40 % could be achieved by laminating several layers with Si quantum dots super lattice. W. J. Nam et al. [82] has reported that the conversion efficiency of 8.2 % has been achieved by forming a-Si:H nanostructured array with the length of 400 nm, and E. C. Garnett et al. [80] has also reported that a radial nanowire structure could increase the conversion efficiency of 0.5 % and obtain higher efficiency with decreasing the resistance of nanowire.

1.2.2 Fabrication process of Si thin film solar cells

As the fabrication method of these thin films and nanostructures, plasma-enhanced chemical vapor depositions (PECVD) has commonly used [85-88], in which SiH_4 is decomposed by glow discharge and the deposited on a glass or plastic substrate. The fabrication process is simply described as follows; SiH_4 gas is induced to the vacuum chamber. SiH_4 gas decomposed to the radical SiH_n ($n = 0 \sim 3$) and H by the generated plasma. SiH_3 is attached to the substrate, and then dangling bonds are formed the abstraction reaction by SiH_3 radical and/or voluntary breaking off the terminated hydrogen. The reaction of these dangling bonds and SiH_3 radical is considered to result in the formation of amorphous Si. Doping can also be conducted by using B_2H_6 and PH_3 , and be controlled from $10^{-11} \sim 10^{-2}$ S/cm [85]. In fabricating Si thin films, the operating temperature is around 200 °C which is lower than that in fabricating crystalline Si (over 1000 °C). However, it has still challenging to fabricate thin films in the fabrication cost, which can not avoid using high vacuum and high voltage equipment, and especially, it is not still easy to fabricate the nanostructures by above technologies.

1.3 The Electrodeposition of Si

Electrodeposition have been widely used as a useful fabrication method of thin films and/or nanostructure, especially of metals in the past, in a large area without using high vacuum and high voltage equipment [89]. On the other hand, the semiconductor electrodeposition such as Si can also be conducted with the recent increase of the research using ionic liquids.

Electrodeposition can also potentially be a way to fabricate the Si thin films solar cells because they have advantages in successive processing of the solar cell structures with nanostructures in a large area without using high vacuum and high voltage equipment. These advantages could provide an effective fabrication process of the Si thin films solar cells with high efficiency in the future. Based on these background, there are several researches to fabricate Si structures by electrodeposition.

In the Si electrodeposition, non-aqueous solvents should be used as electrolytes due to the very negative reduction potential and the high reactivity with water of almost Si precursor. There are three types of ionic liquids for the Si electrodeposition; molten salts, ionic liquids, organic solvents. Here, the study in ionic liquids will be described for considering the characteristics of the ionic liquids described above, while there are several studies in molten salts [90-100] and organic solvents [101-111] on focusing on their characteristics.

The electrodeposition of Si in ionic liquids

Among of three types of non-aqueous solvents, ionic liquids exhibit the advantages such as a low temperature usage, a wide electrochemical window, etc. Following these characteristics, several researches have been performed.

It seems that the electrodeposition in ionic liquids has firstly reported by Katayama et al. [112] in 2001. In that study, they have electrodeposited Si in 1-ethyl-3-methylimidazolium hexafluorosilicate at 90 °C, while opinions are divided whether that ionic liquid can be classified as ionic liquids because that ionic liquids are called as low

temperature molten salt by some researchers. In that study, the condition of the electrodeposited Si was oxidized one, resulting in the difficulties to decide whether they were semiconductor or not as well as the process of oxidation of the films because they were exposed to the air after the electrodeposition. From these results, Katayama et al. has not reported the aspects relating to the semiconductor, while it is seemed to be able to electrodeposit Si in ionic liquids at low temperature. In 2004, it has been reported that the semiconductor Si can be electrodeposited by S. Zein El Abedin et al. [113]. They electrodeposited Si in 1-butyl-1-methylpyrrolidinium bis(trifluoromethylsulfonyl)amide ([Py_{1,4}] TFSA) saturated with SiCl₄ using a highly oriented pyrolytic graphite (HOPG) as working electrode, in which in situ current/voltage tunneling spectroscopy was used, and those techniques indicated a symmetrical band gap of 1.0 ± 0.2 eV that the intrinsic elemental semiconductor of Si have typically have. It was challenging to maintain the adhesion of Si to the HOPG substrate because there was a weak interaction between the electrodeposited Si and the substrate. For this, Borisenko et al. [114] and Al-Salman et al. [115] have exhibited to use Au substrate as working electrode, and same semiconductor property was confirmed and the Si thin films with 1 μm thickness and the spherical morphology of the small grain of 10–50 nm was obtained in 1-butyl-1-methylpyrrolidinium bis(trifluoromethylsulfonyl)imide ([Py_{1,4}] TFSI) with 0.1 M SiCl₄, while it has also confirmed the oxygen inclusion to the films due to the exposure to the air in the analysis. Bebensee et al. [116] have also confirmed the elemental Si by X-ray photoelectron spectroscopy analysis in the electrodeposited Si thin films in [Py_{1,4}] TFSA with 0.1 M SiCl₄. At the almost same time, Nishimura et al. [117, 118] has been reported the electrodeposition of Si from different ionic liquids of in trimethyl-n-hexylammonium bis (trifluoromethylsulfonyl) imide (TMHATFSI) which is the most popular ionic liquids as a hydrophobic at room temperature with high stability against the reduction reaction [119, 120]. This ionic liquid also exhibited the well dissolution of SiCl₄ by van der Waals force, and could hinder the hydrolysis of SiCl₄. Other ionic liquids and precursor also have been used for the Si electrodeposition. Martinez et al. [119] have used N-butyl-N-methyl-pyrrolidinium bis(trifluoromethylsulfonyl) amide (BMPy-TFSA) with SiCl₄ and SiBr₄, and Pulletikurthi et al. [120] have used 1-butyl-1-methylpyrrolidinium trifluoromethylsulfonate ([Py_{1,4}] TfO) and 1-butyl-1-methylpyrrolidinium

tris(pentafluoroethyl)-trifluorophosphate ([Py_{1,4}] FAP). Pulletikurthi et al. has also investigated that the difference of anion in ionic liquids, in which in situ STM revealed the differences in the interfacial behavior of [Py_{1,4}] FAP and [Py_{1,4}] TfO with SiCl₄, resulting in an influence on the deposition process. As for the reaction mechanism of the Si precursor in ionic liquids, Nishimura et al. [121] has reported that the species of Si_mCl_n might be generated during the reduction of SiCl₄ in TMHATFSI from *in-situ* Raman measurement. Komadina et al. [122] has reported that the charge efficiency of the Si electrodeposition was estimated as 190 ~ 250 % for four-electron reduction from electrochemical quartz crystal microbalance (EQCM) method, while it should also be noted that those EQCM analyses might include many deviations in the assumptions for accurate estimation of the mass in the study of the Si electrodeposition, and that the condition of the inclusion of ionic liquids were assumed, resulting in the overestimation of the charge density.

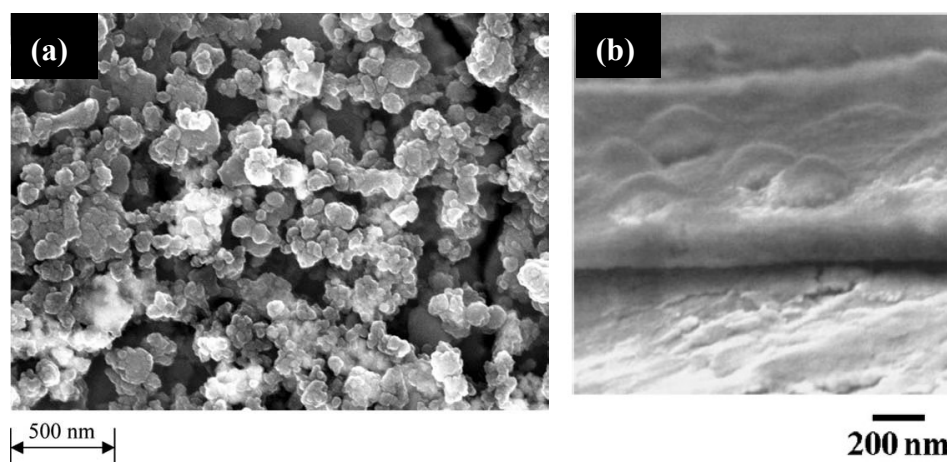


Fig. 1.8 The examples of the Si thin films electrodeposited (a) at -2.7 V vs. Fc/Fc⁺ in [Py_{1,4}] TFSI with 0.1 M SiCl₄ [113] (Copyright 2004 by Electrochemistry Communications. Reproduced with permission of Electrochemistry Communications by Copyright Clearance Center's RightsLink® service) (b) at -2.0 V vs. Pt QRE in TMHATFSI with 0.1 M SiCl₄ for 14,400 s [118] (Copyright 2008 by Electrochem. Solid-State Lett. Reproduced with permission of Electrochem. Solid-State Lett. by Copyright Clearance Center's RightsLink® service)

Si nanostructures have also been fabricated by some researchers as well as the thin films. It seems that Al- Salman et al. and [123] Mallet et al. [124] has firstly reported the electrodeposition of Si nanowires in [Py_{1,4}] TFSA with 0.5 and 1.0 M SiCl₄ with using a polycarbonate membrane, in which the Si nanowires with several diameters of 400, 110, 90 and 15 nm were electrodeposited though they were randomly formed. Three dimensionally ordered macroporous (3DOM) [125] silicon films have been formed in [Py_{1,4}] TFSA with 0.1 M SiCl₄ with using an ordered polystyrene (PS) templates by Liu et al. The sphere of diameters was 235 nm, 455 nm and 515 nm, and then electrodeposited films shows a bandgap in the near infrared region, while there not perfectly electrodeposited in all areas. In addition, Ishibashi et al. [126] have reported that Si nanopillars were able to be fabricated in TMHATFSI with 0.5 M SiCl₄ on the substrate prepared by UV-nanoimprint lithography was employed, in which the thickness of resist was 90-100 nm, and mold feature diameter was 150 nm, with a pitch of 450 nm.

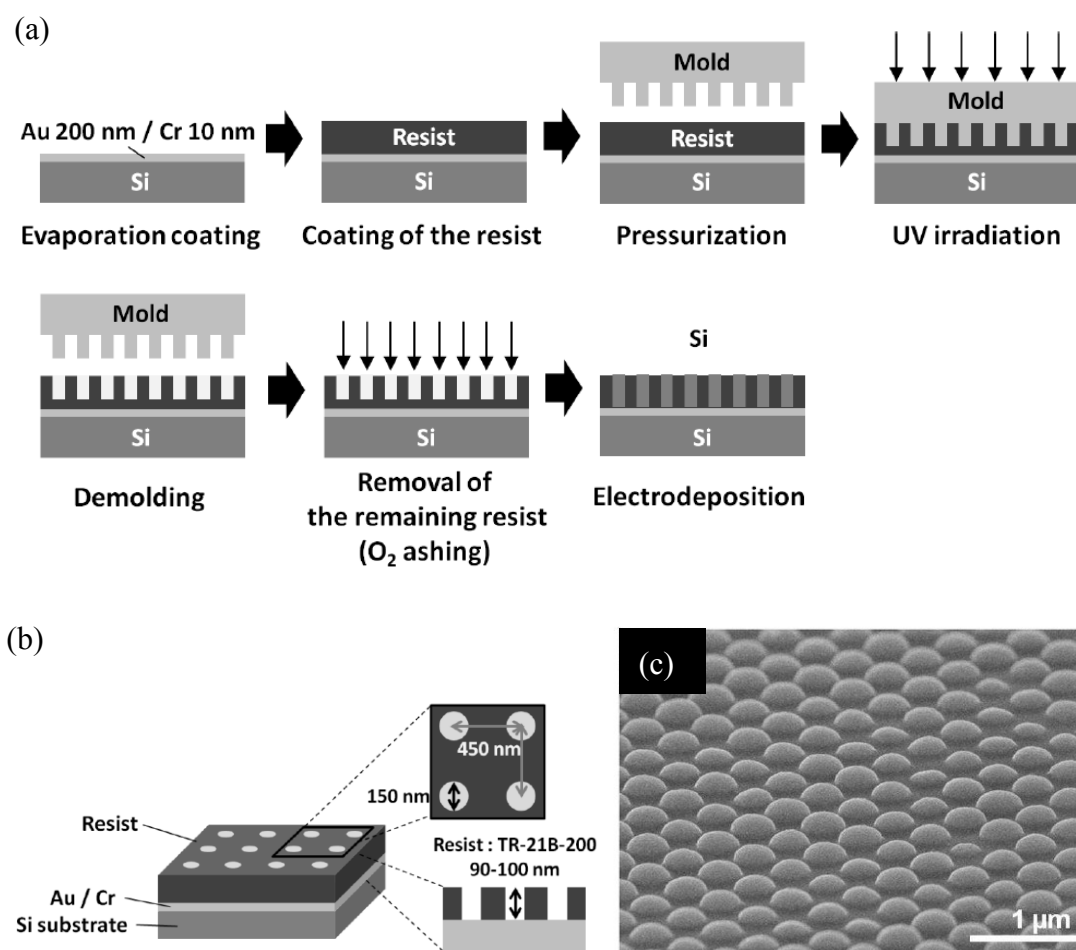


Fig. 1.9 The example of the fabrication of Si nanostructures; (a) the preparation of the patterned substrate by UV-nanoimprint lithography technique, (b) the schematic images of the prepared patterned substrate, and (c) the electrodeposited Si nanopillars [126] (Copyright 2013 by ECS Trans. Reproduced with permission of ECS Trans. by Copyright Clearance Center's RightsLink® service)

1.4 Strategy of this study

As described, Si is widely used in various fields, and it is thought that the demand of Si continuously increases in the future, especially for Si solar cells application. For the fabrication of Si, it has been studied via dry processes. However, these approaches occasionally face difficulties in depositing nanostructures in a large area as well as the fabrication cost due to the high voltage and high vacuum environment.

On the other hand, the electrodeposition has advantages in fabricating nanostructures with nm order in a large area without using high voltage and high vacuum environment. Following these characteristic and the recent availability of ionic liquids, the fabrication of Si by electrodeposition has been attracted as an alternative approach. Although there are several studies of Si electrodeposition in ionic liquids, it still has challenging in the decrease of impurities in the films and the elucidation of reaction mechanism. The reason of these difficulties seems to be strongly related to the insufficient clarification of the reaction system in utilizing the ionic liquids in the electrodeposition, while there are many studies of the electrodeposition in ionic liquids. It is considered that, especially in the Si electrodeposition, the impurities inclusion might relate to the uncertainty of the reaction mechanism. It also indicates that comprehensive understanding of the reaction mechanism will be necessary for the realization that the Si electrodeposition could be controlled more precisely based on the proper understanding of the reaction mechanism, and the impurities inclusion in the films could be suppressed in the future. Therefore, the reaction of the Si electrodeposition in ionic liquids was analyzed in this thesis work focusing on the molecular level understanding at the solid-liquid interface with the view point of establishing the reaction analysis system in non-aqueous solvents. In this thesis work, trimethyl-n-hexylammonium bis(trifluoromethylsulfonyl)imide (TMHATFSI) which has ammonium based cation and sulfonyl based anion was chosen as the ionic liquid because this ionic liquid has relatively low viscos (250 mPa s at 25 °C) and the solubility of SiCl_4 is high (up to 1.0 M) compared with other hydrophobic ionic liquids. Such characteristics, especially basing on hydrophobic characteristics, are important for the electrodeposition of Si.

In order to analyze such reaction at the solid-liquid interface, several interfacial techniques should be used. For this, the combination of experimental measurement and theoretical analysis is focused on as a powerful tool to elucidate the mechanism. Based on these frameworks, experimental measurements are firstly conducted, and then, the validity of suggested mechanisms are evaluated by theoretical calculations in ionic liquids and indicate molecular level behaviors. In addition, the elucidation of the cause of the impurities inclusion, application of the reaction system to other non-aqueous solvents, and the formation of thin films in terms of the application, especially focusing on the solar cell applications, are focused on as well as the reaction mechanism analysis.

References

- [1] K. Nishikawa, Y. Ouchi, T. Itoh, H. Ohno, M. Watanabe, *Ionekitainokagaku: Shinsedaiekitaihenocyouosen*, Maruzenshuppan, Tokyo, 2012.
- [2] J. S. Wilkes, M. J. Zawarotko, *J. Chem. Soc., Chem. Commun.*, 965 (1992).
- [3] P. Bonhote, A. P. Dias, N. Papageorgiou, K. Kalyanasundaram, M. Gratzel, *Inorg. Chem*, **35**, 1168 (1996).
- [4] M. J. Earle, K. R. Seddon, *Pure Appl. Chem.*, **72**, 1391 (2000).
- [5] F. Endres, *ChemPhysChem*, **3**, 144 (2002).
- [6] M. Buzzeo, R. Evans, R. Compton, *ChemPhysChem*, **5**, 1106 (2004).
- [7] D. Silvester, R. Z. Compton, *Phys. Chem.*, **220**, 1247 (2006).
- [8] D. R. MacFarlane, M. Forsyth, P. C. Howlett, J. M. Pringle, J. Sun, G. Annat, W. Neil, E. I. Izgorodina, *Acc. Chem. Res.*, **40**, 1165 (2007).
- [9] D. Wei, A. Ivaska, *Anal. Chim. Acta*, **607**, 126 (2008).
- [10] M. Armand, F. Endres, D. R. MacFarlane, H. Ohno, B. Scrosati, *Nat. Mater.* **8**, 621 (2009).
- [11] Y. Z. Su, Y. C. Fu, Y. M. Wei, J. W. Yan, B. W. Mao, *ChemPhysChem*, **11**, 2764 (2010).
- [12] M. Opallo, A. Lesniewski, *J. Electroanal. Chem.*, **656**, 2 (2011).
- [13] A. P. Abbott, G. Frisch, K. S. Ryder, *Annu. Rev. Mater. Res.*, 43 (2013).
- [14] J. S. Wilkes, *Green Chem.*, **4**, 73 (2002).
- [15] R. D. Rogers, K. R. Seddon, *Science*, **302**, 792 (2003).
- [16] K. R. Seddon, *Nat. Mater.*, **2**, 363 (2003).
- [17] C. Verma, E. E. Ebenso, M. A. Quraish, *J. Mol. Liq.*, **233**, 403 (2017).
- [18] N. V. Plechkova, K. R. Seddon, *Chem. Soc. Rev.*, **37**, 123 (2008).
- [19] A. Stark, *Top. Curr. Chem.*, **290**, 41 (2009).
- [20] A. Lewandowski, *J. Power Sources*, **194**, 601 (2009).
- [21] Ohno, H., Ed., *In Electrochemical Aspects of Ionic Liquids*, John Wiley & Sons Inc., 35-54 (2005).
- [22] D. R. MacFarlane, J. M. Pringle, P. C. Howlett, M. Forsyth, *Phys. Chem. Chem. Phys.*, **12**, 1659 (2010).
- [23] P. Hapiot, C. Lagrost, *Chem. Rev.*, **108**, 2238 (2008).
- [24] G. H. Lane, *Electrochim. Acta*, **83**, 513 (2012).
- [25] M. Hayyan, F. S. Mjalli, M. A. Hashim, I. M. AlNashef, T. X. Mei, *J. Ind. Eng.*

- Chem.*, **19**, 106 (2013).
- [26] R. Hagiwara, Y. Ito, *J. Fluorine Chem.*, **105**, 221 (2013).
- [27] J. A. P. Coutinho, P. J. Carvalho, N. M. C. Oliveira, *RSC Adv.*, **2**, 7322 (2012).
- [28] H. Tokuda, K. Hayamizu, K. Ishii, M. A. B. H Susan, M. Watanabe, *J. Phys. Chem. B*, **109**, 6103 (2005).
- [29] F. Endres, D. MacFarlane, A. Abbott, *Electrodeposition from Ionic Liquids*, John Wiley & Sons, New York, 2008.
- [30] B. D. Falola, I. I. Suni, *Curr. Opin. Solid State Mater. Sci.*, **19**, 77 (2015).
- [31] S. Lee S Eds. *Encyclopedia of chemical processing*, New York, 2006.
- [32] P. Bonhôte, A. Dias, N. Papageorgiou, K. Kalyanasundaram, and M. Grätzel, *Inorg. Chem.*, **35**, 1168 (1996).
- [33] D.R. MacFarlane, P. Meakin, J. Sun, N. Amini, and M. Forsyth, *J. Phys Chem. B.*, **103**, 4164 (1999).
- [34] Y.-F. Lin, and I-W. Sun, *Electrochim. Acta*, **44**, 2771 (1999).
- [35] P.-Y. Chen, and I-W. Sun, *Electrochim. Acta*, **46**, 1169 (2001).
- [36] A.P. Abbott, G. Capper, K. J. McKenzie, and K.S. Ryder, *J. Electroanal. Chem.*, **599**, 288 (2007).
- [37] F. Endres, and A. Schweizer, *Phys. Chem. Chem. Phys.*, **2**, 5455 (2000).
- [38] P.-Y. Chen, and I.-W. Sun, *Electrochim. Acta*, **45**, 441 (1999).
- [39] K. Murase, K. Nitta, T. Hirato, and Y. Awakura, *J. Appl. Electrochem.*, **31**, 1089 (2001).
- [40] T. N. Rostovshchikova, V. V. Smirnov, V. M. Kozhevnikov, D. A. Yavsin, M. A. Zabelin, I. N. Yassievich, and S. A. Gurevic, *Appl. Catal. A: General*, **296**, 70 (2005).
- [41] X.-H. Xu, and C. L. Hussey, *J. Electrochem. Soc.*, **139**, 1295 (1992).
- [42] Y. Katayama, S. Dan, T. Miura, and T. Kishi, *J. Electrochem. Soc.*, **148**, C102 (2001).
- [43] P. He, H. T. Liu, Z. Y. Li, Y. Liu, X. D. Xu, and J. H. Li, *Langmuir*, **20**, 10260 (2004).
- [44] S. A. Meiss, M. Rohnke, L. Kienle, S. Zein El Abedin, F. Endres, and J. Janek, *Chem. Phys. Chem.*, **8**, 50 (2007).
- [45] P. He, H. Liu, Z. Li, and J. Li, *J. Electrochem. Soc.*, **152**, E146 (2005).
- [46] J.-F. Huang, and I.-W. Sun, *Electrochim. Acta*, **49**, 3251 (2004).
- [47] M. R. Ali, A. Nishikata, and T. Tsuru, *Electrochimica Acta*, **42**, 2347 (1997).
- [48] T. Tsuda, C. L. Hussey, and G. R. Stafford, *J. Electrochem. Soc.*, **151**, C379 (2004).
- [49] S. Zein El Abedin, E. Moustafa, R. Hempelmann, H. Natter, and F. Endres, *Chem. Phys. Chem.*, **7**, 1535 (2006).

- [50] Brausch, A. Metlen, and P. Wasserscheid, *Chem. Commun.*, **13**, 1552 (2004).
- [51] Y. Katayama, T. Morita, M. Yamagata, and T. Miura, *Electrochemistry*, **71**, 1033 (2003).
- [52] P. C. Howlett, D. R. MacFarlane, and A. F. Hollenkamp, *Electrochem. Solid-State Lett.*, **7**, A97 (2004).
- [53] G. W. Mellors, and S. Senderoff, *J. Electrochem. Soc.*, **112**, 840 (1965).
- [54] A. J. B. Dutra, J. C. Vazquez, and A. Espinola, *Miner. Eng.*, **6**, 663 (1993).
- [55] P. Chamelot, P. Palau, L. Massot, A. Savall, and P. Taxil, *Electrochim. Acta*, **47**, 3423 (2002).
- [56] F. Lantelme, A. Barhoun, G. Li, and J. P. Besse, *J. Electrochem. Soc.*, **139**, 1255. (1992)
- [57] G. M. Haarberg and J. Thonstad, *J. Appl. Electrochem.*, **119**, 789 (1989).
- [58] F. Endres, and C. Schrodtt, *Phys. Chem. Chem. Phys.*, **2**, 5517 (2000).
- [59] F. Endres, *Phys. Chem. Chem. Phys.*, **3**, 3165 (2001).
- [60] F. Endres and S. Zein El Abedin, *Phys. Chem. Chem. Phys.*, **4**, 1640 (2002).
- [61] L. Chen, K. Wang, X. Xie, J. Xie, *Electrochem. Solid-State Lett.*, **9** (11), A512, (2006).
- [62] T. L. Kulova, A. M. Skundin, Y. V. Pleskov, E. I. Terukov, O. I. Kon’Kov, *J. Electroanal. Chem.*, **600** (1), 217, 2007.
- [63] EDMC, 2015 EDMC Handbook of Japan's & World Energy & Economic Statistics
- [64] United Nations Framework Convention on Climate Change, available: http://unfccc.int/meetings/paris_nov_2015/meeting/8926.php [Accessed 7 December 2017]
- [65] O. Konagai and Y. Ueda Eds., *Solar Cell Technology Handbook 1st ed.*, Ohmsha, Japan (2013).
- [66] “*Photovoltaics Roadmap (PV2030+) revised version*”, New Energy and Industrial Technology Development Organization, Tokyo (2009).
- [67] F. Aratani, *Progress in Photovoltaics: Research and Applications*, **13**, 463, (2005)
- [68] C. Wadia, A. P. Alivisatos, D. M. Kammen, *Environ. Sci. Technol.*, **43** (2009) 2072.
- [69] D. M. Powell, M. T. Winkler, H. J. Choi, and C. B. Simmons, *Energy Environ. Sci.*, **5** (2012) 5874.
- [70] M. A. Green, *Progr. Photovolt.: Res. Appl.*, **17**, 183 (2009).
- [71] M. D. Kempe, *Sol. Energy Mater. Sol. Cells*, **94**, 246 (2010).
- [72] J. Zhao, A. Wang, M. A. Green, *Prog. Photovolt: Res. Appl.*, **7**, 471 (1999).

- [73] K. Masuko, M. Shigematsu, T. Hashiguchi, D. Fujishima, M. Kai, N. Yoshimura, T. Yamaguchi, Y. Ichihashi, T. Yamanishi, and T. Takahama, *IEEE J. Photovolt.*, **4**, 1433 (2014).
- [74] C. Battaglia, A. Cuevas, and S. D. Wolf, *Energy Environ. Sci.*, **9**, 1552, 2016.
- [75] T. Homma, N. Matsuo, X. Yang, K. Yasuda, Y. Fukunaka, T. Nohira, *Electrochim. Acta*, **179**, 512 (2015).
- [76] M. A. Green, *Proc. 15th Int. Photovoltaic Science & Engineering Conference Shanghai, China*, p.7 (2005)
- [77] K. Peng, Y. Xu, Y. Wu, Y. Yan, S.-T. Lee, and J. Zhu, *Small*, **11**, 1062 (2005).
- [78] B. Tian, X. Zheng, T. J. Kempa, Y. Fang, N. Yu, G. Yu, J. Huang, and C. M. Lieber, *nature*, **449**, 885 (2007).
- [79] E-C. Cho, S. Park, X. Hao, D. Song, G. Conibeer, S-C. Park, and M. A Green, *Nanotechnology*, **19**, 245201 (2008).
- [80] E. C. Garnett and P. Yang, *J. AM. CHEM. SOC.*, **130**, 9224 (2008).
- [81] V. Sivakov, G. Andrä, A. Gawlik, A. Berger, J. Plentz, F. Falk, and S. H. Christiansen, *Nano Lett.*, **9**, 1549 (2009).
- [82] W. J. Nam, L. Ji, T. L. Benanti, V. V. Varadan, S. Wagner, Q. Wang, W. Nemeth, D. Neidich, and S. J. Fonash, *Appl. Phys. Lett.*, **99**, 073113 (2011).
- [83] S. Yamada, Y. Kurokawa, S. Miyajima, and M. Konagai, *Jpn. J. Appl. Phys.*, **52**, 04CR02 (2013).
- [84] R. C. Chittik, J. H. Alexander, and H. F. Stealing, *J. Electrochem. Soc.*, **116**, 77 (1969).
- [85] W. E. Spear and P. G. LeComber, *Solid State Commun.*, **17**, 1193 (1975).
- [86] D. E. Carlson and C. R. Wronski, *Appl. Phys. Lett.*, **28**, 671 (1976).
- [87] D. L. Staebler and C. R. Wronski, *J. Appl. Phys.*, **51**, 3262 (1980).
- [88] M. Stutzmann, W. B. Jackson, and C. C. Tsai, *Phys. Rev. B*, **32**, 23 (1985).
- [89] Denkitokin-kenkyuukai, *Gendai-Mekki-kyoukai*, Nikkan Kogyo Simbun Ltd., Tokyo, 2011.
- [90] T. Matsuda, S. Nakamura, K. Ide, K. Nyudo, S. Yae, Y. Nakato, *Chem. Lett.*, **7**, 569 (1996).
- [91] T. Nohira, K. Yasuda, Y. Ito, *Nat. Mater.*, **2**, 397 (2003).
- [92] P. Spinelli, V. E. Ferry, J. van de Groep, M. van Lare, M. A. Verschuuren, R. E. I. Schropp, H. A. Atwater, and A. Polman, *J. Opt.*, **14**, 024004 (2012).
- [94] S. K. Cho, F-R. F. Fan, A. J. Bard, *Electrochim. Acta*, **65**, 57 (2012).
- [95] S. Sokhanvaran and M. Barati, *J. Electrochem. Soc.*, **161**, E6 (2014).
- [96] Y. Sakanaka, T. Goto, *Electrochem. Acta*, **164**, 139 (2015).

- [97] J. Zhao, H. Yin, T. Lim, H. Xie, H-Y. Hsu, F. Forouzan, and A. J. Bard, *J. Electrochem. Soc.*, **163**, D506 (2016).
- [98] X. Zou, L. Ji, X. Yang, T. Lim, E.T. Yu, and A. J. Bard, *J. Am. Chem. Soc.*, **139**, 16060 (2017).
- [99] X. Yang, L. Ji, X. Zou, T. Lim, J. Zhao, E.T. Yu, and A. J. Bard, *Angew. Chem. Int. Ed.*, **56**, 15078 (2017).
- [100] K. Yasuda, K. Maeda, R. Hagiwara, T. Homma, T. Nohira, *J. Electrochem. Soc.*, **164**, D67-71 (2017).
- [101] Takeda, R. Konno, and O. Yamamoto, *J. Electrochem. Soc.*, **128**, 1221 (1981).
- [102] A. K. Agrawal and A. E. Austin, *J. Electrochem. Soc.*, **128**, 2292 (1981).
- [103] J. Gobet and H. Tannenberger, *J. Electrochem. Soc.*, **135**, 109 (1988).
- [104] Y. Nishimura and Y. Fukunaka, *Electrochim. Acta*, **53**, 111 (2007).
- [105] Y. Nishimura and Y. Fukunaka, *ECS Trans.*, **6**, 77 (2007).
- [106] R. Epur, M. Ramanathan, F. R. Beck, A. Manivannan, and P. N. Kumta, *Mater. Sci. Eng., B*, **177**, 1157 (2012).
- [107] D. Elwell, *J. Cryst. Growth*, **52**, 741 (1981).
- [108] T. Munisamy and A. J. Bard, *Electrochim. Acta*, **55**, 3797 (2010).
- [109] J.P. Nicholson, *J. Electrochem. Soc.*, **152**, C795 (2005).
- [110] M. Bechelany, J. Elias, P. Brodard, J. Michler, and L. Philippe, *Thin Solid Films*, **520**, 1895 (2012).
- [111] C. Vichery, V. Le Nader, C. Frantz, Y. Zhang, J. Michler, and L. Philippea, *Phys. Chem. Chem. Phys.*, **16**, 22222 (2014).
- [112] Y. Katayama, M. Yokomizo, T. Miura, T. Kishi, *Electrochemistry*, **69**, 834 (2001).
- [113] S. Zein El Abedin, N. Borissenko, F. Endres, *Electrochemistry Communications*, **6**, 510 (2004).
- [114] N. Borisenko, S. Zein El Abedin, F. Endres, *J. Phys. Chem. B*, **110**, 6250 (2006).
- [115] R. Al-Salman, S. Zein El Abedin, F. Endres, *Phys. Chem. Chem. Phys.* **31**, 4650 (2008).
- [116] F. Bebensee, N. Borissenko, M. Frerichs, O. Höfft, W. Maus-Friedrichs, S. Zein El Abedin, F. Endres, *Z. Phys. Chem.*, **222**, 671 (2008).
- [117] Y. Nishimura and Y. Fukunaka, *ECS Transactions*, **6** (13), 77 (2007).
- [118] Y. Nishimura, Y. Fukunaka, T. Nishida, T. Nohira, and R. Hagiwara, *Electrochem. Solid-State Lett.*, **11** (9), D75 (2008).
- [119] A. M. Martinez, K. S. Osen, O. E. Kongsteinb, E. Sheridan, A. Ulyashina, and G. M. Haarbergc *ECS Trans.*, **25** (27), 107 (2010).
- [120] G. Pulletikurthi, A. Lahiri, T. Carstens, N. Borisenko, S. Zein El Abedin and F.

- Endres, *J. Solid State Electrochem.*, **17**, 2823 (2013).
- [121] Y. Nishimura, Y. Fukunaka, C. R. Miranda, T. Nishida, T. Nohira, and R. Hagiwara, *ECS Trans.*, **16** (24), 1 (2009).
- [122] J. Komadina, T. Akiyoshi, Y. Ishibashi, Y. Fukunaka, and T. Homma, *Electrochim. Acta*, **100**, 236 (2013).
- [123] R. Al-Salman, J. Mallet, M. Molinari, P. Fricoteaux, F. Martineau, M. Troyon, S. Zein El Abedin, F. Endres, *Phys. Chem. Chem. Phys.*, **10**, 6233 (2008).
- [124] J. Mallet, M. Molinari, F. Martineau, F. Delavoie, P. Fricoteaux, and M. Troyon, *Nano Lett.*, **8** (10), 3468 (2008).
- [125] X. Liu, Y. Zhang, D. Ge, J. Zhao, Y. Li and F. Endres, *Phys. Chem. Chem. Phys.*, **14**, 5100 (2012).
- [126] Y. Ishibashi, T. Akiyoshi, J. Komadina, Y. Fukunaka, and T. Homma, *ECS Trans.*, **50** (48), 117 (2013).

Chapter 2:

***Overall Reaction Mechanism Analysis of Si
Electrodeposition in Ionic Liquids***

2.1 Introduction

For considering the fabrication of the electrodeposited Si structure for the application, it is required to electrodeposit Si with an appropriate electrodeposition condition and avoid the impurities inclusion to the structures after understanding the detailed reaction mechanism.

As for the analysis of the reaction mechanism of the Si electrodeposition in ionic liquids, the detailed mechanism has not been reported yet, while several researches were engaging in the Si electrodeposition [1-12]. As the most recent example until now, S. Ivanov et al. [12] has reported the Si electrodeposition in 1-butyl-1-methylpyrrolidinium bis(trifluoromethylsulfonyl)imide with SiCl_4 as Si source. However, it has also been still unclear in that paper with the respect to the details of reduction processes even though they have confirmed several cathodic peaks with / without frequency decreases, in which the decrease of frequency suggests the silicon deposition, with using the technique of electrochemical quartz crystal microbalance.

The objective of the study in this chapter is to investigate three aspects, focusing on an overall reaction mechanism of the Si electrodeposition. First, films electrodeposited at several potentials are characterized. Second, X-ray photoelectron spectroscopy (XPS) and electrochemical quartz crystal microbalance (EQCM) measurement are used to obtain the electrodeposition rate of Si in the films. Third, the electrodeposited films are characterized using Raman spectroscopy. XPS and Raman spectroscopy provide complementary information regarding Si electrodeposition, in particular ionic liquid inclusion into Si thin films and the possibility of its binding with the films. These analyses allow us to partially understand the Si electrodeposition reaction mechanism in ionic liquids.

2.2 Experimental

The ionic liquid trimethyl-n-hexylammonium bis(trifluoromethylsulfonyl)imide (TMHATFSI) containing less than 10 ppm H₂O and less than 1 ppm Cl⁻ were used with 0.5 M SiCl₄ (99.98% purity) (Stella Chemifa). This ionic liquid is hydrophobic and exhibits high solubility of SiCl₄ up to 1.0 M. The working electrode (deposition substrate) was a 6 MHz AT-cut quartz crystal with Au contacts (Hokuto Denko). Its surface area was 1.32 cm². Pt wires 0.1 cm in diameter were used as a quasi-reference electrode (QRE) and as a coiled counter electrode. The Pt QRE was insulated by a heat-shrinkable tube, leaving the tip of the Pt wire exposed, and it was immersed directly in the ionic liquid. The surface area of the QRE tip was 0.01 cm², whereas that of the Pt wire coil counter electrode was about 5 times larger than that of the working electrode. The working electrode was pretreated in oxygen plasma for 2 min, and the Pt electrodes were pretreated in 20 % sulfuric acid solution before electrodeposition. The potential of ferrocene/ferrocenium (Fc/Fc⁺) was measured to be -0.23 V vs. Pt QRE (Fig. 2.1), resulting in the discussion of our potential with the standard of Fc/Fc⁺.

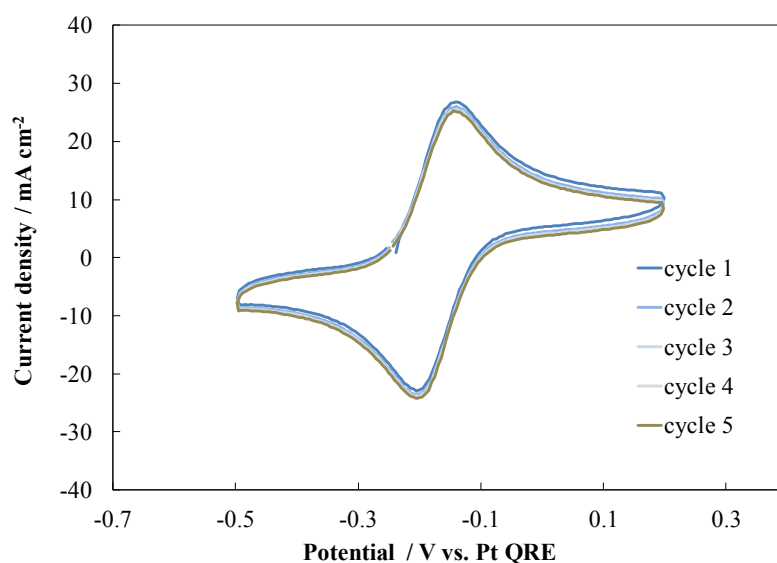


Fig. 2.1 Cyclic voltammogram (scan rate = 10 mV s^{-1}) in TMHATFSI with 1.0 M Fc/Fc^+ at $40 \text{ }^\circ\text{C}$

The EQCM apparatus was mounted in an aluminum block, and the electrolyte temperature was maintained at 18, 30 and $40 \text{ }^\circ\text{C}$ during all the experiments using this Al thermo-block (NISSIN, COOL/HEAT BLOCK NDC-100). After the measurements, all the electrodes were cleaned by rinsing with 99.5 % dimethyl carbonate and dried in vacuum for 10 min. In the EQCM analysis, the Sauerbrey equation [Eq. (1)] and the related equations for damping [Eqs. (2), (3)] were used to calculate the mass change during electrodeposition [12].

$$\Delta f_{\text{mass}} = \frac{-2f_s^2 \Delta m}{A(\mu_q \rho_q)^{1/2}} \quad (1)$$

$$\Delta f_{\text{viscosity}} = \frac{-\Delta w}{2} = \frac{-f_s^{3/2} [\Delta(\eta\rho)^{1/2}]}{(\pi\mu_q \rho_q)^{1/2}} \quad (2)$$

$$\Delta f_s = \Delta f_{\text{mass}} + \Delta f_{\text{viscosity}} = \Delta f_{\text{mass}} - \frac{\Delta w}{2} \quad (3)$$

where

Δf_{mass} is the resonance frequency change deriving from the mass,

$\Delta f_{\text{viscosity}}$ is the resonance frequency change deriving from viscous damping,

Δf_s is the series resonance frequency change (frequency of peak in conductance),

Δm is the mass change,

A is the surface area,

$\mu_q \rho_q$ is the product of the quartz crystal's shear modulus and density,

Δw is the change in the half-width at half-maximum of the conductance peak, and $\eta\rho$ is the product of the ionic liquid's viscosity and density.

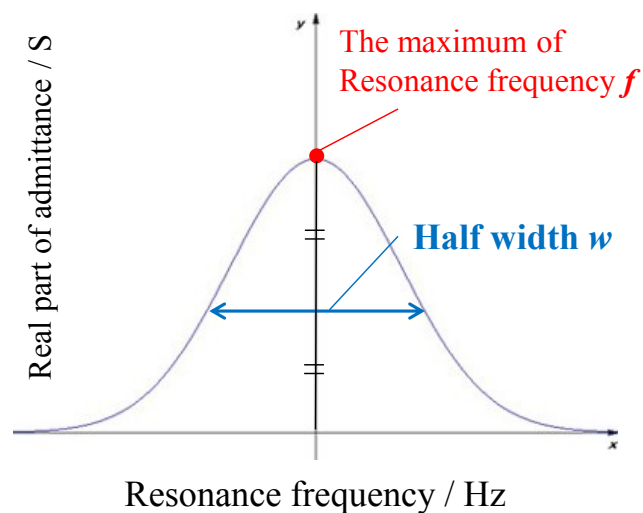


Fig. 2.2 The mean of uncommon parameters in EQCM analysis

Cyclic voltammetry (CV) and constant potential measurements were then performed using a potentiostat/galvanostat (Hokuto Denko, HZ-5000). EQCM (Hokuto Denko quartz crystal mount and Agilent Technologies Frequency Analyzer, E5061A) measurement was also performed. CV was conducted from open circuit potential (OCP) to -3.0 V vs. Pt QRE at a scan rate of 10 mV s^{-1} , and constant potential electrodeposition was performed at -2.0, -2.5, and -3.0 V vs. Pt QRE. The reproducibility of the OCP measurement was within 50 mV at -0.20 V vs. Pt QRE in the ionic liquid containing 0.5 M SiCl_4 . All electrochemical measurement was performed in an Ar-filled glove box.

XPS (ULVAC, PHI 5000 Versa Probe WS) using $\text{Al-K}\alpha$ irradiation and 4 kV Ar ion etching was employed to measure the content profiles of elements. One minute of Ar sputter time etches approximately 50 nm in SiO_2 . A transfer vessel was used to prevent Si thin films from oxidizing in the air before XPS measurement as possible as I could, however, it might not be avoided the oxidation perfectly. The XPS peaks were fitted using the MultiPak software utility (ULVAC, PHI 5000 Versa Probe WS).

The electrodeposited thin films were also characterized using focused ion beam scanning electron microscopy (SEM, HITACHI High-Technologies, NB 5000) with Ga ion etching to measure cross-sectional views, and scanning transmission electron microscopy (TEM, HITACHI High-Technologies, HD 2700) as well as by Raman spectroscopy (TOKYO INSTRUMENTS SOLAR TII, Nanofinder 30). Detailed analysis of the Raman spectra was performed using Origin (OriginLab Corporation). It can compensate for the background noise level in each measurement so that the modified spectrum represents the essential chemical signal strength corresponding to each peak. As-deposited Si films were subjected to rapid thermal annealing (ULVAC, MILA 3000) at 350 and 700 °C for 1 h in Ar (90 %) and H_2 (10 %) atmosphere.

2.3 Results and Discussion

To understand the electrochemical behavior of SiCl_4 in TMHATFSI, the current transient and EQCM measurement were conducted. Figure 2.3 illustrates those results along the dotted line during the anodic scan in the ionic liquid alone (containing no SiCl_4). The increase in the cathodic current density and decrease in the mass recorded at -3.8 V vs. Pt QRE stemmed from decomposition of the ionic liquid. Then, EQCM measurement during CV measurement was conducted in the ionic liquid with 0.5 M SiCl_4 .

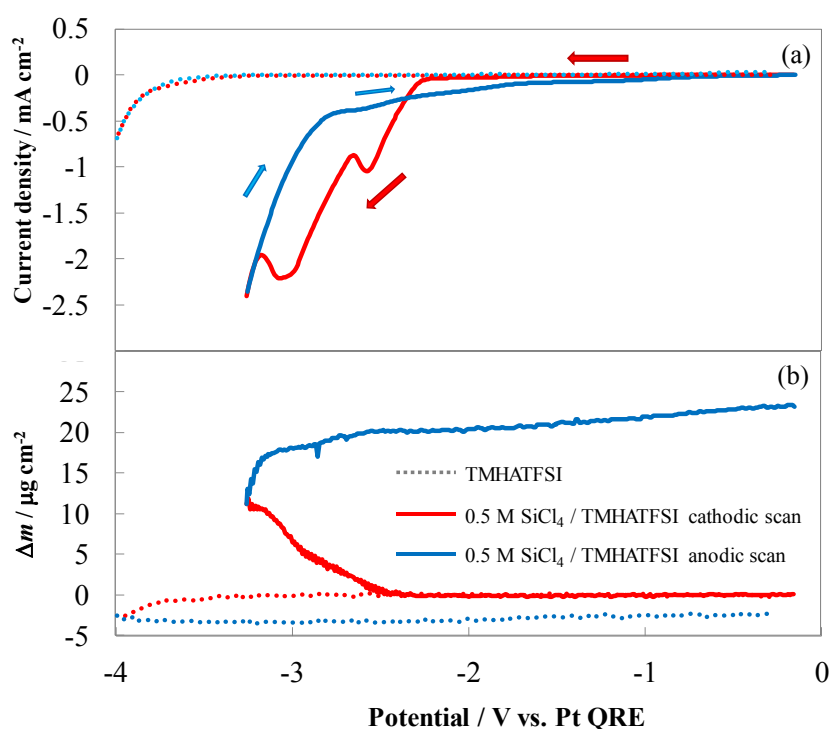


Fig. 2.3 (a) Cyclic voltammogram (scan rate = 10 mV s^{-1}) (b) Mass change calculated from EQCM measurement during CV in TMHATFSI with (continuous line) and without (dotted line) 0.5 M SiCl_4 at $40 \text{ }^\circ\text{C}$ (Arrows show the path of voltammogram.)

The uncommon parameters are described in Fig. 3. In the above equations, f_s represents the series resonance frequency, and Δf_s represents the series resonance frequency change, which is equal to the sum of the contributions to the resonance shift from the mass and viscosity: Δf_{mass} and $\Delta f_{\text{viscosity}}$, respectively (assuming that $\Delta f_{\text{viscosity}} \ll \Delta f_{\text{mass}}$). This viscosity component is almost equivalent to the change in the half-width at half-maximum of the conductance peak relative to the quartz crystal in air (no liquid contact). The viscosity of the electrolytes appears to change during electrodeposition in ionic liquids. Therefore, the resonance frequency change deriving from the viscosity must be calibrated in order to calculate the mass gain.

The cathodic current starts to increase slightly from -1.0 to -1.5 V vs. Pt QRE and then rises significantly around -2.0 V vs. Pt QRE, as seen in the inset of Fig. 2.3. Two current peaks, on the other hand, appear around -2.5 and -3.0 V vs. Pt QRE with an associated mass increase that is likely due to SiCl_4 reduction. These EQCM results suggest that SiCl_4 reduction may progress in multiple stages, i.e., via intermediary electroreduction reactions, although further detailed study is necessary to clarify the stages of SiCl_4 reduction.

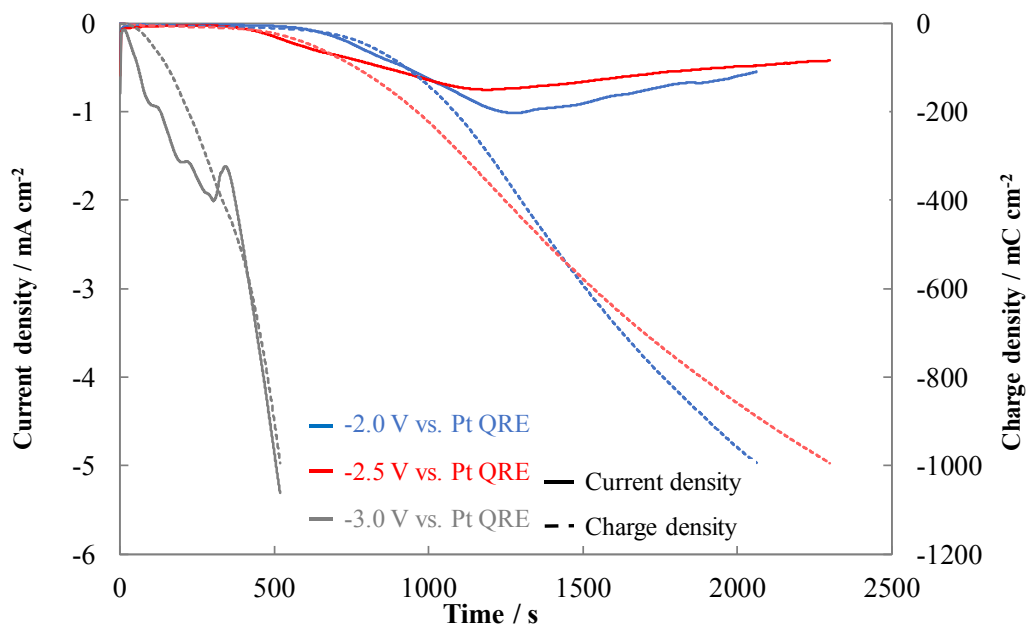


Fig. 2.4 Current density (continuous line) and charge density (dotted line) during potentiostatic electrodeposition in TMHATFSI with 0.5 M SiCl_4 at 40 °C at each potential at 1000 mC cm^{-2}

Next, the mass change during potentiostatic electrodeposition at three potentials was investigated using the EQCM. Figure 2.4 shows the transient variations in the current density and charge density at each potential. The current density recorded at -2.0 and -2.5 V vs. Pt QRE over the initial 400 to 600 s is negligibly small. An incubation period for Si electrodeposition may be expected.

After this incubation period, a current increase is observed from 400 to 1250 s at both potentials. Two solid curves reach the minimum values around 1250 s, indicating that the current tends to decrease after 1300 s. On the other hand, the current density rapidly increases just after potentiostatic electrodeposition starts, with a quite short incubation period, at -3.0 V vs. Pt QRE. It increases in a zigzag manner over the initial 300 s, and then the current tends to increase more smoothly. (Three peaks are observed, which represent reactions that are difficult to identify at present.) These current increases

are surely attributed to the electroreduction of SiCl_4 . Morphological variations in Si films electrodeposited at the three potentials were examined at 500 mC cm^{-2} (Fig. 2.5). A cross-sectional image of a compact, dense Si film on a Au substrate is observed at -2.0 V vs. Pt QRE. A much thicker film with some pores in its cross section appears at -2.5 V vs. Pt QRE. The surface morphology is rather uniformly composed of precipitated grains 50 nm in diameter. This surface roughness may be enhanced by coagulated precipitated grain ensembles with submicron diameter at -3.0 V vs. Pt QRE.

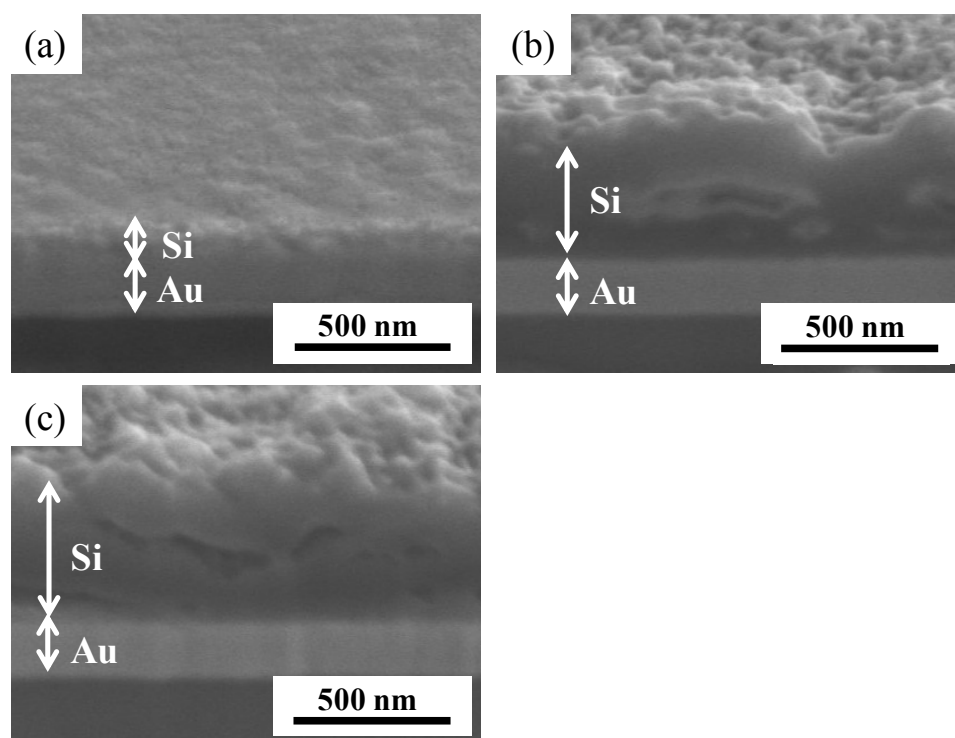
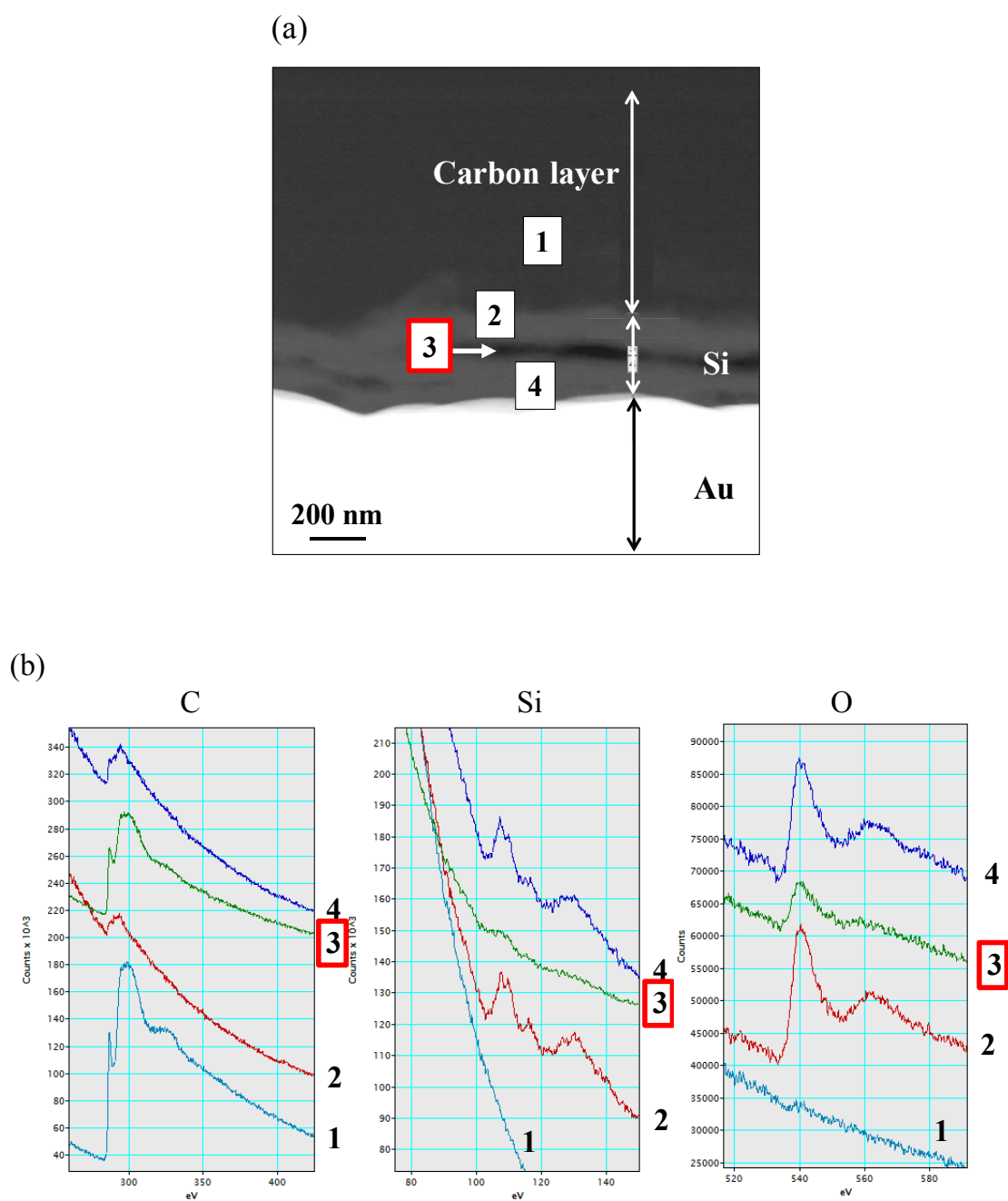


Fig. 2.5 SEM images of the Si thin films electrodeposited at $40 \text{ }^\circ\text{C}$ at 500 mC cm^{-2} at each potential: (a) -2.0 V vs. Pt QRE (b) -2.5 V vs. Pt QRE (c) -3.0 V vs. Pt QRE

The current density starts to decrease after 1300 s at -2.0 and -2.5 V vs. Pt QRE, as seen in Fig. 2.4. This decreasing tendency may be caused by the resistance of the electrodeposited dense Si thin films, as the electrodeposited Si thin films might be a semiconductor. On the other hand, the current density continues to increase as electrodeposition progresses, accompanying the formation of a porous film structure at -

3.0 V vs. Pt QRE. The porous film structure enhances the effective electrode surface area, increasing the current density under potentiostatic electrolysis.

In the SEM images, it was confirmed that voids were existed inside the films. To analyze these voids whether some elements are existed or not, the films were observed by TEM. The results are shown in Fig. 2.6. From these analyses, the peak derived from carbon, which is considered as ionic liquids, was strongly observed in voids (No. 3), while the peak derived from Si was strongly observed in grey area (No. 2 and 4). These results suggest that the impurities deriving from the ionic liquids are incorporated during the Si growth. As the condition of the ionic liquids, it is possible that ionic liquids themselves are incorporated in the films because they are not decomposed at -2.5 V vs. Pt QRE with the reference to their electrochemical windows to -3.5 V vs. Pt QRE as shown in Figure 2.1, while very small amount of ionic liquids are decomposed despite the electrochemical window. It was also confirmed that oxygen was existed in the films. In the region in grey area (No. 2 and 4), the exposure to the air cause the oxidation of the sample, and the existence of oxygen in voids (No. 3) also suggest that the ionic liquids are incorporated in the films. Then, the structure of the included ionic liquids was investigated by Raman spectroscopy. The result of Raman spectrum of Si thin films electrodeposited at -2.5 V vs. Pt QRE is shown as Fig. 2.7. From this result, the peak deriving from C-C-C, S=O, C-F, C-H were observed, in which C-C-C and C-H should derive from the cation, and S=O and C-F should derive from the anion. It also indicates that ionic liquids themselves were incorporated into the films during the Si growth. However, it should be noted here that it can not mention that it is hard for ionic liquids to decompose at -2.5 V vs. Pt QRE because CV of the blank ionic liquid shows the small cathodic current, meaning the decomposition of a part of ionic liquids. Therefore, the result by Raman spectrum might include the decomposed products of ionic liquids.



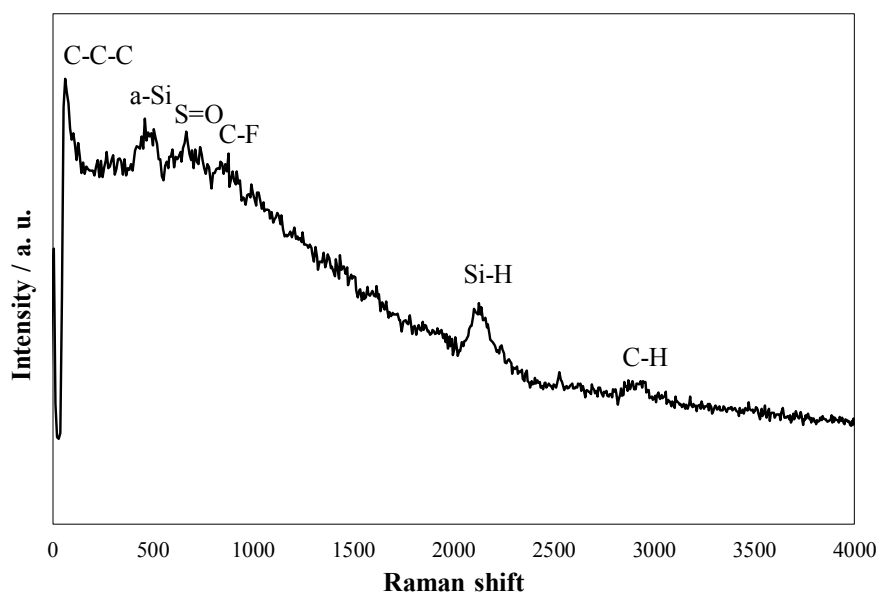


Fig. 2.7 Raman spectrum of the film electrodeposited at -2.5 V vs. Pt QRE

The Si binding energy of the topmost surface of the deposits at each potential are shown in Fig. 2.8. These data were analyzed using MultiPak to obtain detailed peak fitting information. The black lines show the original data measured by XPS, and the red and blue lines show the analyzed data. The jagged red lines are the background spectrum. At all the potentials, Si-Si and Si-O_x bonding were observed at the topmost surface. The ratio of the Si-Si bonding peak intensity to that for SiO_x is increased as the potential is decreased from -2.0 to -2.5 V vs. Pt QRE. It is almost saturated at -3.0 V vs. Pt QRE. This behavior is also expected from the depth profile measurement shown in Fig. 2.10, where the O concentration is highest near the topmost surface (until 1 min of Ar sputter time).

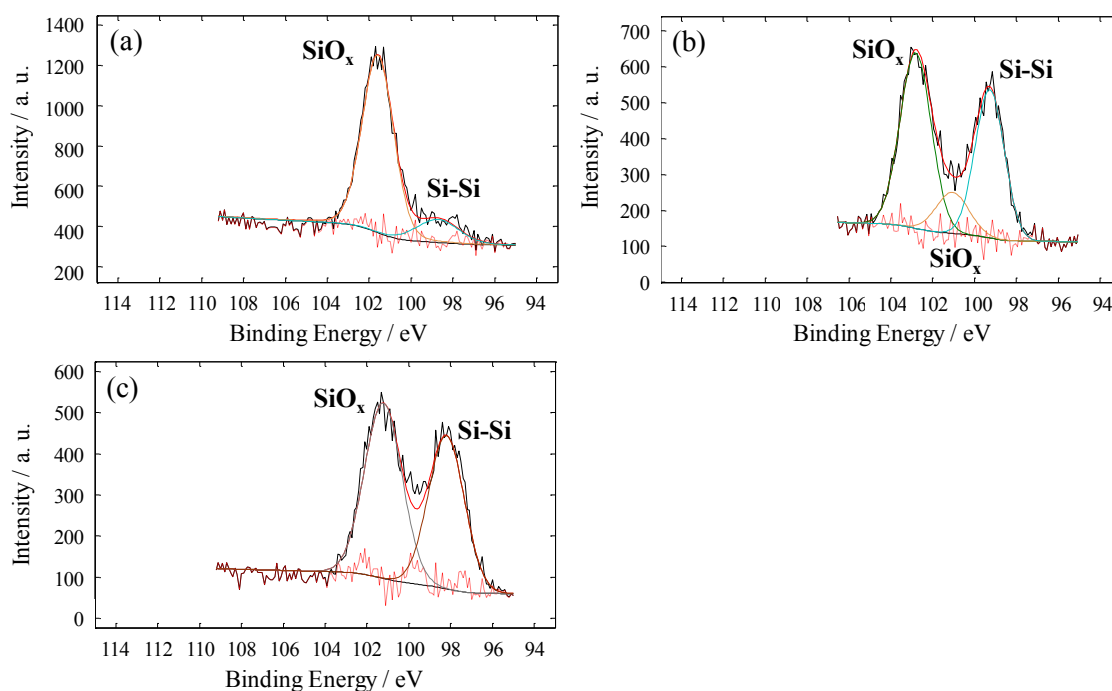


Fig. 2.8 Si 2p binding energy of the top most surface of the thin films electrodeposited at 40 °C at each potential: (a) -2.0 V vs. Pt QRE (b) -2.5 V vs. Pt QRE, (c) -3.0 V vs. Pt QRE

Raman spectra are shown in Fig. 2.9. A peak around 480 cm^{-1} was observed in the Si thin films electrodeposited at all the potentials. This peak was analyzed using Origin [Fig. 2.9 (d)]. The pink dots show the original data measured by Raman spectroscopy, and the continuous lines show fitting results. This analysis confirms the existence of a peak around 480 cm^{-1} . The peak at around 480 cm^{-1} generally originates from amorphous Si (a-Si) inside Si thin films. The other peaks in Fig. 2.9 are thought to be derived from ionic liquids. For example, the peak around 770 cm^{-1} probably indicates S=O bonding, and that around 300 cm^{-1} indicates C–C–C bonding. CH₃ bonding appears around 2950 cm^{-1} . It becomes sharper as the electrode potential is shifted in the negative direction. This may suggest that cations including CH₃ bonding may participate in the cathodic reduction process. These peaks due to such chemical bonding may be caused by adsorption of the fragment ion in ionic liquids, which is in good agreement with the previous

discussion in SEM and TEM analysis.

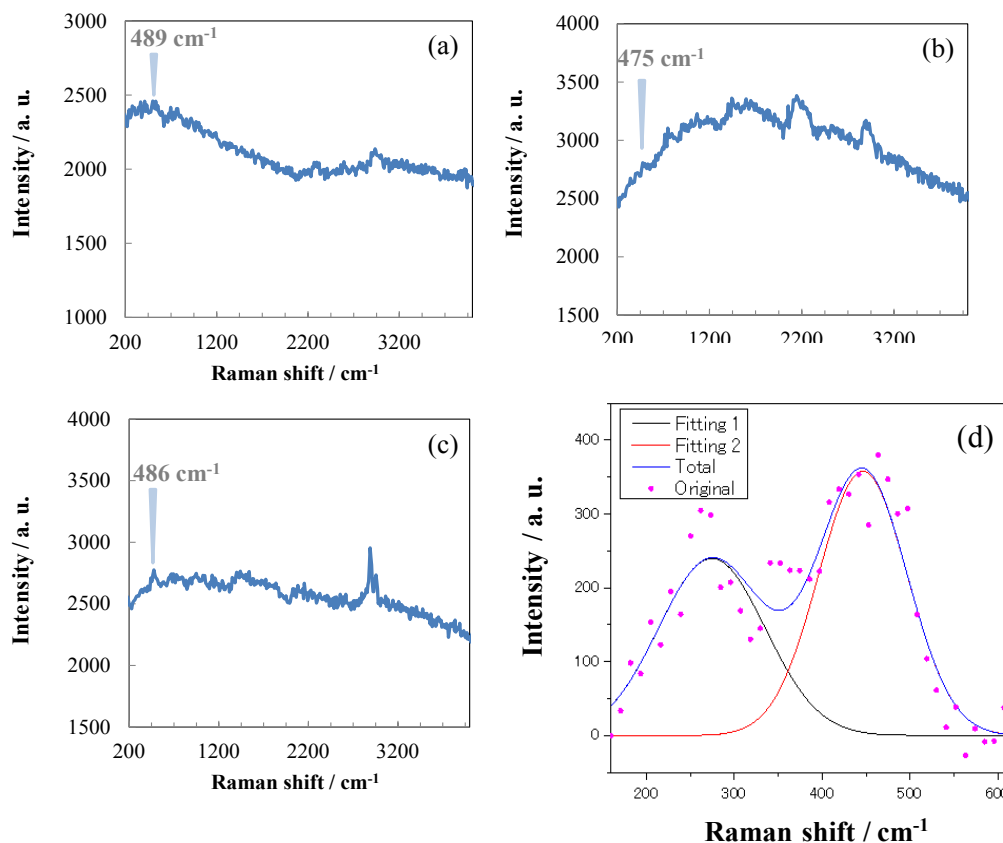


Fig. 2.9 Raman spectra, with possible weak Si peaks (wavenumbers indicated in the figures), of thin films electrodeposited at 40 °C at each potential: (a) -2.0 V vs. Pt QRE (b) -2.5 V vs. Pt QRE (c) -3.0 V vs. Pt QRE (d) analyzed result of the peak around 480 cm⁻¹

The concrete content profiles of the Si thin films electrodeposited at each potential were measured by XPS. Figure 2.10 shows the composition depth profiles of thin films produced at each potential. In these depth profiles, the Au substrate was detected only after around 4 min of Ar sputtering (Au content not shown in this figure). The profiles are divided into three regions, (1), (2), and (3), in this figure. Region (1) is close to the top surface layer, where the sputtering time is limited to 1 min, region (2) is an intermediate area with a substantially uniform concentration profile through the Si film, and region (3)

is the zone close to the Au substrate, which corresponds to 3 to 4 min of sputtering time. Region (1) is characterized by an increasing Si profile and the resulting decrease in the O and C profiles along its depth. When the electrodeposited sample is characterized, its surface is always rinsed by dimethyl carbonate, which contains oxygen atoms. Moreover, the film may be instantaneously exposed to a slightly oxidizing atmosphere when it is placed in the XPS instrument, even if a transfer vessel is employed. Thus, region (2) may represent compositions characterized primarily by the electrodeposition conditions. Table 1 demonstrates the averaged mass concentration of each element in region (2). The Si mass concentration is 57 %, 65 %, and 53 % at -2.0, -2.5, and -3.0 V vs. Pt QRE, respectively, in region (2). The concentration level of Cl is quite low compared with that of Si in the film. Thus, SiCl_4 molecules are electrochemically reduced to Si, leaving Cl^- ions in the electrolyte. Note that the C content increases and the O content decreases with the shift toward negative potential. The potential dependence of the other element is, however, not clearly observed. These data may suggest that the SiCl_4 reduction reaction partially accompanies cation decomposition.

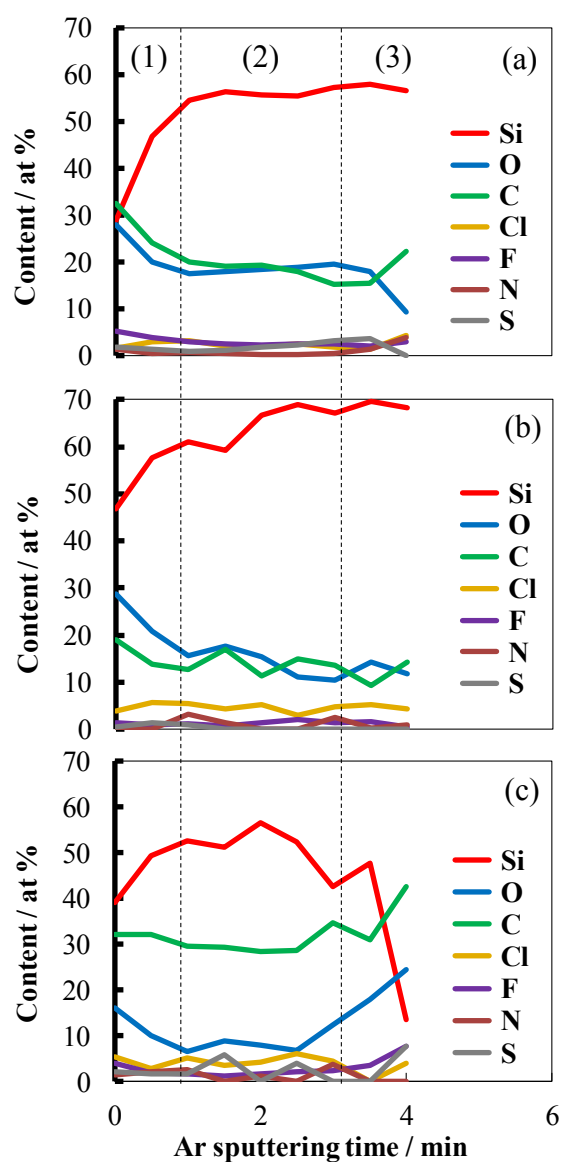


Fig. 2.10 XPS depth profiles of the Si thin films electrodeposited at 40 °C at each potential: (a) -2.0 V vs. Pt QRE, (b) -2.5 V vs. Pt QRE, and (c) -3.0 V vs. Pt QRE

Table 1 Average % of mass concentration of each element in region (2) in Fig. 2.9

	-2.0 V _{vs. Pt QRE}	-2.5 V _{vs. Pt QRE}	-3.0 V _{vs. Pt QRE}
N	1	1	1
S	2	1	2
O	18	14	7
C	17	14	31
F	3	1	2
Cl	2	4	4
Si	57	65	53

Another concern is the high content of C and O in the electrodeposited a-Si film. It is likely that even after rinsing with dimethyl carbonate, some ionic liquid remains on the surface of the deposits. In addition, for considering the ionic liquids incorporation in the films, annealing treatment could be helpful to get rid of them because the thermal decomposition of ionic liquids of TMHATFSI is nearly 380 °C. Then, the as-deposited Si film was annealed at 700 °C in the Ar gas stream. The composition of each thin film was measured by XPS depth profiling before and after annealing, as shown in Fig. 2.11. The carbon content was significantly decreased by annealing, suggesting that there are no covalent bonds between carbon and silicon. The increase in the oxygen content after annealing is due to the exposure to air in the annealing treatment during sample transfer to the annealing apparatus.

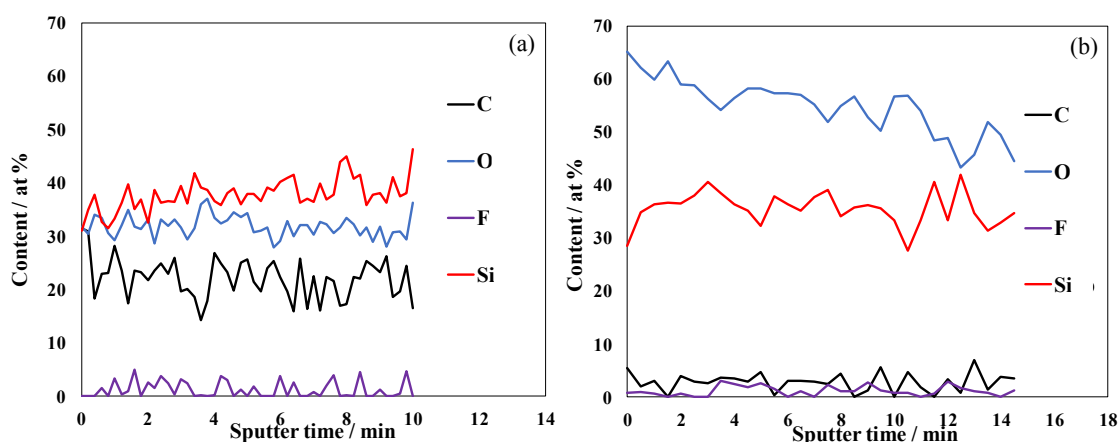


Fig. 2.11 XPS depth profiles of the thin films electrodeposited -2.5 V vs. Pt QRE (a) before and (b) after annealing (at 700 °C for 1 h)

Figure 2.11 (a) shows the frequency change measured by the EQCM during potentiostatic electrodeposition. The mass change calculated from the frequency change in Fig. 2.11 (b) is the total mass change calculated from frequency change in (a). Based on these results, the mass of Si accumulated on the substrate due to SiCl_4 reduction is obtained by multiplying the total mass changes with the Si mass concentrations obtained from the XPS depth profiles, as illustrated in Fig. 2.12 as a function of the charge density. The straight line expressing the relationship between the mass of Si and the charge density is drawn using Faraday's law assuming a four-electron transfer reaction.

$$\Delta m = \frac{M_{\text{Si}} Q}{zF} \quad (2.1)$$

where,

Δm = the mass change

M_{Si} = the molar mass of Si

Q = the charge density

z = the number of the electron

F = the Faraday constant

The measured data follow this straight line during the initial stage and start to deviate slightly above 400 mC cm^{-2} at -2.0 and $-2.5 \text{ V vs. Pt QRE}$. The agreement with Faraday's law is maintained to 150 mC cm^{-2} at $-3.0 \text{ V vs. Pt QRE}$. The deviation from this straight line may be caused by enhanced surface roughness of the Si thin films [13]. SEM images of Si thin films with rough surface morphology electrodeposited at all potentials at a charge density of 500 mC cm^{-2} actually showed those tendency.

By comparing the mass change due to SiCl_4 reduction with Faraday's law at 400 mC cm^{-2} , the current efficiency of SiCl_4 reduction was calculated to be 94.6 %, 93.4 %, and 73.2 % at -2.0 , -2.5 , and $-3.0 \text{ V vs. Pt QRE}$, respectively. Thus, Si may apparently be electrodeposited by four-electron electroreduction. The poorer efficiency is probably caused by the difficulty of converting the frequency data to the mass gain in the film with a rough surface at $-3.0 \text{ V vs. Pt QRE}$.

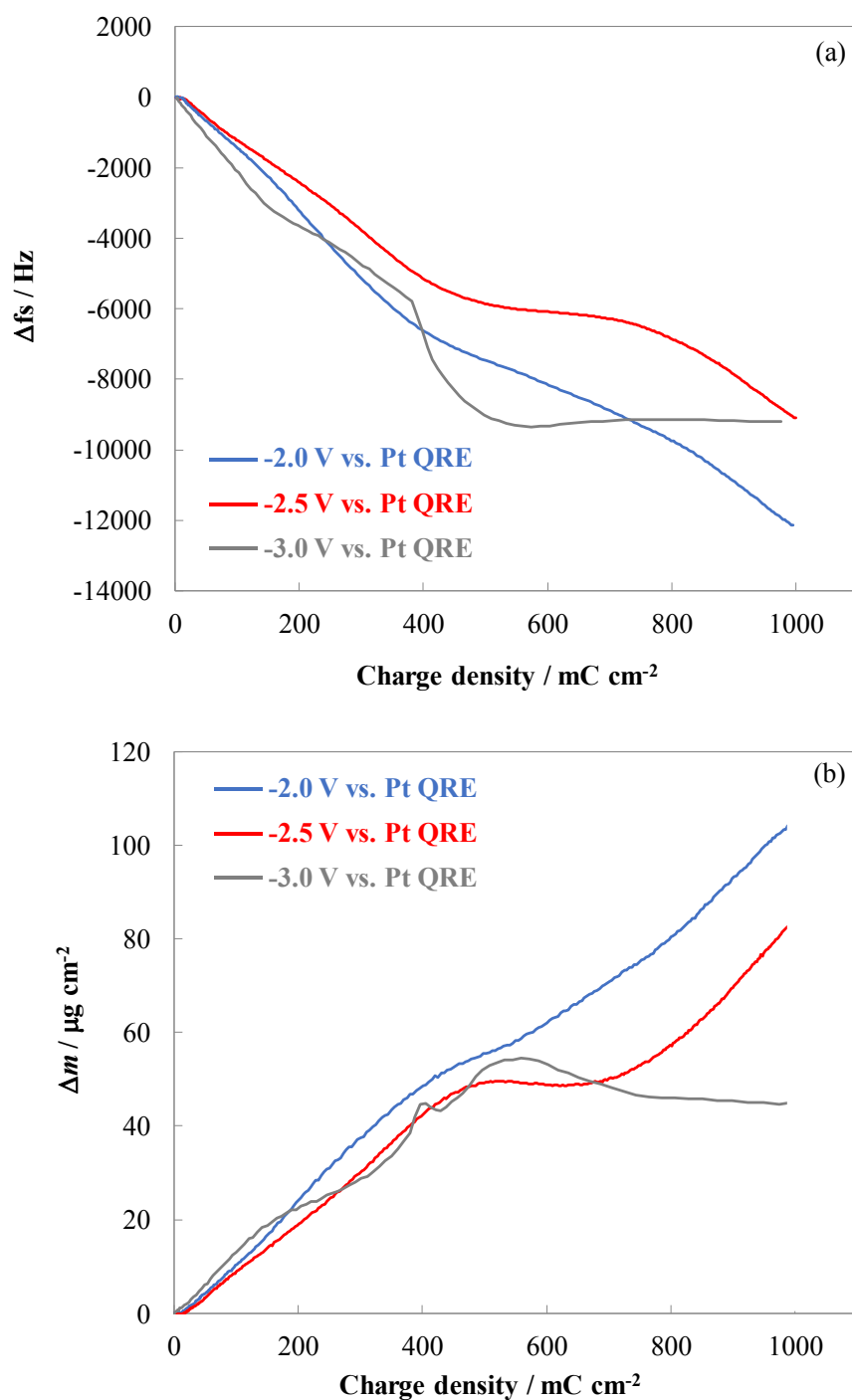


Fig. 2.12 (a) Frequency change measured by EQCM during potentiostatic electrodeposition at each potential (b) the total mass change calculated from frequency change in (a)

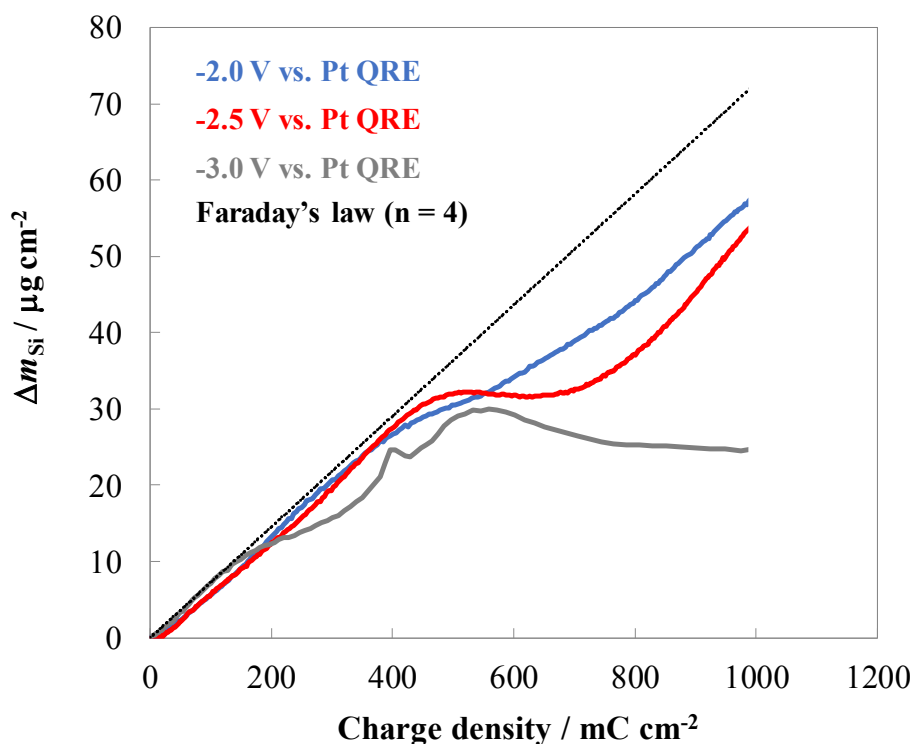


Fig. 2.13 Accumulation of mass of Si on the films estimated from average % Si determined by XPS

Here, the stage of mass changes is clarified as three regions; (i) $0 \sim 20 \text{ mC cm}^{-2}$, (ii) $20 \sim 400 \text{ mC cm}^{-2}$, (iii) $400 \text{ mC cm}^{-2} \sim$. In stage (i), there were no mass changes at -2.0 and $-2.5 \text{ V vs. Pt QRE}$, while the mass changes at $-3.0 \text{ V vs. Pt QRE}$ was proportionally increased with the increase of charge density. The enlarged figure focusing on -2.5 and $-3.0 \text{ V vs. Pt QRE}$ to see the difference clearly is shown as Fig. 2.14. It is clearly seen that there are no mass changes from 0 to 15 mC cm^{-2} at $-2.5 \text{ V vs. Pt QRE}$. Same result was observed at $-2.0 \text{ V vs. Pt QRE}$. For this, morphologies at -2.5 and $-3.0 \text{ V vs. Pt QRE}$ at approximately 10 mC cm^{-2} were shown in Fig. 2.14. More detailed discussions depending on the charge density will be described in Chapter 5.

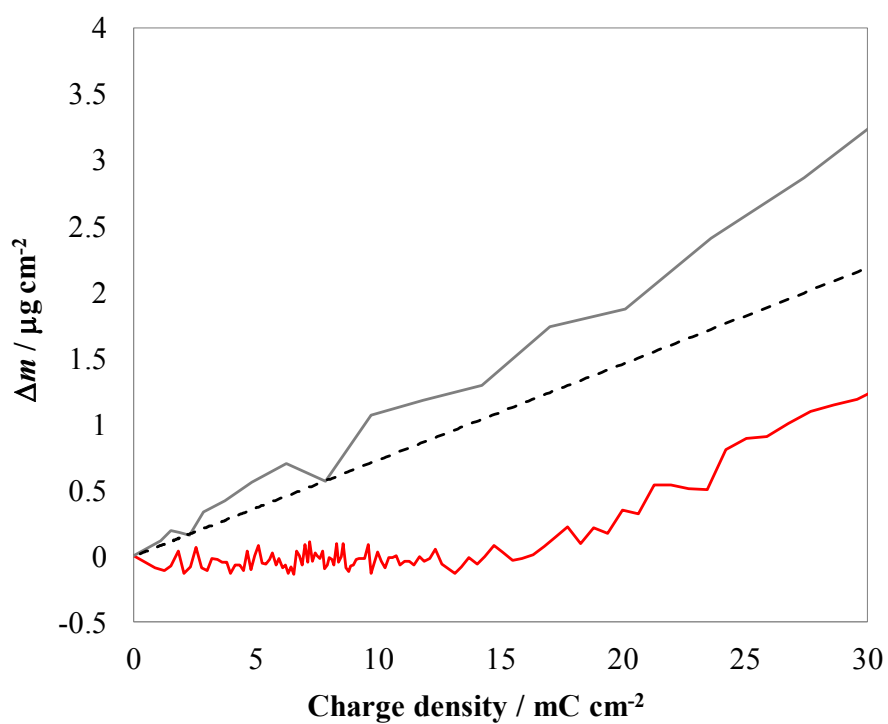


Fig. 2.14 The mass change calculated from frequency change in Fig. 2.12 (a) focusing on 0 ~ 30 mC cm⁻²

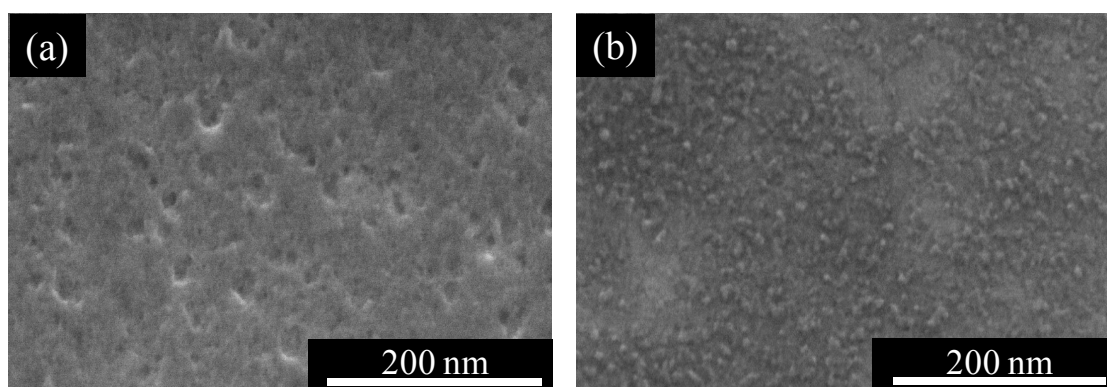


Fig. 2.15 The morphology of the films electrodeposited at (a) -3.0 and (b) -2.5 V vs. Pt QRE at charge density of 10 mC cm⁻²

As seen in Fig. 2.15, the electrodeposited Si entirely covered the surface at -3.0 V vs. Pt QRE, while the area where Si was not electrodeposited was observed at -2.5 V vs. Pt QRE. This tendency might cause the results that there were no mass changes in the very initial stage -2.5 V vs. Pt QRE. In general, in EQCM measurement using high viscous solvents, the frequency derived from viscosity was compensated as described above, and such effect seems to be large. Therefore, the frequency deriving from small amount of deposition like this structure might be buried and not be detected [14, 15]. When the influence of the viscosity was not compensated, the mass changes are shown as Fig. 2.16. It is difficult to mention whether mass changes are observed or not, however, it seems that the noise increased with the increase of the charge density, implying the mass increase. These results also suggest that the compensation of the viscous in EQCM analysis buried the information of small amount of the electrodeposited Si at the very initial stages.

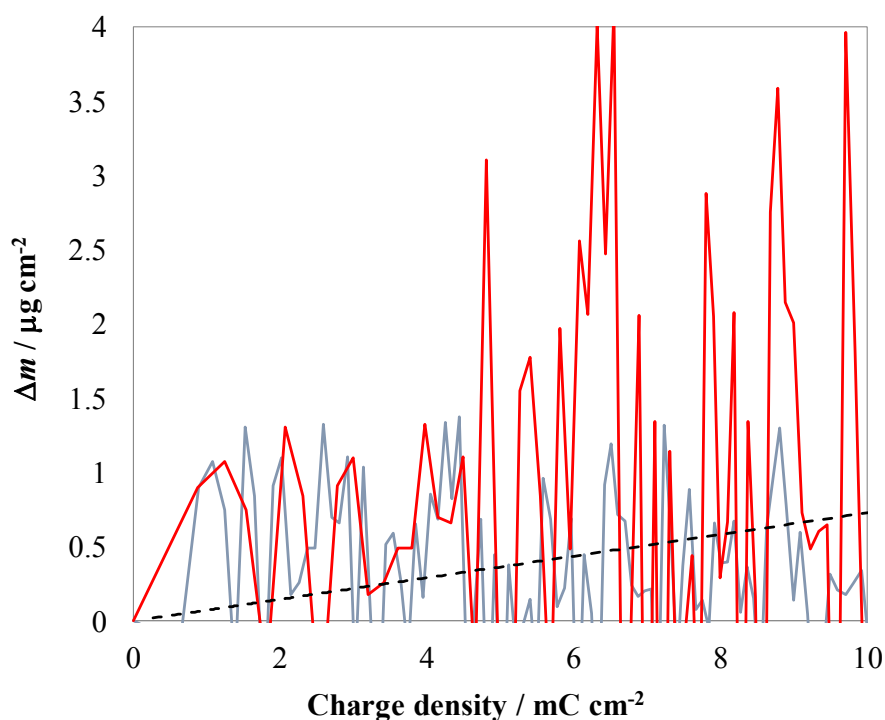


Fig. 2.16 The mass changes without the consideration of the viscosity of ionic liquids

In stage (ii), the proportional mass changes with the increase of charge density were observed at -2.0 and -2.5 V vs. Pt QRE, while there were non-proportional mass changes at -3.0 V vs. Pt QRE. This might be due to the crack formation (Fig. 2.17). In EQCM measurement, it is generally mentioned that this crack formation affects the measured frequency during the electrodeposition, in which one example is the increase of the roughness deriving from the crack. There are some researches discussing the influence of roughness on the frequency [12]. Among them, following theory is well discussed and might apply to this case. The frequency changes relating to the roughness is described as Eq. (2.2). In general, the roughness changes during the electrodeposition, therefore, it is difficult to consider the time dependence changes of the roughness to the total frequency changes. This background also causes the difficulties to consider the influence of the roughness.

$$\Delta f_{\text{roughness}} = -\frac{2\pi^2}{\lambda^3} \delta_r^2 \quad (2.2)$$

Where,

δ_r is the absolute value of the mean roughness

When the influence of the roughness is considered with this equation, $\Delta f_{\text{roughness}}$ becomes positively with the increase of the roughness, resulting in positive increase of the total change of measured frequency. In this case, the roughness was not considered, therefore, the positive increase of the frequency directly affected the Δf_{mass} . It means that mass changes indicate the negative value as shown in Fig. 2.12 and 2.13.

In stage (iii), the electrodeposited films had very rough surfaces as shown in Fig. 2.17. Those roughness also cause the error in measuring the frequency described above. Therefore, the mass changes showed the decrease tendencies.

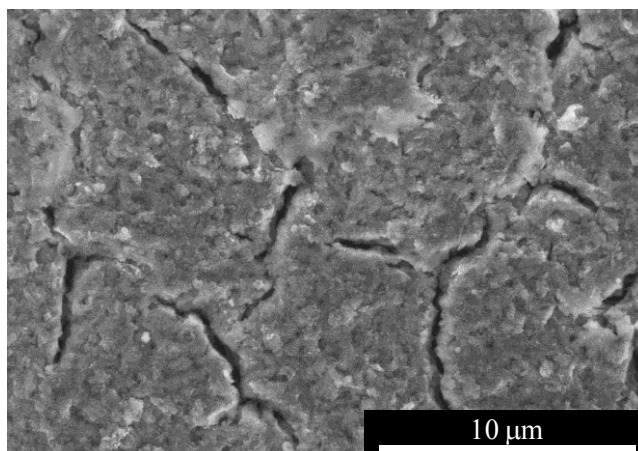


Fig. 2.17 Morphology of the film electrodeposited at -3.0 V vs. Pt QRE at 150 mC cm⁻²

Conclusions

In this chapter, to understand the overall reaction of the Si electrodeposition in the ionic liquids with SiCl_4 , the impurities incorporation mechanism and reaction mechanism was analyzed via the formation of the films electrodeposited under several conditions.

Form the analysis of the effect of the applied potential and the electrodeposition temperature, the ionic liquids are incorporated as the impurities, which was also suggested by the annealing treatment effect that mainly carbon content was dramatically decrease. The primarily amorphous Si thin films with Si–Si bonding were obtained, while impurities driving form ionic liquids incorporated to the films during the Si growth. Based on these results, it is suggested the apparent Si electrodeposition with a net four-electron reduction from SiCl_4 of $\text{SiCl}_4 + 4 e^- \rightarrow \text{Si} + 4 \text{Cl}^-$ by EQCM measurement. Especially, the current efficiency was calculated as 94.6 and 93.4 % at -2.0 and -2.5 V vs. Pt QRE, respectively at the very initial stage.

This analysis technique of the combination of EQCM and XPS, in which the total mass changes was multiplied with the mass concentrations of the films obtained from the XPS depth profiles in order to analyze the accumulated amount on the substrate relating to the precursor's reduction.

References

- [1] S. Z. E. Abedin, N. Borrisenko, and F. Endres, *Electrochem. Comm.*, **6**, 510 (2004).
- [2] N. Borisenko, S. Z. E. Abedin, and F. Endres, *J. Phys. Chem. B*, **110**, 6250 (2006).
- [3] Y. Nishimura and Y. Fukunaka, *Electrochim. Acta*, **53**, 111 (2007).
- [4] R. Al-Salman, S. Z. E. Abedin, and F. Endres, *Phys. Chem. Chem. Phys.*, **10**, 4650 (2008).
- [5] R. Al-Salman, X. Meng, J. Zhao, Y. Li, U. Kynast, M. M. Lezhnina, and F. Endres, *Pure Appl. Chem.*, **82**, 1673 (2010).
- [6] A.M. Martinez, K.S. Osen, O.E. Kongstein, E. Sheridan, A. Ulyashin, and G.M. Haarberg, *ESC Trans.*, **25**, 107 (2010).
- [7] J. Mallet, M. Molinari, F. Martineau, F. Delavoie, P. Fricoteaux, and M. Troyon, *Nano Lett.*, **8**, 3468 (2010).
- [8] T. Homma, J. Komadina, Y. Nakano, T. Ouchi, T. Akiyoshi, Y. Ishibashi, Y. Nishimura, T. Nishida, and Y. Fukunaka, *ECS Trans.*, **41**,9 (2012).
- [9] J. Park, C.K. Lee, K. Kwon, and H. Kim, *Int. J. Electrochem. Sci.*, **8**, 4206 (2013).
- [10] J. Komadina, T. Akiyoshi, Y. Ishibashi, Y. Fukunaka, and T. Homma, *Electrochim. Acta*, **100**, 236 (2013).
- [11] G. Pulletikurthi, A. Lahiri, T. Carstens, N. Borisenko, S. Z. E. Abedin, and F. Endres, *J. Solid State Electrochem.*, **17**, 2823 (2013).
- [12] S. Ivanov, C. Vlaic, A. Bund, and I. Efimov, *Electrochim. Acta*, **219**, 251 (2016).
- [13] L. Daikhin, E. Gileadi, G. Katz, V. Tsionsky, M. Uriah, D. Zagidulin *Anal. Chem.*, **74**, 554 (2002).
- [14] A. Bund, H. Chmiel, and G. Schwitgenbel, *Phys. Chem. Chem. Phys.*, **1**, 3933 (1999).
- [15] A. R. Hillman, I. Efimov, and K. S. Ryder, *J. AM. CHEM. SOC.*, **127**, 16611 (2005).

Chapter 3:

***Analysis of Cathodic Reaction Process of SiCl₄ in
Ionic Liquids***

3.1 Introduction

To provide details on the reaction of SiCl_4 on the substrate surface, it is important to understand the mechanism for how these reactions proceed or what kind of intermediate are produced by focusing on the molecular level behavior at the solid-liquid interface.

In this chapter, these detailed interfacial reaction mechanisms starting with the elementary steps of the SiCl_4 reduction process in Si electrodeposition with ionic liquids as the solvent are discussed. Here, several precise interfacial analyses are used. The electrochemical quartz crystal microbalance (EQCM) measurement is continuously one of techniques, which proves to be applicable for such interfacial analyses of Si deposition for detecting the formation of intermediates if the effects from solvent viscosity on measurement results were taken into account precisely as discussed in the previous chapter. X-ray reflectivity (XRR) has been used as a selective probe of the interface and has allowed us to suggest a detailed molecular level deposition mechanism including the presence of intermediate states [1-3]. Density functional theory (DFT) calculation is also performed to investigate the theoretical aspects. The ability of DFT to provide a molecular level understanding of several solid-liquid interfacial reaction system behaviors in aqueous solution has been shown [4-6], so that this theoretical calculation was selected to use.

3.2 Experimental

In all experimental measurements, trimethyl-n-hexylammonium bis(trifluoromethylsulfonyl) imide (TMHATFSI) containing less than 10 ppm H₂O was used as the ionic liquid with 0.5 M SiCl₄ (99.98% purity) (Stella Chemifa).

In EQCM measurement, A 6 MHz AT-cut quartz crystal with Au contacts was used as the working electrode with a surface area of 1.32 cm² (Hokuto Denko). A Pt wire was used as the counter electrode. Here, a Ag/Ag⁺ reference electrode would enable to follow the detailed reduction processes in these reactions including the number of reduction processes undergone by the SiCl₄ as well as the possible formation of intermediate states, and then this reference electrode was determined to use. In this application of the Ag/Ag⁺ reference electrode, an Ag wire is immersed into TMHATFSI dissolved 0.05 M AgTFSI (Aldorich) and the reference electrode is separated from the electrolyte of 0.5 M SiCl₄/TMHATFSI by a vycor glass with porous tip. The electrochemical cell for the EQCM measurement was mounted in an aluminum block, and the electrolyte temperature was maintained at 40 °C using an Al thermo-block (NISSIN, COOL/HEAT BLOCK NDC-100) in an Ar-filled glove box. Frequency was measured by a frequency analyzer (Agilent Technologies Frequency Analyzer, E5061A) during cyclic voltammetry (CV). The CV measurement was performed using the potentiostat/galvanostat (Hokuto Denko, HZ-7000). The detailed technique used in our EQCM analysis has been shown in previous chapter.

In XRR measurement, the samples for XRR were fabricated by spinning the ionic liquid with 0.5 M SiCl₄ on a flat Au covered surface that served as the working electrode for the electrochemical deposition. The counter electrode was also a Au film with a 1 mm separation from the working electrode. The Au (100 nm) film was formed on glass substrate with a Cr adhesion layer (10 nm) both deposited by electron beam evaporation (ULVAC, EBX-6D). The ionic liquids were coated as thinly as possible on the Au substrate by spinning at 3000 rpm in order to minimize the absorption of the X-ray intensity during the reflectivity measurements. XRR was performed on beamline 2-1 at the Stanford Synchrotron Radiation Lightsource at an energy of 11.5 keV and measured

with a Pilatus 100k area detector. The substrate temperature was maintained at 30 °C in a controlled Ar or N₂ atmosphere via a thin-film heater. The XRR measurement data were analyzed by GenX software [7].

All calculations were performed by DFT with Gaussian 09 [8]. The exchange-correlation function was B3LYP, the basis set for H and Cl was 6-31+G** [9, 10], and the basis set for Si was LANL 2DZ dp ECP [11]. To model ionic liquids as surrounding reactants, the ONIOM method was applied; the main reactant was expressed by quantum mechanics (QM), and solvent molecules were expressed by molecular mechanics (MM) with universal force field (UFF) parameters [12]. Since ionic liquids generally exhibit complicated behaviors in their dielectric constant, a polarized continuum model (PCM) [13] that usually provides a sufficiently appropriate solvent model in the case of aqueous system is not capable of working well in this situation. The procedure for the DFT calculation was as follows: first, the solvent molecules were periodically located around the QM region. After that, the structural optimization of the prepared model was carried out by a mechanical embedding process in which the QM and MM regions are optimized independently. Finally, the optimized structures were obtained by an electronic embedding process, in which the electrostatic interaction between the QM and MM regions is taken into consideration. Figure 1 shows the structural optimization process used in this study. First, the MM part solvents sphere with vacancy for reactant is prepared (Fig. 1 (a)). The QM part reactant is placed into the vacancy to build the initial geometry (Fig. 1 (b)). Geometrical optimization is performed in two steps in order to more easily reach convergence: (1) the QM part is roughly optimized without considering the force field of the MM part, which is called mechanical embedding, ME (Fig. 1 (c)), and (2) it is optimized with the force field of MM part, and called electrical embedding, EE (Fig. 1 (d)). Figure 2 also shows the examples of equilibrium structure obtained from the optimization.

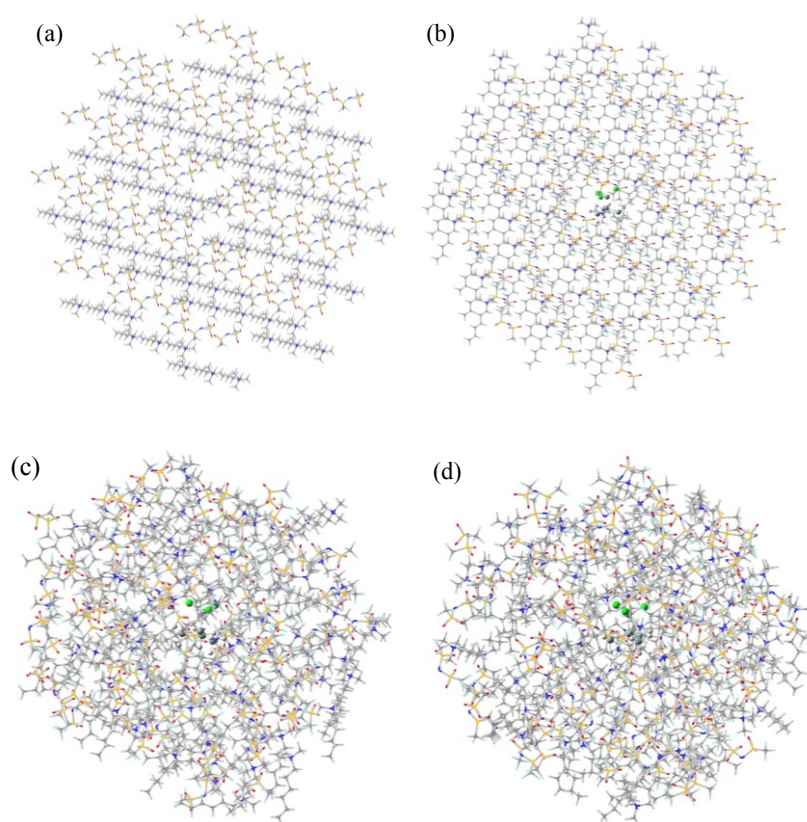


Fig. 3.1 Schematic image of the structural optimization process
(a) after adding solvent molecules, (b) after placing the QM part with the addition of reactants, (c) after ME optimization, and (d) after EE optimization

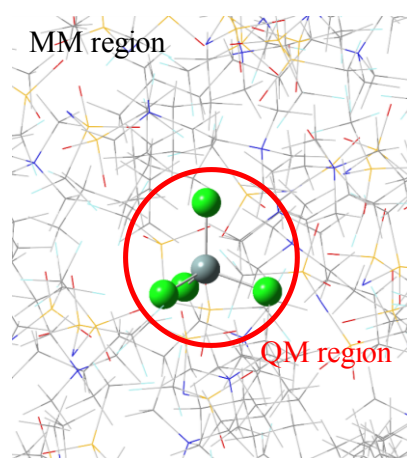


Fig. 3.2 Example of the equilibrium structure obtained from the QM/MM optimization

3.3 Results and Discussion

3.3.1 Analysis of reduction steps during the electrodeposition

To understand the electrochemical behavior of SiCl_4 in TMHATFSI in detail, the electrochemical measurement with Ag/Ag^+ was newly conducted. Figure 3.3 shows the current transient and mass change from the open circuit potential to -2.7 V. This CV measurement identified several reduction peaks: -1.0 , -1.7 , and -2.2 V. There were no mass changes taking place at either the -1.0 or -1.7 V reduction steps, indicating that these two steps corresponded to just reductions of the electroactive species, not deposition. However, mass changes accompanied the reduction peak at -2.2 V in the CV measurement. This was believed to derive from the deposition of Si because the evaluation by X-ray photoelectron spectroscopy showed the existence of Si. This behavior had been also corresponded to the results in the previous chapter. These electrochemical measurements suggest that this Si electrodeposition involves several elementary steps with stable intermediates before the deposition; before reaching -2.2 V, electroactive species, such as SiCl_4 in our case, receive electrons to form some intermediate. Considering the fact that these steps were not observed in the blank ionic liquids as shown in Fig. 3.4, they should derive from SiCl_4 , and they might be oxidized during the anodic CV scan. This mechanism is also demonstrated by S. Ivanov et al. [14]. They electrodeposited Si from 1-butyl-1-methylpyrrolidinium bis(trifluoromethylsulfonyl)imide ([BMP][TFSI]) in the presence of SiCl_4 on copper sputtered quartz piezoelectric resonators. Their EQCM during linear sweep voltammetry identified some reduction peaks before the deposition peak with mass change, which was around -1.87 V vs. Pt QRE. They also attributed these peaks to the adsorption and reduction of electroactive species from electrolyte.

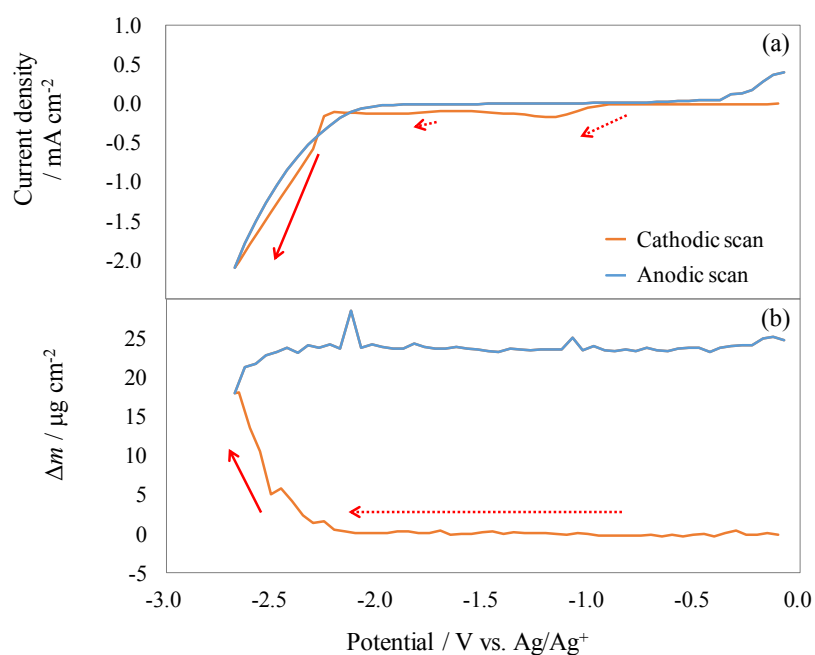


Fig. 3.3 (a) Cyclic voltammogram, scan rate = 10 mVs^{-1} , (b) Mass changes during cyclic voltammetry in 0.5 M SiCl₄/TMHATFSI

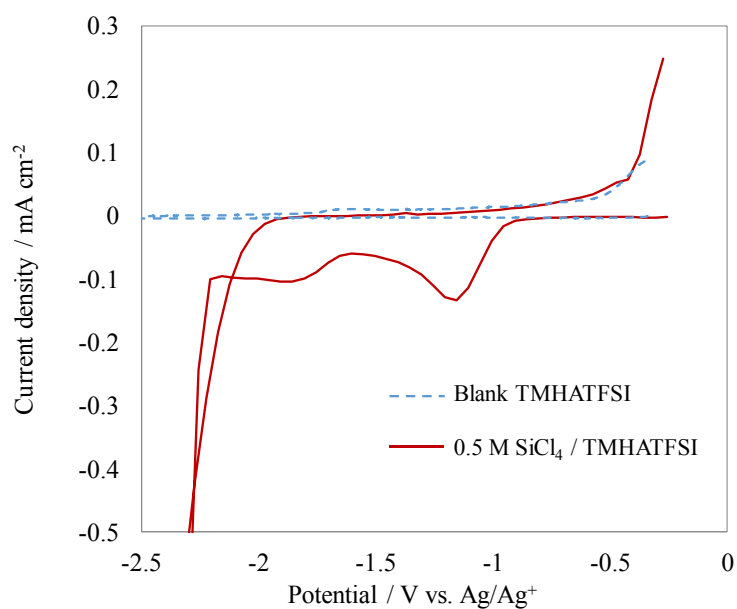


Fig. 3.4 Cyclic voltammogram in TMHATFSI with or without the addition of SiCl₄, scan rate = 10 mVs^{-1}

3.3.2 Analysis of the intermediate state during the electrodeposition

To identify the intermediate species of the deposition reaction, XRR measurement was carried out for the electrode surface during the Si deposition. Fig. 3.5 shows the reflectivity in each case: before applying potential (ionic liquids are adsorbed on Au substrate described as "Au substrate only", black dots), after applying 0 V ("0 V", red dots), and after applying -4 V for each time ("-4 V each time", green and blue dots). In this XRR measurement, the two electrode system described above was used, whereas three electrodes were used in the EQCM measurement described above. The potential of 0 V in XRR corresponds to the potential before -2.2 V vs. Ag/Ag⁺ in EQCM, which is the first cathodic peak implying the formation of an intermediate, because the cathodic current density was observed at 0 V in XRR. As for the current value at each potential, it was also shown such correspondence that -0.001 mA was measured at both 0 V in XRR and -1.7 V vs. Ag/Ag⁺. -4 V in XRR corresponds to the potential after -2.2 V vs. Ag/Ag⁺ in EQCM, which is the second larger cathodic peak attributed to Si deposition. Current values measured at each potential also showed such correspondence that -0.01 mA was measured at both -4 V in XRR and -2.3 V vs. Ag/Ag⁺. This correspondence can be seen in Fig. 3.6.

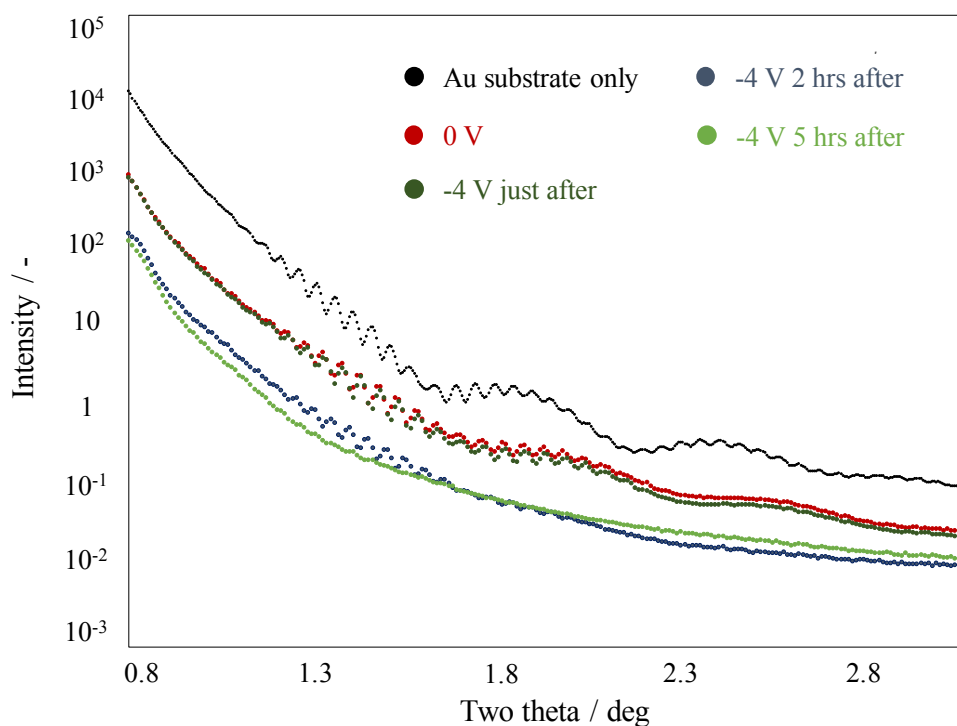


Fig. 3.5 Reflectivity changes during Si electrodeposition at each condition in TMHATFSI with 0.5 M SiCl_4 at 30 °C (Black dots show the reflectivity of only the Au substrate coated by TMHATFSI with 0.5 M SiCl_4 , red, green, blue and light blue dots show the reflectivity after applying 0 V and -4 V for each time, respectively.)

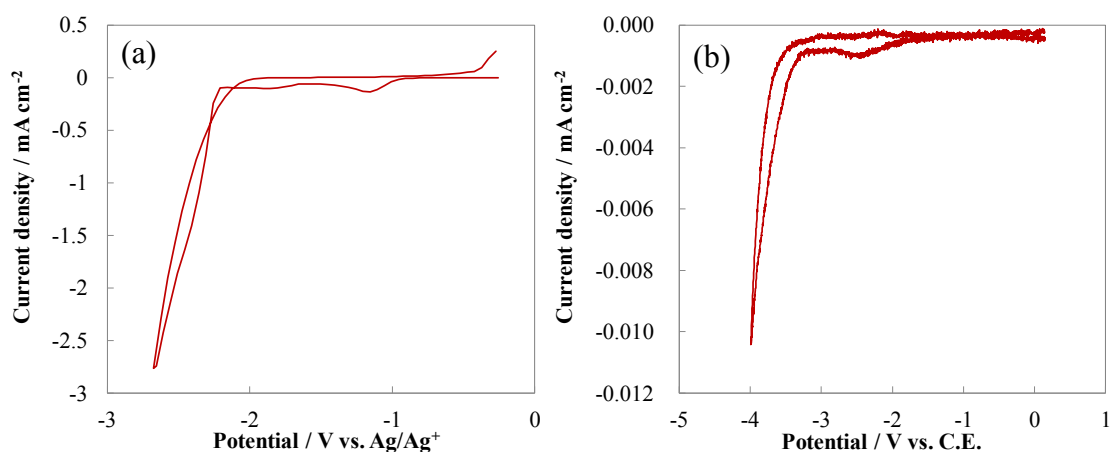


Fig. 3.6 Correspondence of the potential between three electrode system (a) and two electrode system (b)

The black dots demonstrate the structure of the fringes indicating that the surface of the Au electrode adsorbed ionic liquids. In XRR, these fringes reflect mainly the roughness and density of the layer at the surface. This characteristic shape will be changed when some layers form on the surface of electrode. As shown by the red dots, the reflectivity of the substrate after applying 0 V clearly changed compared with black dots, suggesting that some layers are newly formed at this potential. This suggests basically two possibilities: a change in the accumulation of adsorbed ionic liquid molecules at the interface or the formation of some layers on the surface. The XRR measurement in this study should detect interfacial changes thickness is larger than Au substrate's roughness, 1.1~1.4 nm in this case. Since the thickness of the accumulation layer of the ionic liquid molecules adsorbed at the interface of the electrode is less than the substrate's roughness, it can be concluded that a new layer has formed after the application of 0 V. The accuracy of the curve fitting analysis using GenX is shown as Fig. 3.7. The thickness of the prepared Au substrate (Au: 100nm, Cr: 10 nm) was correctly same with the GenX analysis, in which the thickness of Au was assumed as 103 ~ 104 nm and that of Cr was assumed as 10 ~ 11 nm. The roughness of the prepared Au substrate (1.3 ~ 1.7 nm, measured by AFM) also corresponds to the analyzed results by GenX (1.1 ~ 1.4 nm).

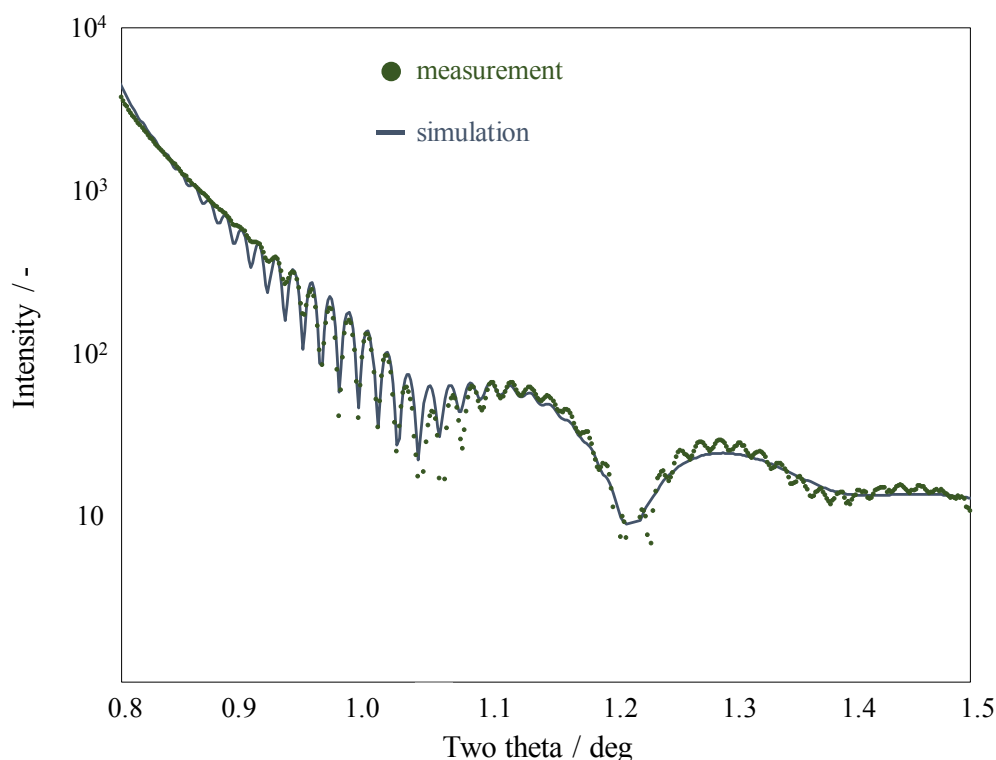


Fig. 3.7 Reflectivity change of Au substrate (Green dots show the measured result, blue lines are simulated result.)

It is assumed that this layer derives from decomposition of the ionic liquids (carbon products) or the result of reduction of the SiCl_4 (i.e., an intermediate). However, based on the correspondence to the potential as discussed above, decomposition of ionic liquids should be hard to occur at 0 V. This is also supported by the curve fitting analysis of the XRR. The shape of the XRR could not be explained by the existence of such a thin layer composed mainly of carbon derived from the decomposition of the ionic liquids. The fact that critical angle changes so little also supports this viewpoint. Only when a layer including Si_2Cl_6 as a part of a reduced species of SiCl_4 was assumed to be at the surface, the measured reflectivity curve could be explained well. By evaluating that how the curves of considered layer model fit the experimental data, the interpretation of the XRR data can be assessed. This suggests that Si_2Cl_6 forms as an intermediate state during the reduction of SiCl_4 , which corresponds to the EQCM results (Fig. 3.8). All these data

suggest that SiCl_4 reduces to Si_2Cl_6 before Si deposition. Therefore, this can be used to demonstrate a layer-by-layer structure involving the ionic liquid (IL), Si_2Cl_6 , and Au substrate (Fig. 3.8 (b)).

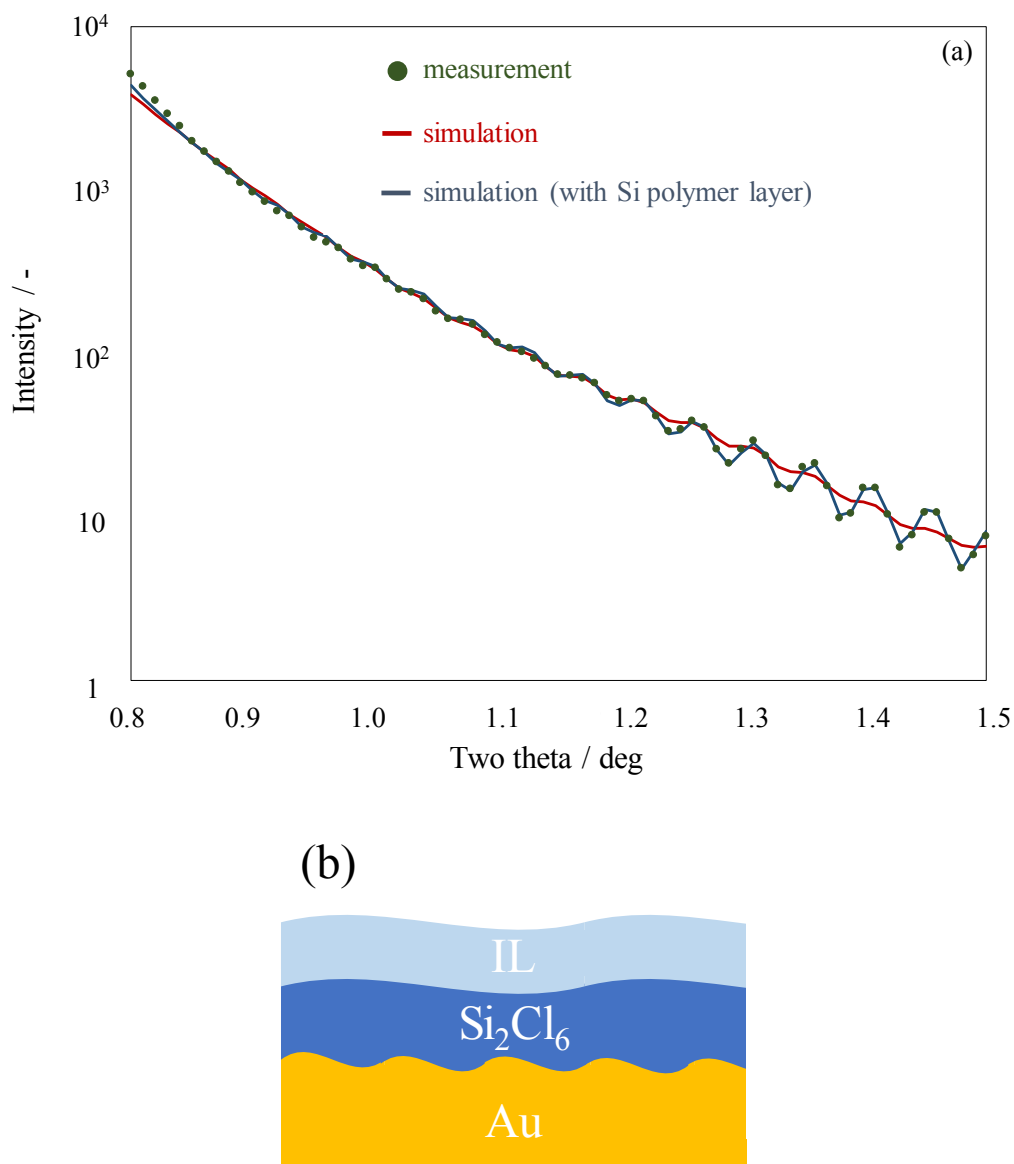


Fig. 3.8 (a) Reflectivity change after electrodeposition at 0 V in TMHATFSI with 0.5 M SiCl_4 at 30 °C (Green dots show the measured result, red and blue lines are simulated results. The different between red and blue lines is with/without assuming a formation of Si polymer layer.), (b) Layer model electrodeposited at 0 V

Similar results have been reported from research on organic electrolytic synthesis [15-17]. The CV studies of X. Wang et al. [17] on the electroreduction scheme of organo-substituted dichlorosilanes in tetrahydrofuran revealed that $RR'SiCl_2$ species reduced to $R_2R'_2Si_2Cl_2$ by radical coupling or nucleophilic substitution. When $RR'SiCl_2$ receives electrons from the electrode, an anion radical of $RR'SiCl_2$ is formed, followed by more electrons being received to form dianionic of $RR'SiCl_2$. These anion radicals and dianionic components release Cl species to react with other neighboring species, resulting in the formation of $R_2R'_2Si_2Cl_2$ (Fig. 3.9).

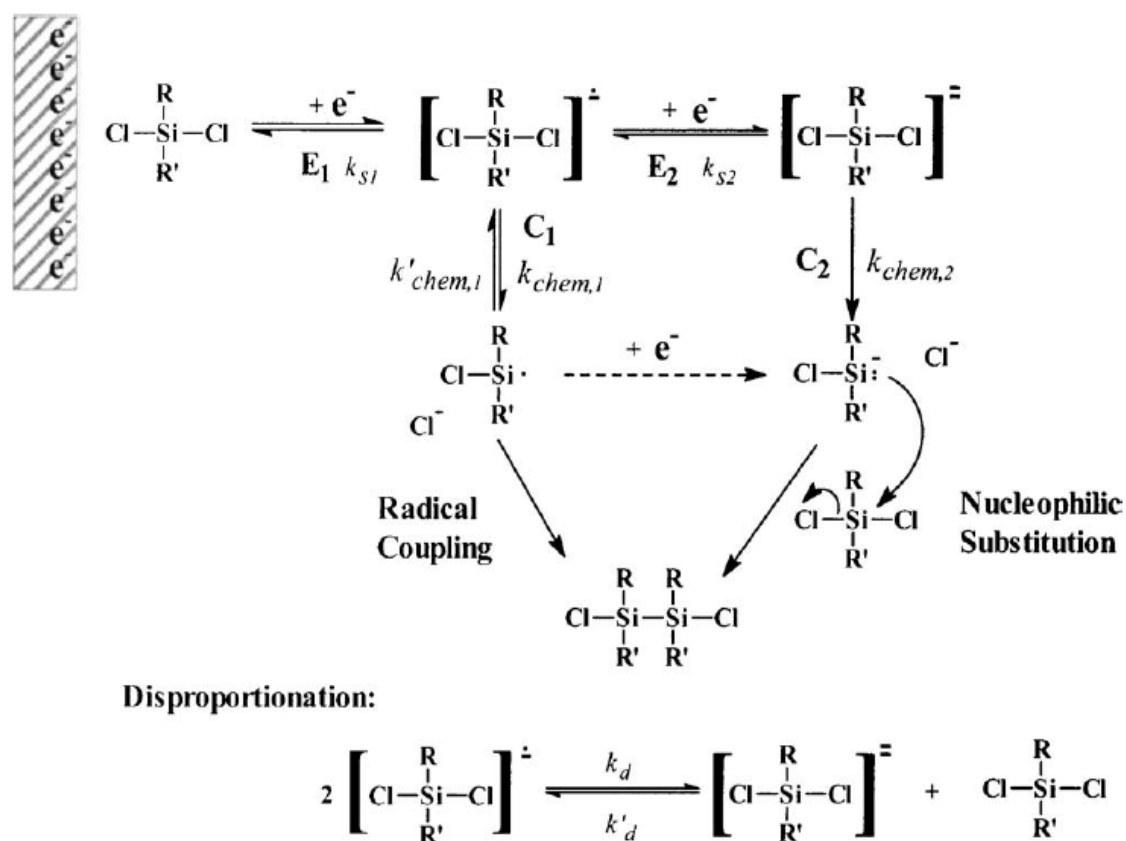


Fig. 3.9 The proposed reduction mechanism of dichlorosilanes [17] (Copyright 2005 by J. Electrochem. Soc. Reproduced with permission of J. Electrochem. Soc. by Copyright Clearance Center's RightsLink® service)

The reflectivity in the case just after when -4 V was applied, did not significantly changed from the red dots (at 0 V, in which a polymer-like intermediate state was formed), suggesting that a polymer-like intermediate state remained just after applying the negative potential even though that potential reached to the formation of Si (Fig. 3.10).

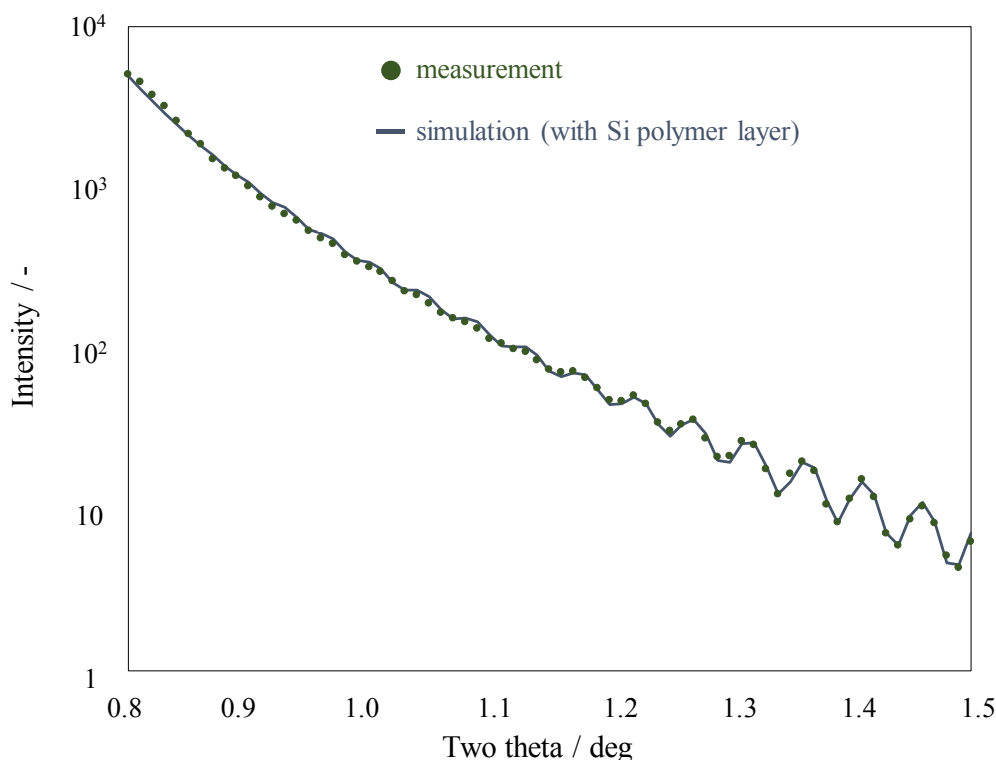


Fig. 3.10 Reflectivity change of the electrodeposited Si film just after applying -4 V in TMHATFSI with 0.5 M SiCl₄ at 30 °C (Green dots show the measured result, blue line is simulated results.)

The reflectivity in the case when -4 V was applied for 2hr described as blue dots in Fig. 3.5, changed dramatically from the original black dots (where ionic liquids were adsorbed on Au substrate) and the red dots (at 0 V, in which a polymer-like intermediate state was formed). In particular, the curve at the low angle of ~0.8 deg., which should reflect the optical state of the topmost surface, changed from a monotonically decreasing shape to a convex shape. As the topmost surface solidifies, the reflectivity generally

increases in that region due to its higher density, thus suppressing the damping of the reflectivity at low angles, which then results in the convex shape of the reflectivity curve. This implies that the polymer-like intermediate state is solidified by the application of -4 V. Fringes at angles higher than 1.3 deg. are reduced, when compared with the red dots, also implying the formation of a new solid layer on the electrode surface as described above. Therefore, it is suggested that applying -4 V deposits Si in the solid state from the polymer-like intermediates. It also appears that the formation of the Si_2Cl_6 species is a reasonable way to explain the measured reflectivity changes shown in Fig. 3.11 (a): the red line represents the case without the assumption of a Si_2Cl_6 deposit on the Si, while blue line includes the Si_2Cl_6 . In the curve without Si_2Cl_6 (red), the experimental result cannot be explained well, whereas the curve with Si_2Cl_6 (blue) is able to describe the experimental results quite well, especially the fringes from 1.0 to 1.3 deg. (Fig. 3.12). These results suggest that Si_2Cl_6 is also formed on the deposited Si thin film at -4 V. Therefore, a layer containing Si_2Cl_6 is considered to be continuously formed during the Si deposition step as described in Fig. 3.11 (b). This Si_2Cl_6 formation pathway is considered as the reaction pathway of polymer intermediate state formation. In this Si_2Cl_6 formation reaction, the following process should be possible: a SiCl_4 molecule is reduced with the release of a Cl^- ion, followed by the reaction between the residual SiCl_3 and another nearby SiCl_4 to produce the intermediate Si_2Cl_6 . It should be noted that Si_2Cl_6 could not be the final product after the electron transfer, which should continuously receive electrons to react with another nearby SiCl_4 and then form a polymer-like structure. No mass changes during the intermediate reaction stage in EQCM implies non-solid layer formation in this stage, supporting this hypothesis. Analysis of the XRR results, which assume Si_3Cl_8 and $\text{Si}_4\text{Cl}_{10}$ as intermediates, successfully reproduced the experimental curve, also suggests that a layer formed after the reduction of SiCl_4 is a polymer-like structure.

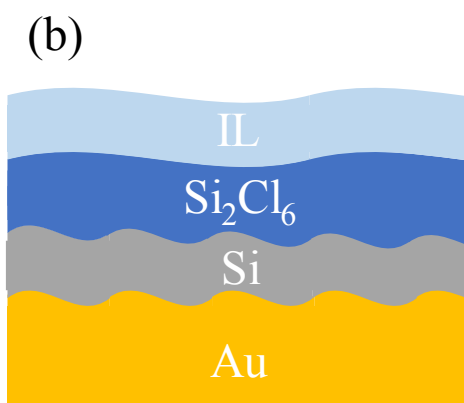
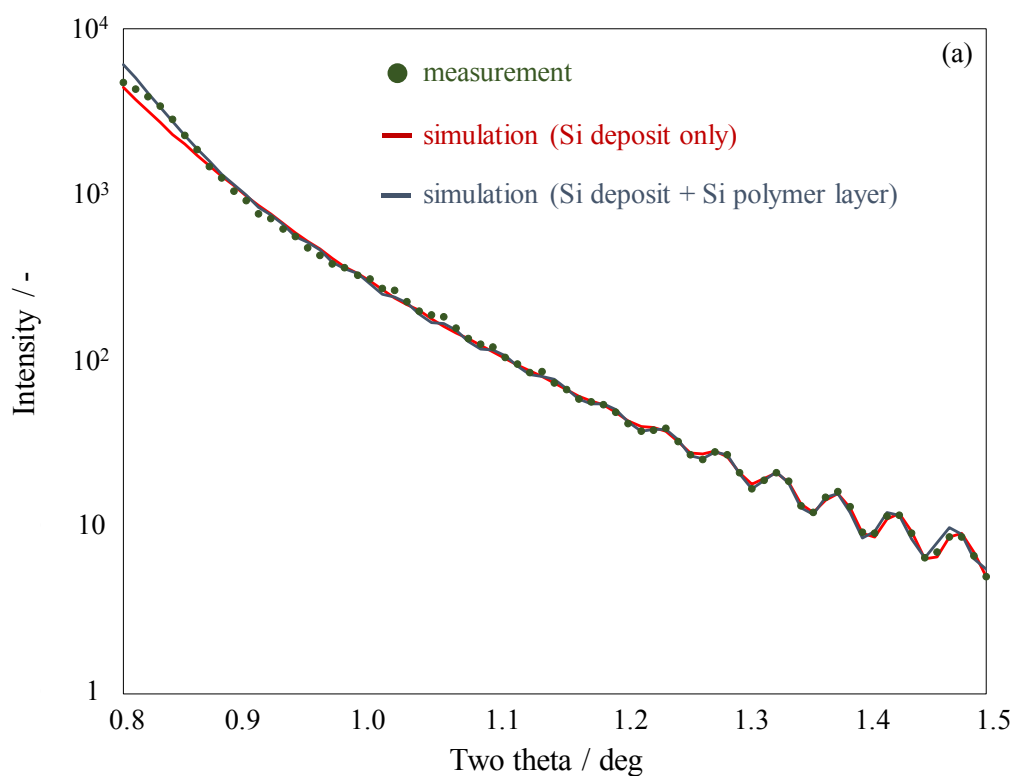


Fig. 3.11 (a) Reflectivity change of the Si film electrodeposited at -4 V for 2 hrs in TMHATFSI with 0.5 M SiCl_4 at 30 °C (Green dots show the measured result, red line and blue line are simulated results. The different between red line and blue line results is with/without assuming a formation of Si polymer layer on Si deposit.), (b) Layer model electrodeposited at -4 V for 2 hrs

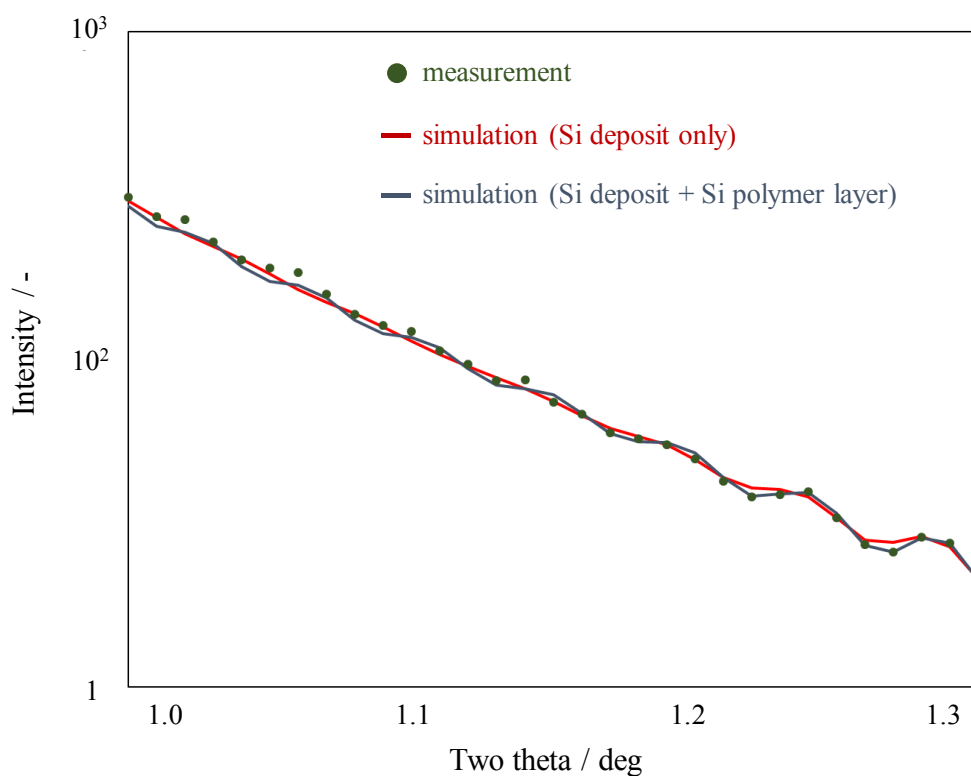


Fig. 3.12 Enlarged reflectivity changes between 1.0 and 1.3 deg of Fig. 3.11.

The reflectivity in the case when -4 V was applied for 5 hrs was a little bit different from the results with after applying -4 V for 2 hrs, especially focusing on the observed fringes. This is because the thickness is considered to be increased with the increase of the electrodeposition time, which might interfere to observe the information driving from the substrate. The analysis by GenX definitely showed the tendency of the thickness changes relating to the Si thin films from 1.8 ~ 1.9 nm (after 2 hrs) to 4.8 ~ 5.3 nm (after 5 hrs). These differences were observed, whereas it is considered to have the same layer model after applying -4 V for 2 hrs (Fig. 3.13).

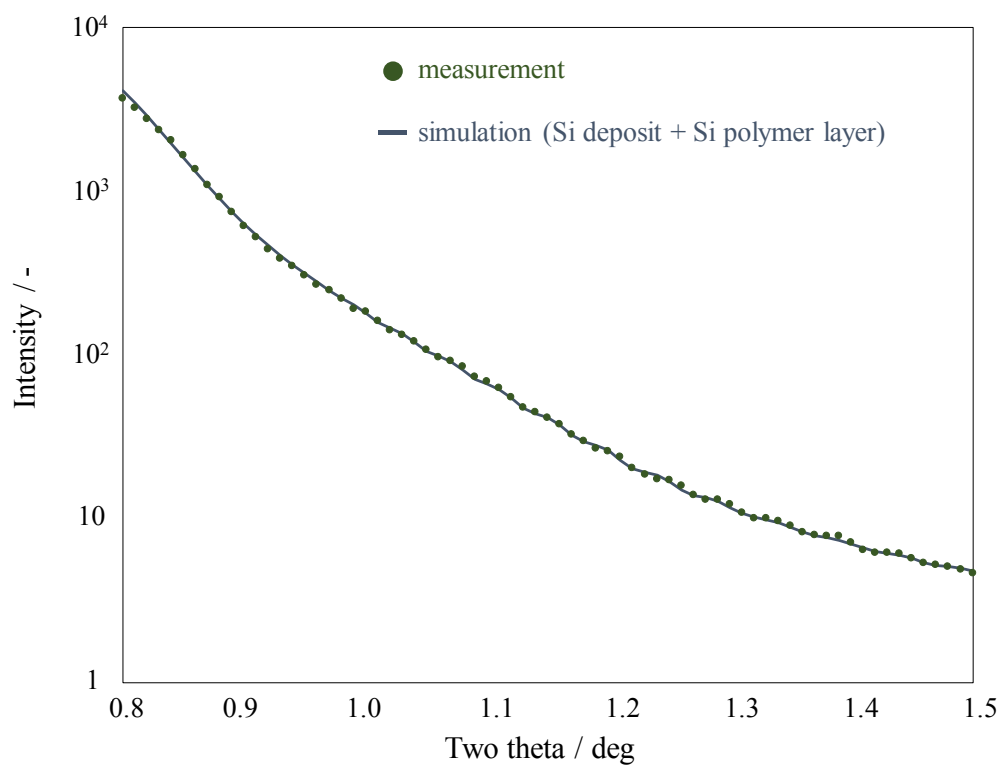


Fig. 3.13 Reflectivity change of the Si film electrodeposited at -4 V for 2 hrs in TMHATFSI with 0.5 M SiCl₄ at 30 °C (Green dots show the measured result, blue line is simulated results.)

3.3.3 Analysis of the pathway of the intermediate state formation

To examine the possibility of the Si_2Cl_6 formation scheme described above, stability of the Si-Si bond of this product is theoretically analyzed. The pathway in forming the intermediate state can be investigated by the experiment. However, as described later, the formed specie, especially anion, will be same in each considerable pathway, implying the experiment might not be suitable to decide the concrete pathway in this case. Therefore, this theoretical analysis was conducted here. For this, we compared two different types of Si-Si bonds as follows; (i) Si-Si formation between two SiCl_4 molecules which are located close to each other to form Si_2Cl_6 (“scheme 1”) and (ii) Si-Si formation between the SiCl_4 molecule and Si surface, which is referred as direct deposition (“scheme 2”). In the scheme 1, there are possibilities to occur via three types of intermediate formation reaction; SiCl_3 anion intermediate formation, SiCl_3 radical intermediate formation, and SiCl_3 anion intermediate formation with the formation of Cl_2 (Fig. 3.14). To estimate which is the more favorable pathway, energy profiles of scheme 1 from DFT calculations were compared (Fig. 3.15).

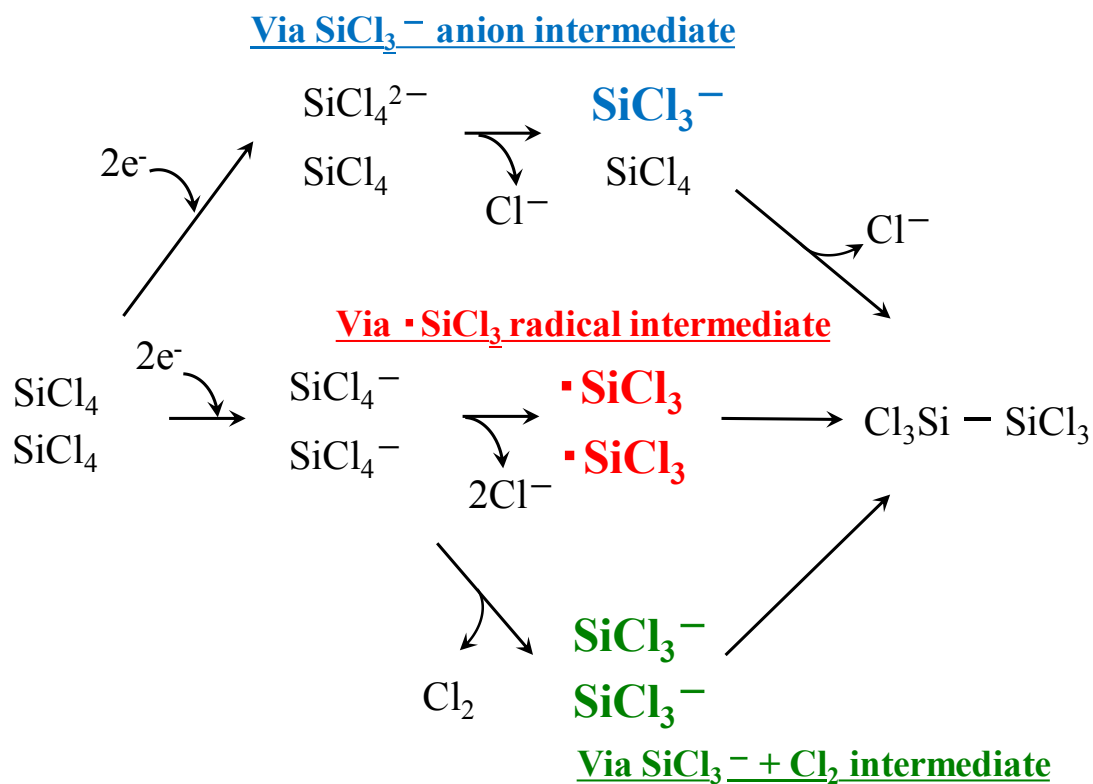
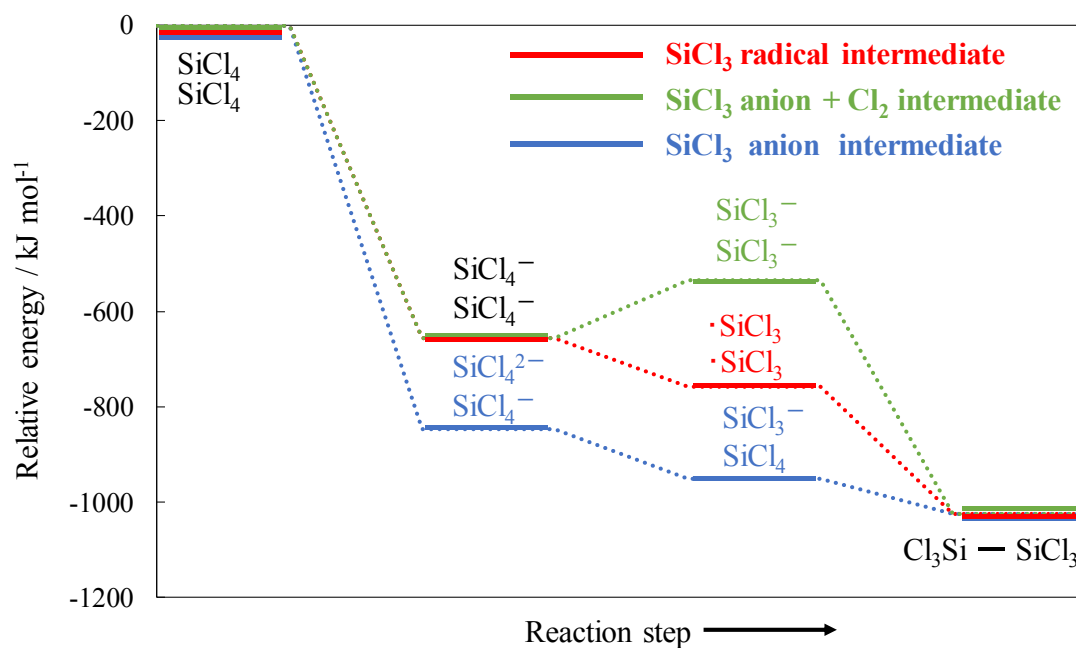
Fig. 3.14 Three types of the reaction pathway to form Si_2Cl_6 

Fig. 3.15 Energy profiles of each reaction of Fig. 3.14

This energy profiles shows that the reaction via SiCl_3 anion intermediate formation is the most favorable reaction. In the scheme 2, there are possibilities to occur via three types of intermediate formation reaction; SiCl_3 radical intermediate formation, SiCl_3 anion intermediate formation, and anion surface intermediate formation (Fig. 3.15). To estimate which is the more favorable pathway, energy profiles of scheme 2 from DFT calculations were compared (Fig. 3.16).

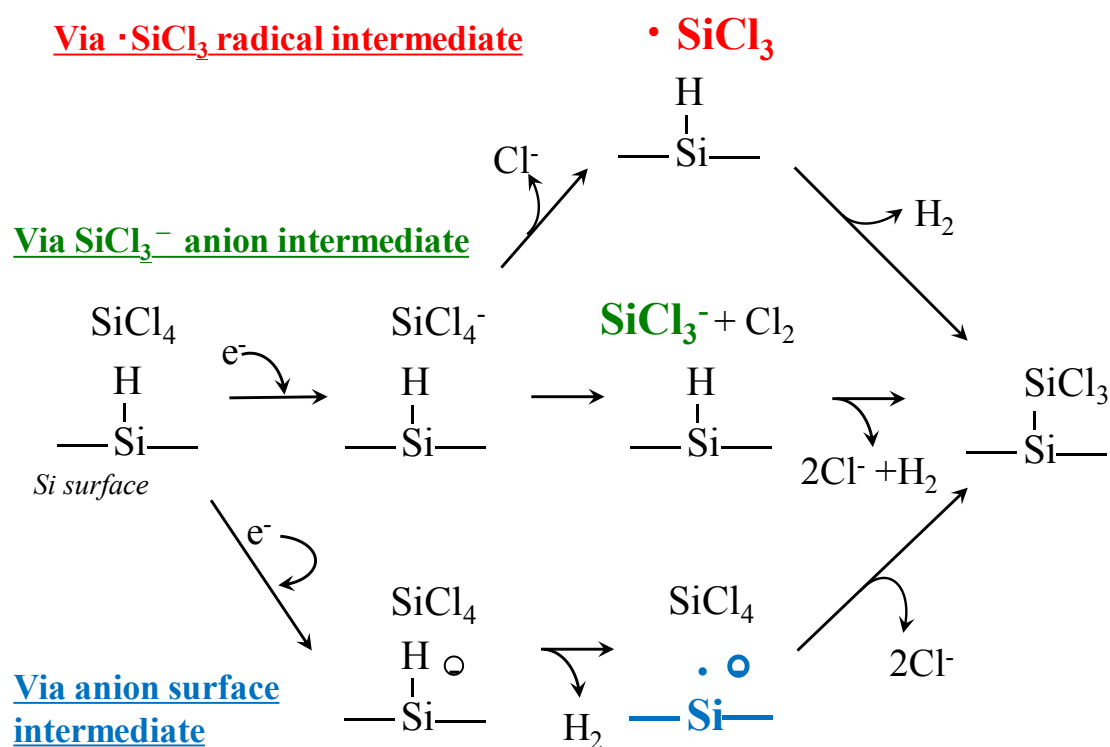


Fig. 3.15 Three types of the reaction pathway to form Si species directly on the surface

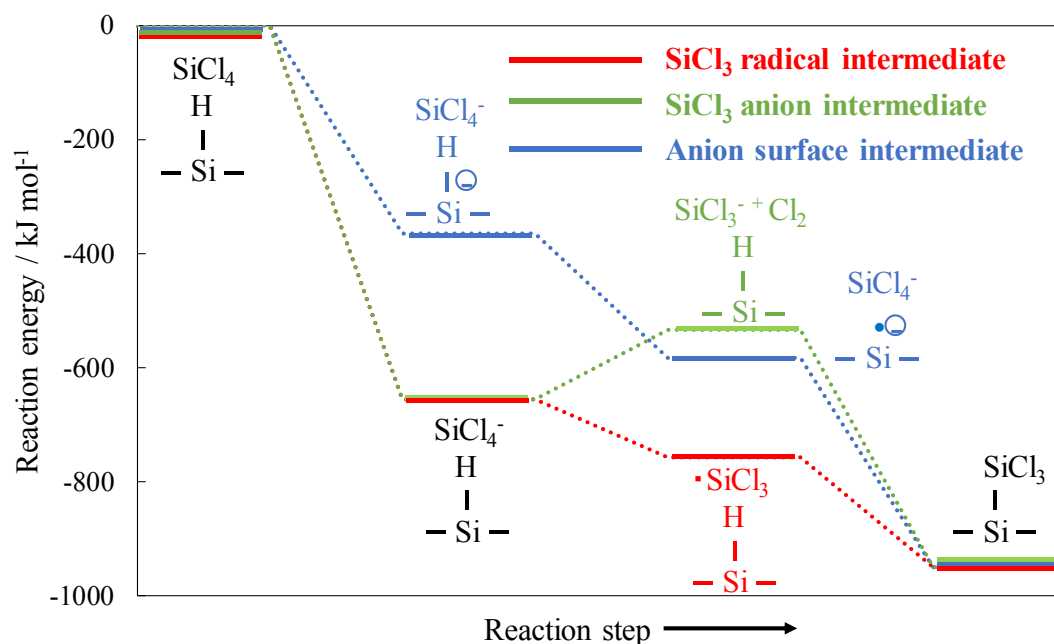


Fig. 3.16 Energy profiles of each reaction of Fig. 3.15

This energy profiles shows that the reaction via SiCl₃ radical intermediate formation is the most favorable reaction. To estimate which is the more favorable pathway, energy profiles of the reaction via SiCl₃ anion intermediate formation in scheme 1 and the reaction via SiCl₃ radical intermediate formation in scheme 2 from DFT calculations were compared. Fig. 3.17 shows the energy profiles of the two schemes, in which the profile for scheme 1 is always below the scheme 2, indicating that the reaction scheme 1 is more favorable. This means that SiCl₄ reacts with another SiCl₄ to form the intermediate just after receiving electrons from the surface.

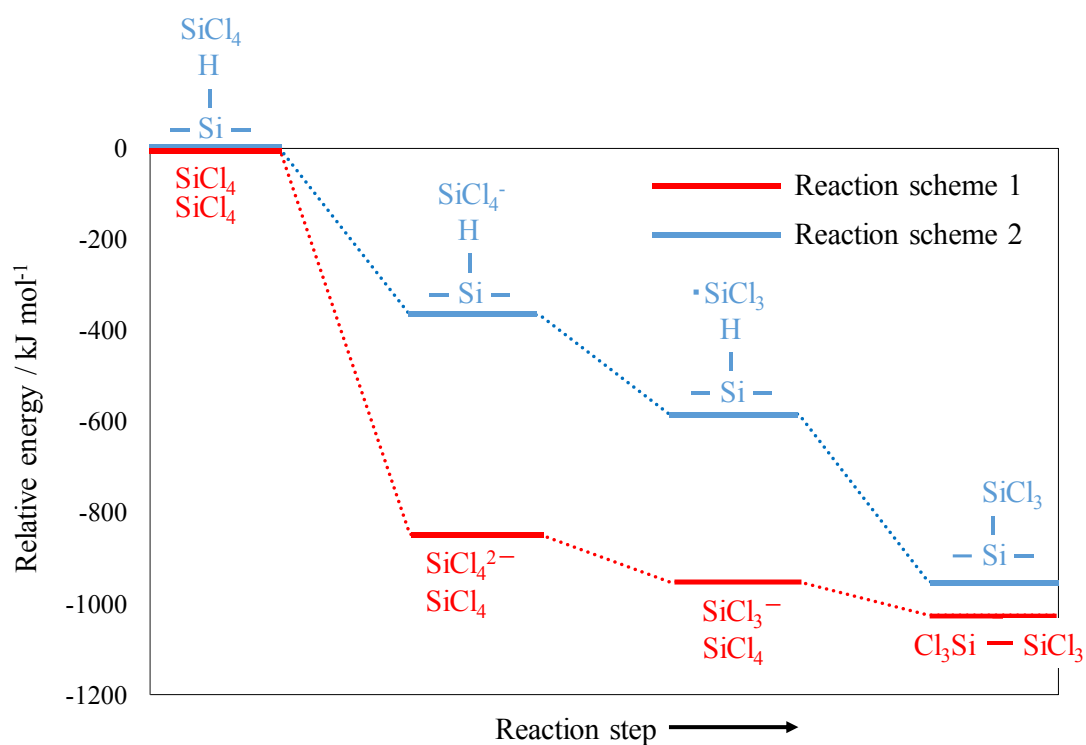


Fig. 3.17 Energy profiles of reaction scheme 1 and 2

(Scheme 1 shows the reaction of SiCl_4 with another SiCl_4 to form Si_2Cl_6 via SiCl_3^- anion intermediate formation in scheme 1. Scheme 2 shows the reaction of SiCl_4 with Si surface the reaction via SiCl_3^\cdot radical intermediate formation.)

From these comprehensive works have revealed that the elementary steps of the SiCl_4 reduction process in Si electrodeposition with TMHATFSI was described as Fig. 3.18.

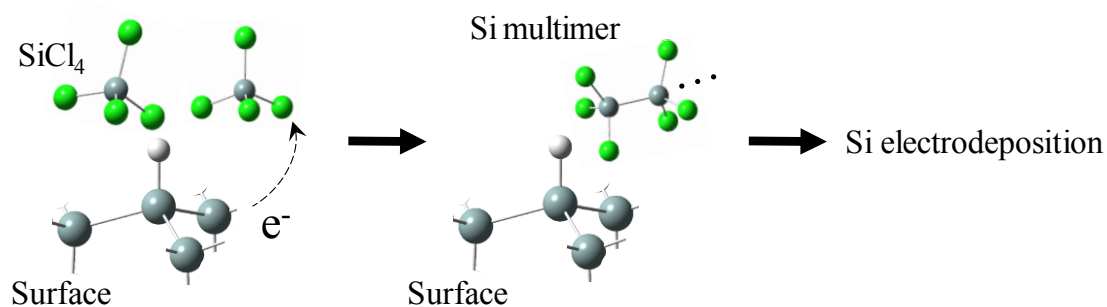


Fig. 3.18 Schematic image of the Si electrodeposition

In addition, to investigate the difference between scheme 1 and 2, Mulliken population analysis of the final products in each scheme was carried out (Fig. 3.18); the electron population of the Si-Si bonds in the Si surface model (in which all value is 0.72) turned out to decrease after reacting with SiCl_4 in scheme 2 (in which each value shows 0.72, 0.72, and 0.70). Since the Si-Si bond is considered to be categorized as a covalent bond, such a decrease of electron population in the bond should result in reducing the strength of the Si-Si bond, which affects the stability of reaction intermediates and products. This result indicates that the reaction between the Si surface and SiCl_4 does not fully stabilize the Si-Si bonds on the Si surface. Solvation effects were also considered to contribute the difference between these two schemes.

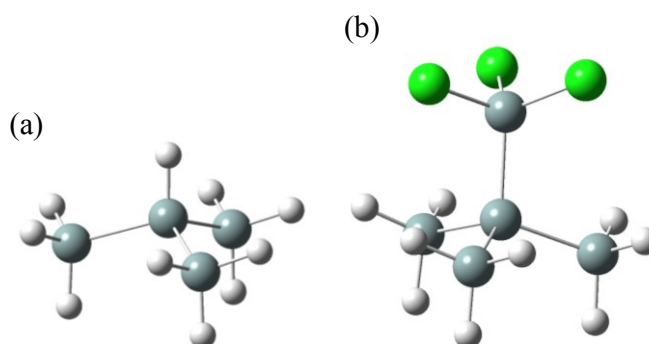


Fig. 3.18 Mulliken population analysis of the product in the reaction scheme 2; (a) before (Si surface only), (b) after (SiCl₃ with Si surface) the reaction with SiCl₄ (Dark and light grey dots are Si and H, respectively, and green dots are Cl. All electron population of Si-Si bond of Si surface before the reaction is 0.75, while that after the reaction changes to 0.72, 0.72, and 0.70, respectively.)

The solvation structures of reaction schemes 1 and 2 (Fig. 3.19) suggests that the final products interact with only the TMHA⁺ cation to stabilize themselves in reaction scheme 2, while the final products of reaction scheme 1 interact with both the cation of TMHA⁺ and anion of TFSI⁻ to be stabilized. Such a difference should be caused by the steric factor of the structure of ionic liquid; since ionic liquid molecules applied to the present work have relatively larger molecular volume and are bulky, their interaction should be sterically restricted. Thus, it is expected that the number of ionic liquids which are capable of interacting with the product species will be different, due to the molecular structure of the ionic liquids, measurably determining the favorable reaction pathway. Therefore, it is concluded that Si bonding to electronegative Cl (Si of SiCl₄) is more active for Si-Si bond formation rather than Si bonding to surrounding Si (Si of the Si surface). From the view point of these calculations, the intermediate formation of Si₂Cl₆ described above is theoretically reasonable. In addition, the released Cl⁻ was interacted and stabilized with two cations, suggesting the favorability of the discussed reaction as shown in Fig. 3.20.

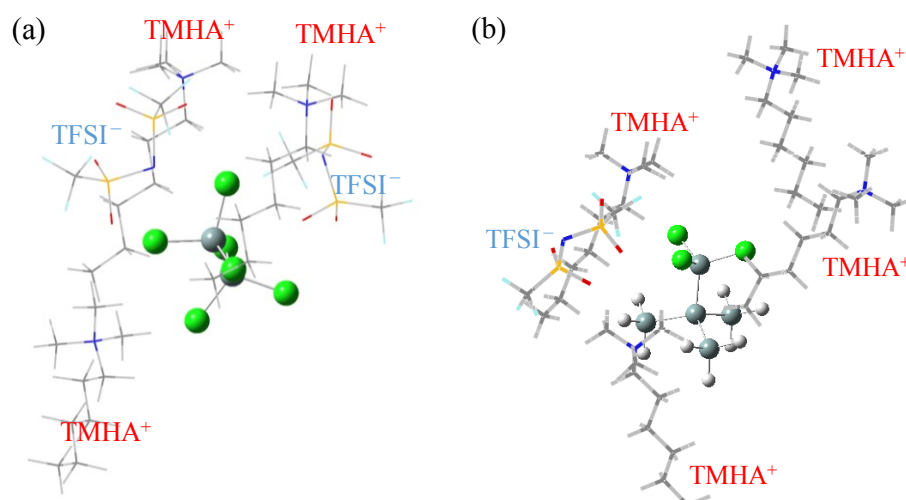


Fig. 3.19 The solvation structure of the final products in (a) reaction scheme 1; Si₂Cl₆ and (b) reaction scheme 2; SiCl₃ with Si surface (Dark and light grey dots are Si and H respectively, and green dots are Cl. Cation and anion of ionic liquids are described directly in Fig.)

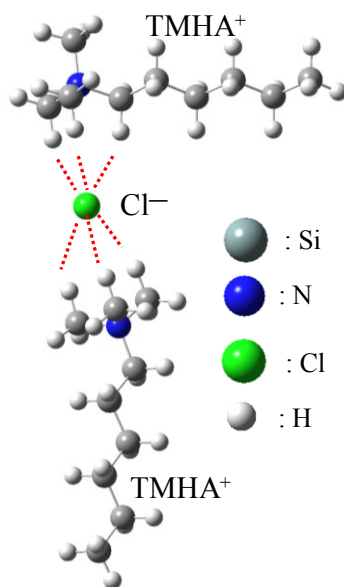


Fig. 3.20 The interaction of Cl⁻ and cations of the ionic liquids

As for the transition state in scheme 1, more detailed calculation was performed. The existence of transition state formation is shown in Fig. 3.21. First, as for the transition state when two electrons trapped into SiCl_4 , and then SiCl_3^- was formed, it was suggested that there is no transition state formation. Such mechanism is described in Fig. 3.22. Figure 3.22 shows each electron density distribution in HOMO orbital. As described above, SiCl_4^{2-} could act as transition state, however, the reaction process can progress smoothly. From these results, it was revealed that Cl^- could be easily dissociated from Si when two electrons were trapped, and it seemed not to have activation energy to release Cl^- because SiCl_4^{2-} should be more stable than SiCl_4 , and SiCl_3^- should also be stable than SiCl_4^{2-} .

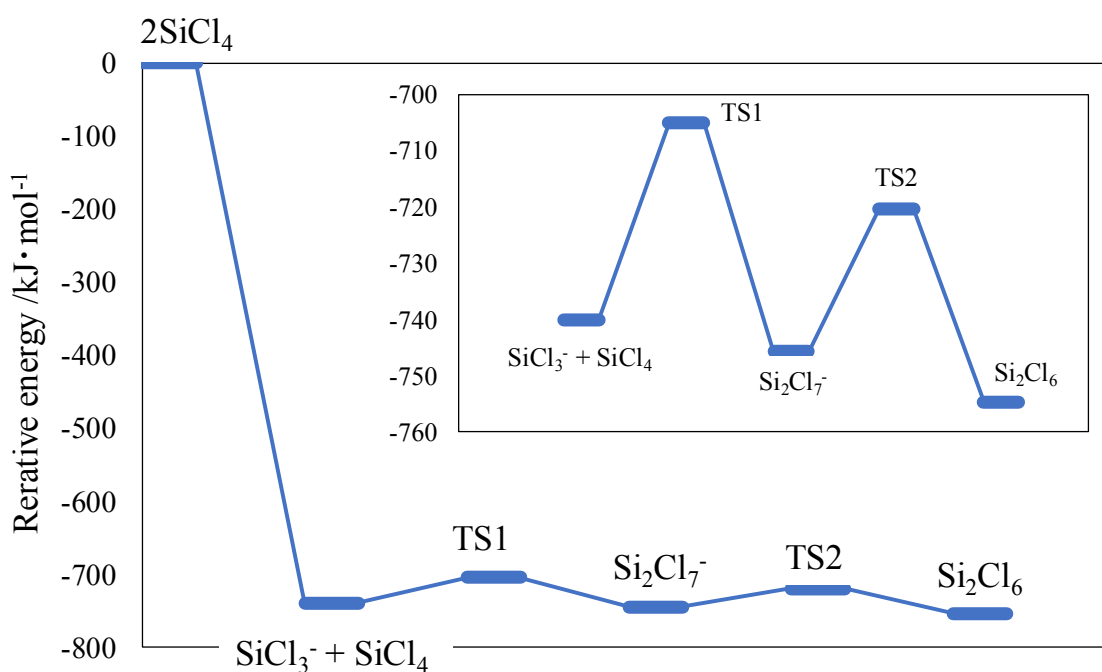


Fig. 3.21 Transition state in Si dimer formation as intermediate state during electrodeposition

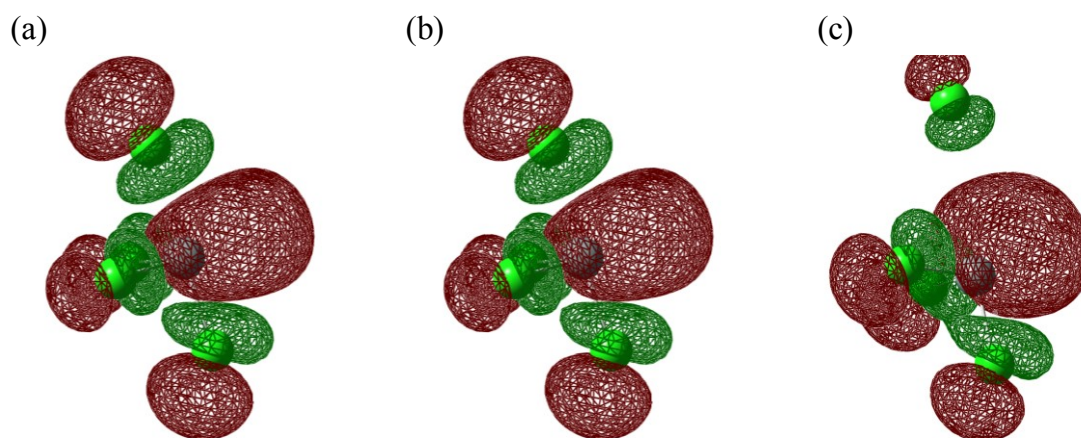


Fig. 3.22 Electron density distribution in HOMO orbital; (a) SiCl_4^{2-} in which the bond length between Si and Cl is 2.1 Å, (b) SiCl_4^{2-} in which the bond length between Si and Cl is 2.5 Å, and (c) SiCl_3^- in which the bond length between Si and Cl is 4.0 Å

Second, the transition state from SiCl_3^- to Si_2Cl_6 was investigated. As a result, two transition state were considered. For this, Si_2Cl_7^- acted as an intermediate state. In general, Si tends to form the structure of three center four electron bonding [18], which turn out to be an intermediate state in this case. Each transition state structure is shown in Fig. 3.23. In the formation of three center four electron bonding of Si_2Cl_7^- , SiCl_4 and SiCl_3^- were bonded after reaching to 2.8 Å that is the bond length between Si and Si. After the formation of Si_2Cl_7^- , the Cl⁻ in the rightest side in Fig. 3.23 (b) will tend to be dissociated after releasing to 2.9 Å.

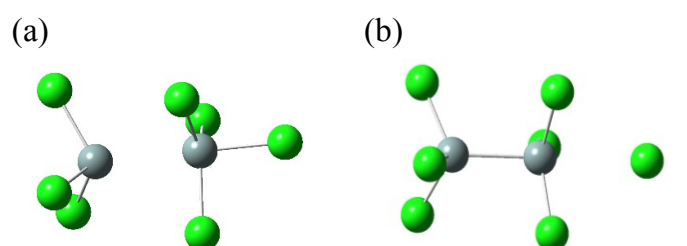


Fig. 3.23 Transition state in Fig. 3.21, (a) TS1 with the bond length between Si and Si of 2.8 Å, (b) TS2 in Fig. 3.21 with the bond length between Si and Cl of 2.9 Å

To predict whether the further reaction of this Si_2Cl_6 intermediate species behaves like a polymer or not, as discussed above, the DFT calculation was continuously conducted for Si_2Cl_6 that had received another electron from the Si surface. The calculated reaction energy indicated that dissociation of Cl^- ions to generate Si_2Cl_5 took place favorably, mainly because the structure of the released Cl^- ion that strongly interacts with the ionic liquids becomes stable as described above. That reaction energy was calculated as -374.6 kJ/mol, while the reaction energy was calculated as -306.8 kJ/mol if the reaction that Si_2Cl_6 receives electrons to form SiCl_3 and SiCl_3^- , which means the reverse reaction of the formation of polymer. The structural analysis also shows that the Si-Cl bond of Si_2Cl_6 is extended after receiving additional electrons from 2.04 Å to 2.21 Å, which also indicates that a Si_2Cl_6 emits a Cl^- ion and proceeds the reaction by receiving an electron. Si of Si_2Cl_5 that has already releases a Cl^- tends to exhibit bond formation with another Si of SiCl_4 due to its strong activity, generating a Si trimer species. This reaction eventually leads to the formation of a polymer structure during Si electrodeposition, as discussed in the XRR measurement. This polymer-like intermediate is expected to be finally deposited as Si on the substrate.

Conclusions

In this chapter, the interfacial reaction mechanism of the elementary steps of the SiCl_4 reduction process in Si electrodeposition with an ionic liquid was analyzed, focusing on the molecular level behavior of the reactants at solid-liquid interface to provide details on the reaction of SiCl_4 on the substrate surface.

It has been revealed that there is an intermediate formation step, in which a polymer-like structure such as Si_2Cl_6 , is formed during the reduction of SiCl_4 , in which the electrochemical behavior was analyzed by EQCM measurement, and based on those results, the possibility of the intermediate formation was discussed by XRR measurement. Then, proposed scheme was confirmed from the view point of reaction energy and solvation effect by using DFT calculation.

The following process is proposed to describe the detailed interfacial reaction mechanism of the SiCl_4 reduction process from molecular point of view: a SiCl_4 molecule reduces with the release of a Cl^- ion, followed by the reaction between the residual SiCl_3^- and another nearby SiCl_4 to produce the intermediate states containing Si_2Cl_6 . This intermediate formation takes place successively, generating a polymer-like species, which is finally deposited as Si on the substrate.

From these results, these comprehensive works would be greatly helpful to understand the reaction mechanism focusing on the reductant itself in the electrodeposition using non-aqueous solvents.

References

- [1] O. M. Magnussen, B. M. Ocko, M. J. Regan, K. Penanen, P. S. Pershan, and M. Deutsch, *Phys. Rev. Lett.*, **74**, 444 (1995).
- [2] M. Mezger, H. Schröder, H. Reichert, S. Schramm, J. S. Okasinski, S. Schöder, V. Honkimäki, M. Deutsch, B. M. Ocko, J. Ralston, M. Rohwerder, M. Stratmann, and H. Dosch, *Science*, **322**, 424 (2008).
- [3] T. A. Petach, A. Mehta, R. Marks, B. Johnson, M. F. Toney, and D. Goldhaber-Gordon, *ACS Nano*, **10**, 4565 (2016).
- [4] M. Kunimoto, A. Otomo, N. Takahashi, H. Nakai, and T. Homma, *Electrochim. Acta*, **113**, 785 (2013).
- [5] B. Jiang, M. Kunimoto, M. Yanagisawa, and T. Homma, *J. Electrochem. Soc.*, **160**, D366 (2013).
- [6] M. Kunimoto, K. Endo, H. Nakai, and T. Homma, *Electrochim. Acta*, **100**, 311 (2013).
- [7] M. Björck and G. Andersson, *J. Appl. Cryst.*, **40**, 1174 (2007).
- [8] M. J. Frisch, G. W. Trucks, H. B. Schlegel, G. E. Scuseria, M. A. Robb, J. R. Cheeseman, G. Scalmani, V. Barone, B. Mennucci, G. A. Petersson, H. Nakatsuji, M. Caricato, X. Li, H. P. Hratchian, A. F. Izmaylov, J. Bloino, G. Zheng, J. L. Sonnenberg, M. Hada, M. Ehara, K. Toyota, R. Fukuda, J. Hasegawa, M. Ishida, T. Nakajima, Y. Honda, O. Kitao, H. Nakai, T. Vreven, J. A. Montgomery, Jr., J. E. Peralta, F. Ogliaro, M. Bearpark, J. J. Heyd, E. Brothers, K. N. Kudin, V. N. Staroverov, R. Kobayashi, J. Normand, K. Raghavachari, A. Rendell, J. C. Burant, S. S. Iyengar, J. Tomasi, M. Cossi, N. Rega, J. M. Millam, M. Klene, J. E. Knox, J. B. Cross, V. Bakken, C. Adamo, J. Jaramillo, R. Gomperts, R. E. Stratmann, O. Yazyev, A. J. Austin, R. Cammi, C. Pomelli, J. W. Ochterski, R. L. Martin, K. Morokuma, V. G. Zakrzewski, G. A. Voth, P. Salvador, J. J. Dannenberg, S. Dapprich, A. D. Daniels, Ö. Farkas, J. B. Foresman, J. V. Ortiz, J. Cioslowski, and D. J. Fox, Gaussian 09, Revision A.01, Gaussian, Inc., Wallingford, CT (2009).
- [9] W. J. Hehre, R. Ditchfield, and J. A. Pople, *J. Chem. Phys.*, **56**, 2257 (1972).

- [10] M. J. Frisch, J. A. Pople, and J. S. Binkley, *J. Chem. Phys.*, **80**, 3265 (1984).
- [11] P. J. Hay and W. R. Wadt, *J. Chem. Phys.*, **82**, 270 (1985).
- [12] S. Dapprich, I. Komaromi, K. S. Byun, K. Morokuma, and M. J. Frisch, *J. Mol. Struct. Theochem*, **462**, 1 (1999).
- [13] E. Cancès, B. Mennucci, and J. Tomasi, *J. Chem. Phys.*, **107**, 3032 (1997).
- [14] S. Ivanov, C. Vlaic, A. Bund, and I. Efimov, *Electrochim. Acta*, **219**, 251 (2016).
- [15] M. Umezawa, M. Takeda, H. Ishikawa, T. Ishikawa, T. Koizumi, T. Fuchigami, and T. Nonaka, *Electrochim. Acta*, **36**, 621 (1991).
- [16] S. Kashimura, M. Ishifune, N. Yamashita, H- B. Bu, M. Takebayashi, S. Kitajima, D. Yoshiwara, Y. Kataoka, R. Nishida, S. Kawasaki, H. Murase, and T. Shono, *J. Org. Chem.*, **64**, 6615 (1999).
- [17] X. Wang, Y. Yuan, and I. Cobasso, *J. Electrochem. Soc.*, **152**, 259 (2005).
- [18] M. Kira, K. Tamao, *Gendaikeisokagaku*, Kagakudojin, Chapter 1, Japan (2013).

Chapter 4:

***Overall Reaction Mechanism Analysis of Si
Electrodeposition in Ionic Liquids***

4.1 Introduction

In previous chapter (chapter 2 and 3), the solvent of ionic liquid was focused on. On the other hand, among the non-aqueous solvents, organic solvents are also the promising solvent for the electrodeposition of Si at low temperatures. Several studies of the Si electrodeposition have also been conducted because organic solvents have characteristics that their low viscosity can allow us a faster electrodeposition at room temperature, which could turn out to be useful for practical applications [1-11]. In this chapter, focusing on such characteristics of organic solvents, the electrodeposition using organic solvents is described.

Several studies of the electrodeposition of Si using organic solvents have been reported. In the 1980's, in which acetic acid containing tetramethylammonium chloride or tetraethylammonium chloride with tetraethylorthosilicate [1], propylene carbonate containing tetrabutylammonium chloride [2] or tetrabutylammonium perchlorate [3] with SiHCl_3 were used as electrolytes. In recent, the growth process of electrodeposited Si has been gradually discussed. Y. Nishimura et al. [7] has reported that the Si electrodeposition process in propylene carbonate containing tetrabutylammonium chloride with SiCl_4 might involve the formation of Si_mCl_n species, and T. Munisamy et al. [8] has studied the initial growth of the electrodeposited Si in acetonitrile and tetrahydrofuran containing tetrabutylammonium chloride with SiCl_4 and SiHCl_3 . For further developing such Si electrodeposition in organic solvents, it is necessary to overcome current problems such as the inclusion of impurities into the films and uncertainty of the reaction mechanism. As for the impurities, there are some reports that an annealing treatment is effective to decrease the impurities in Si thin films [3, 6, 8, 10]. On the other hand, the influence of as-deposited conditions on the electrodeposition process, which could also have an influence on the film composition, is still unclear. For this, two possible concerns have been discussing, which might affect the electrodeposition process; species of oxidized and non-oxidized solvents [10,11], and the water content in organic solvents [8]. The presence of water is believed to cause hydrolysis reaction of the Si precursors [12], thereby affecting the electrodeposition process. However, the details of such influences

have not been reported. Also, when using SiCl_4 as the Si source, the reduction step and the intermediate species remain to be clarified. In this regard, Y. Nishimura et al. [7] hypothesized that the Si electrodeposition process in propylene carbonate containing tetrabutylammonium chloride with SiCl_4 might involve the formation of Si_mCl_n .

Therefore, in this chapter, the author investigates the influence of as-deposited condition, namely the oxidized/non-oxidized solvent species and the water content in the solvent, on the deposited Si film, as well as the reduction mechanism of SiCl_4 . To elucidate such interfacial reactions during the electrodeposition, electrochemical quartz crystal microbalance (EQCM) and Raman spectroscopy experiments were conducted, since these methods were proven to be useful for analyzing the interface during the Si electrodeposition process in previous chapter. Additionally, density functional theory (DFT) was used to provide a molecular-level understanding of the solid-liquid interfacial reactions as shown in previous chapter.

4.2 Experimental

The Si electrodeposition was carried out with a three-electrode system. The bath was SiCl_4 (0.5 M) in acetonitrile (CH_3CN) or PC, with the addition of tetrabutylammonium chloride (TBACl, 0.3 M for CH_3CN and 0.1 M for PC) as a supporting electrolyte. PC containing approximately 30 ppm water was purchased from Kishida Chemical Corporation, non-dehydrated CH_3CN containing approximately 30 ppm water was purchased from Kanto Chemical Corporation, and dehydrated CH_3CN containing approximately 10 ppm water was purchased from Wako Pure Chemical Industries. SiCl_4 and TBACl were purchased from Sigma-Aldrich. As a working electrode, an Au film (200 nm) was formed on a Si (111) substrate with a Cr adhesion layer (10 nm), both layers being deposited by electron beam evaporation (ULVAC, EBX-6D). A Pt wire was used as the counter electrode; and the reference electrode was Ag/Ag^+ in which an Ag wire was immersed into the organic solvent containing 0.05 M AgNO_3 (Kanto Chemical Corporation). The reference electrode was separated from the electrolyte by a vycor glass with a porous tip. The rotating disk electrode was used in the electrodeposition in the PC bath. The electrodeposition potential in PC and CH_3CN was -2.5 and -2.3 V vs. Ag/Ag^+ , respectively, and the Si thin films were normally electrodeposited at 1000 mC cm^{-2} unless specified otherwise. For the EQCM measurement, a 6 MHz AT-cut quartz crystal with Au contacts was used as the working electrode with a surface area of 1.32 cm^2 . Frequency was measured by a frequency analyzer (Agilent Technologies, E5061A) during linear sweep voltammetry (LSV). The detailed technique used for EQCM analysis can be found in our previous report^{5,17}. All electrochemical measurements were performed using a potentiostat/galvanostat (Hokuto Denko, HZ-7000) at room temperature in an Ar-filled glove box. For measurements carried out under light irradiation, a quartz halogen lamp of 30 W m^{-2} was used.

Before each characterization experiment, the deposited Si films were rinsed with dehydrated CH_3CN several times to remove the residual solvents. The average composition of the samples was measured by X-ray photoelectron spectroscopy (ULVAC, PHI 5000 Versa Probe WS) using $\text{Al-K}\alpha$ irradiation and 4 kV Ar ion etching. A transfer

vessel was used to prevent the Si thin films from oxidization during transport to the XPS apparatus. The deviation of the average composition measured with this apparatus was ± 3 at.%. The chemical species in the electrodeposited films were characterized by Raman spectroscopy (TOKYO INSTRUMENTS, Nanofinder 30). Before the Raman measurement, the Au substrate with the electrodeposited film was attached to a cover glass with a Kapton tape to prevent exposure to air. The morphology of the samples was characterized by a scanning electron microscope (Hitachi High-Technologies, SU-4800). The electrodeposited Si films were annealed at 700 °C for 1 h in Ar (90 %) and H₂ (10 %) gas atmosphere using a rapid thermal annealing apparatus (ULVAC, MILA 3000).

All calculations were performed by density functional theory (DFT) with Gaussian 09 [13]. The exchange-correlation function was B3LYP [14, 15], and the basis set for each element was 6-311++(2d, 2p). Solvation effect was considered by using polarized continuum model (PCM) [16]. In this PCM, surrounding solvents were assumed by using their dielectric constant as shown in Fig. 4.1.

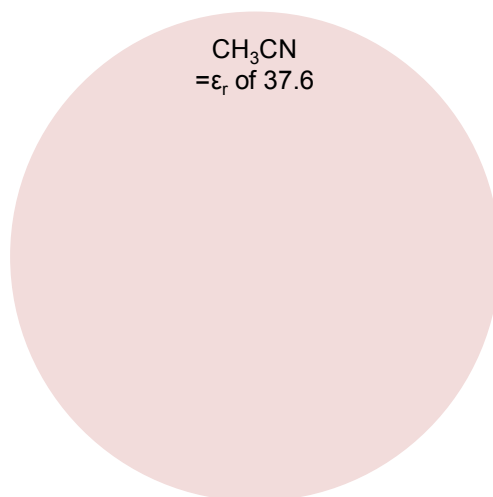


Fig. 4.1 Schematic diagram of PCM (ϵ_r is the dielectric constant of solvents)

4.3 Results and Discussion

4.3.1 Analysis of the effect of electrodeposition conditions on as-deposited films

As mentioned in the section of Introduction, the annealing treatment effect on the composition of the electrodeposited films is described here. The electrochemical behavior was shown in Fig. 4.1. The current density increased around -1.5 V, suggesting the reduction of SiCl_4 , while the current density deriving from the decomposition of solvents themselves also increased. The decomposition mechanism of PC has been theoretically reported [17]. Then, the electrodeposition potential was set at -2.5 V, and the average atomic percentage of each element of the films electrodeposited at -2.5 V in the PC bath before and after the annealing treatment are shown in Fig. 4.2 and Table 4.1. The impurities were dramatically decreased by the annealing. The increase of oxygen content is considered to drive from the exposure to the air of the samples even though the samples were transferred to the rapid thermal annealing apparatus as quickly as possible. These decreases of the impurities by the annealing also suggested that one of the reason why the impurities included into the electrodeposited films was the incorporation of the solvents themselves or their decomposed products. Actually, it has been reported that PC is thermally decomposed over 400 °C [18], indicating that the incorporated PC in the films was decomposed by the annealing. Then, the fundamental aspects of Si electrodeposition in the as-deposited condition are described below.

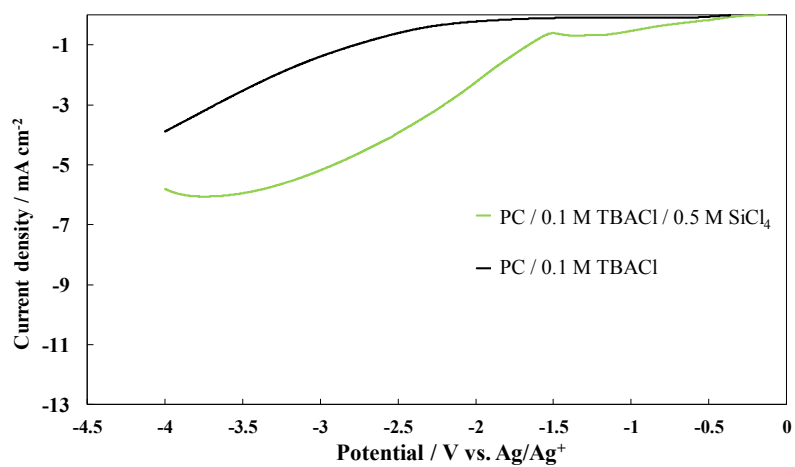


Fig. 4.1 Linear sweep voltammogram (scan rate = 10 mV s^{-1}) in TMHATFSI with and without 0.5 M SiCl_4

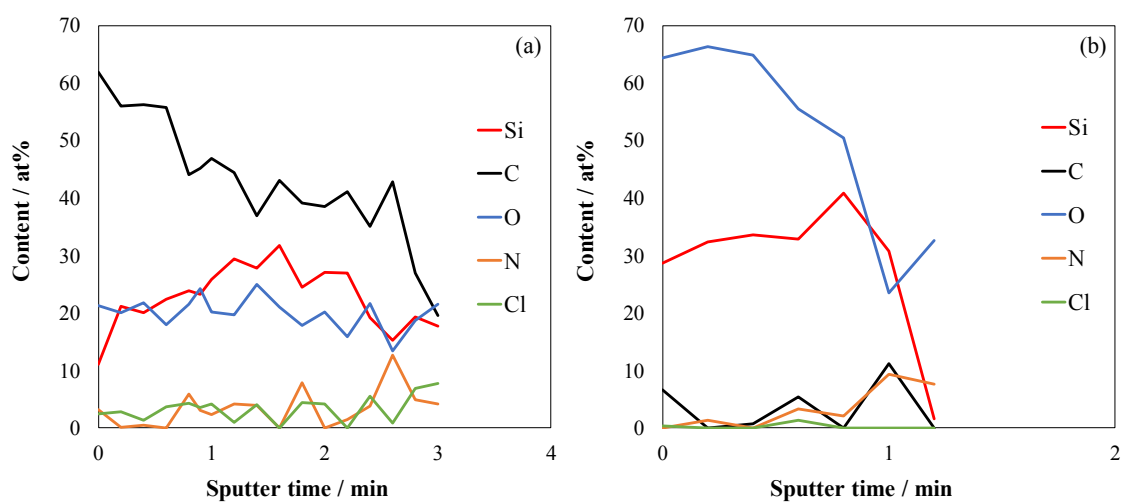


Fig. 4.2 The XPS depth profiles of the Si thin films electrodeposited at -2.5 V in the PC bath; (a) before annealing, (b) after annealing

Table 4.1 The average atomic percentage of each element of the electrodeposited films in the PC bath before and after the annealing treatment in Fig. 4.1

	Content / at %				
	Si	C	O	N	Cl
Before	20	45	24	6	5
After	31	2	65	1	1

First, to discuss the influence of the diffusion of SiCl_4 , the rotating disk electrode was used. The electrochemical behavior with and without rotating (300 rpm) are shown in Fig. 4.3. As seen in Fig., the current density increased with the rotating. In the blank solution, it did not confirm the increase of the current density which is entirely same with the black curve in Fig. 4.3 when the electrochemical measurement was conducted under the rotating of 300 rpm condition, so that it is considered that only reduction of SiCl_4 was enhanced by accelerate the diffusion of SiCl_4 .

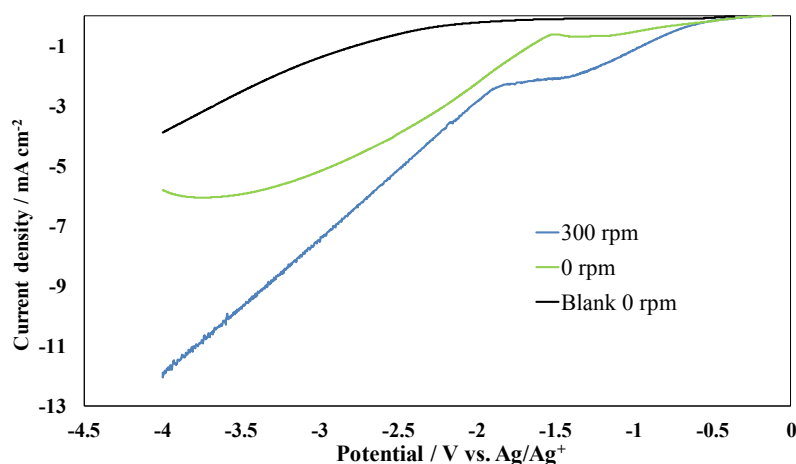


Fig. 4.3 Linear sweep voltammogram (scan rate = 10 mV s^{-1}) in the PC bath with and without rotating

This tendency was also confirmed in the current transients during the constant electrodeposition at -2.5 V with and without the rotating were shown in Fig. 4.4. The current density gradually decreases during the electrodeposition without the rotating, while the current density kept the same value during the electrodeposition under the rotating condition, suggesting a stable supply of SiCl_4 to the electrode surface. Following these results, the composition analyses showed the same tendency that the content of Si increased, while the content of carbon which is the dominant of impurities decreased (Fig. 4.5). It is suggested that the reduction of SiCl_4 is competitively occurred with the decomposition of the solvents.

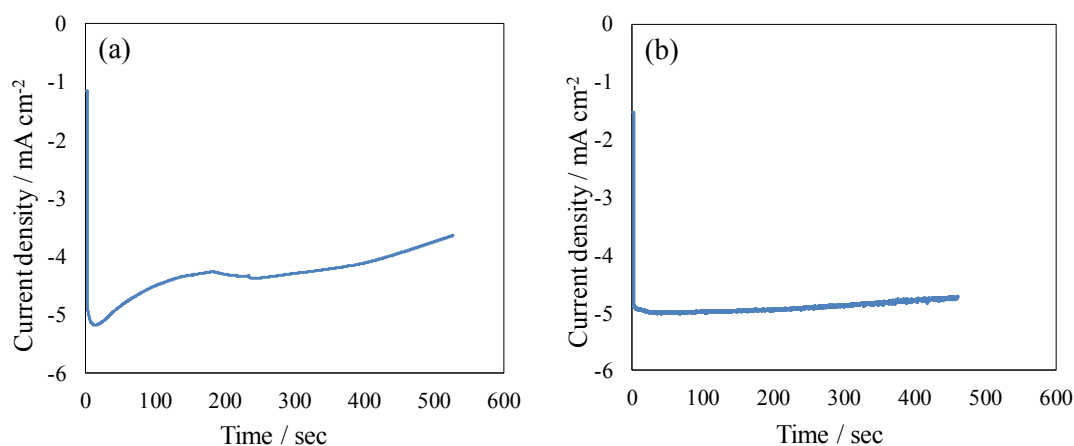


Fig. 4.4 Current transient during the electrodeposition at -2.5 V in the PC bath (a) without and (b) with rotating

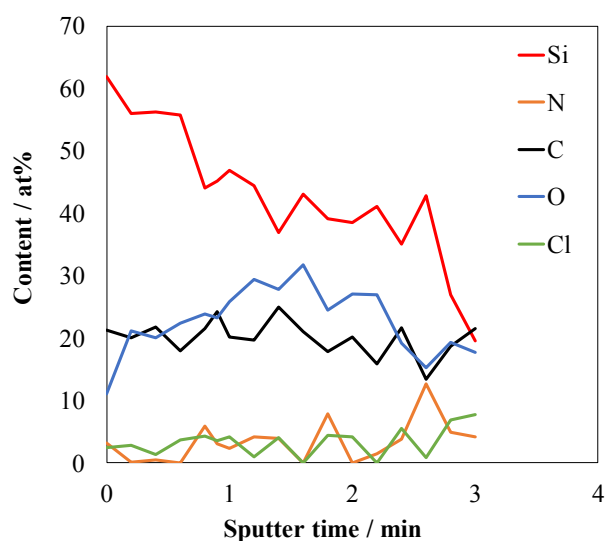


Fig. 4.5 XPS depth profiles of the Si thin films electrodeposited at -2.5 V in the PC bath with rotating at 300 rpm

Next, Since the organic solvent species, especially the oxygen content can affect the Si film composition, PC and CH₃CN as representative oxidized and non-oxidized solvents, respectively were used. In the beginning, the electrochemical measurement was performed in the CH₃CN bath. In Fig. 4.6, the result of dehydrated CH₃CN was also shown, which will be mentioned later. The increase of the current around -2.0 V vs. Ag/Ag⁺ was considered to derive from the reduction of SiCl₄. Then, the electrodeposition potential was set at -2.3 V vs. Ag/Ag⁺ in the CH₃CN bath.

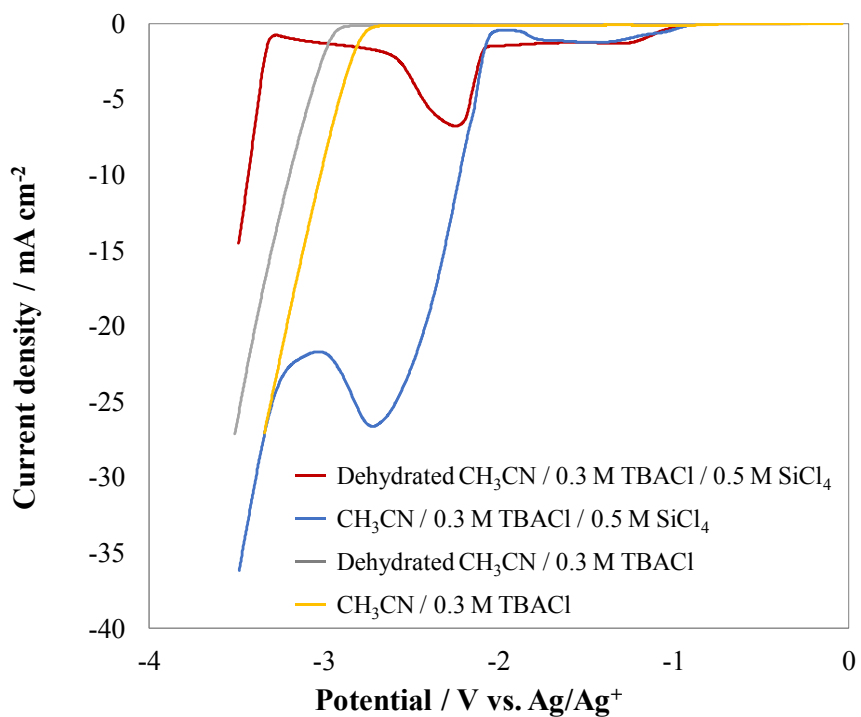


Fig. 4.6 Linear sweep voltammogram (scan rate = 10 mV s⁻¹) in the CH₃CN bath

The average compositions of the electrodeposited films from XPS measurement in CH₃CN are shown in Fig. 4.7 and Table 4.2. In Table 4.2, the average composition of each element of the electrodeposited films in the PC bath also represented as the comparison.

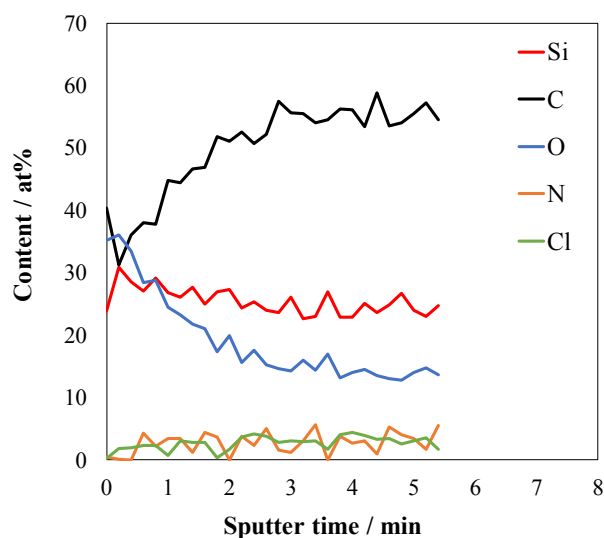


Fig. 4.7 XPS depth profiles of the Si thin films electrodeposited at -2.3 V in the CH₃CN bath

Table 4.2 The average atomic percentage of each element of the electrodeposited films in the PC and CH₃CN bath

Solvents	Content / at %				
	Si	C	O	N	Cl
PC	20	45	24	6	5
CH ₃ CN	26	50	19	2	3

Compared to PC, the use of CH₃CN only reduced the oxygen content by 5 at.%, a small amount that could be attributed to the incorporation of the oxidized solvent. Therefore, we concluded that the film composition did not change much between the oxidized and non-oxidized solvents. Based on these results, in order to consider the influence of water on the films composition, non-dehydrated and dehydrated CH₃CN containing approximately 30 and 10 ppm water, respectively was used as the solvent. As shown in Fig. 4.6, the current density in the non-dehydrated CH₃CN was larger than that in dehydrated CH₃CN. The consideration mechanism will be described later. The average composition of each element of the electrodeposited films in the non-dehydrated CH₃CN

bath and the dehydrated CH₃CN bath are shown in Fig. 4.8 and Table 4.3.

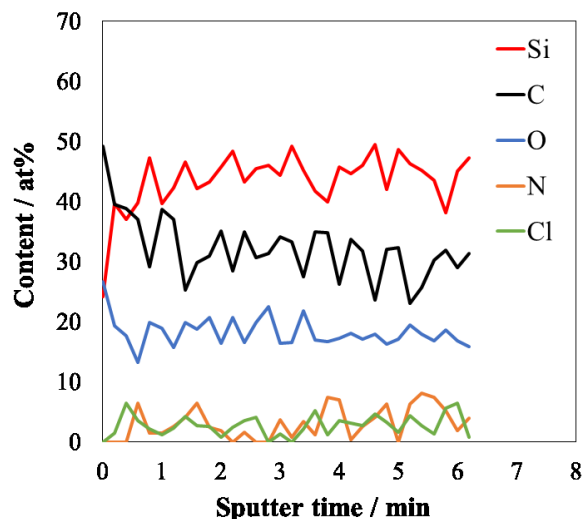


Fig. 4.8 XPS depth profiles of the Si thin films electrodeposited at -2.3 V in the dehydrated CH₃CN bath

Table 4.3 The average atomic percentage of each element of the electrodeposited films depending on the water content in the dehydrated CH₃CN bath

Water content / ppm	Content / at %				
	Si	C	O	N	Cl
30	26	50	19	2	3
10	41	33	19	4	3

The carbon content increased with increasing water content in the solvent, while the oxygen content did not increase. It is considered that this oxygen was not incorporated during the electrodeposition *process*. Instead, the oxygen could come from oxidation during the cleaning process after the electrodeposition, and/or during the transfer to the XPS apparatus despite using a transfer vessel. The reason is that, when we used the vacuum-dried samples without cleaning for the XPS apparatus, the oxygen content decreased to 6 at %, while the carbon content increased because it could be considered that the solvents were not perfectly removed by using only vacuuming. In order to confirm

the effect of the annealing treatment, that process was also conducted against the films, and the significant carbon decrease was observed (Fig. 4.9).

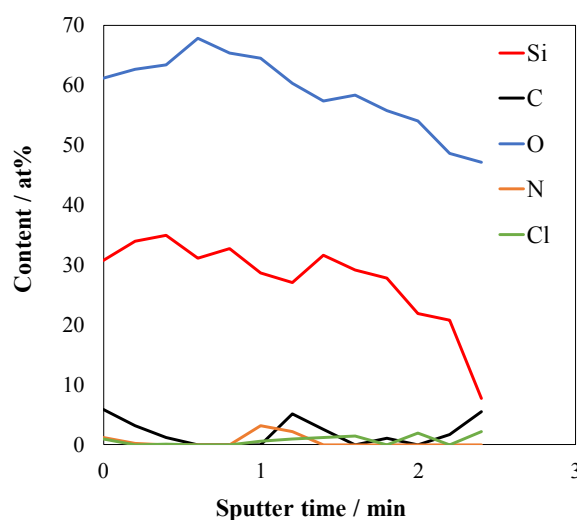


Fig. 4.9 XPS depth profiles of the Si thin films electrodeposited at -2.3 V in the dehydrated CH₃CN bath after annealing

In order to understand the molecular-level effect of residual water, DFT calculation was performed for the Si electrodeposition in CH₃CN. SiCl₄ is assumed to hydrolyze in the presence of water [12] ($\text{SiCl}_4 + \text{H}_2\text{O} \rightarrow \text{SiCl}_3\text{OH} + \text{HCl}$), with a negative reaction energy of -19.6 kJ/mol compared with the formation of a hydrated structure (Fig. 4.10). Here, it should be mentioned that the hydrolysis reaction seems to progress more favorable than the formation reaction of the hydrated structure, however, such hydrated structure formation might be considered as a transition state in the hydrolysis reaction. It is thought that the hydrolysis reaction could proceed after the hydrated structure formation because water should get close to SiCl₄ to form the hydrolysis product. The reaction energy also suggests this phenomenon because it was +7.7 kJ/mol. If this reaction energy would be an activation energy, the reaction can be occurred without the reaction barrier.

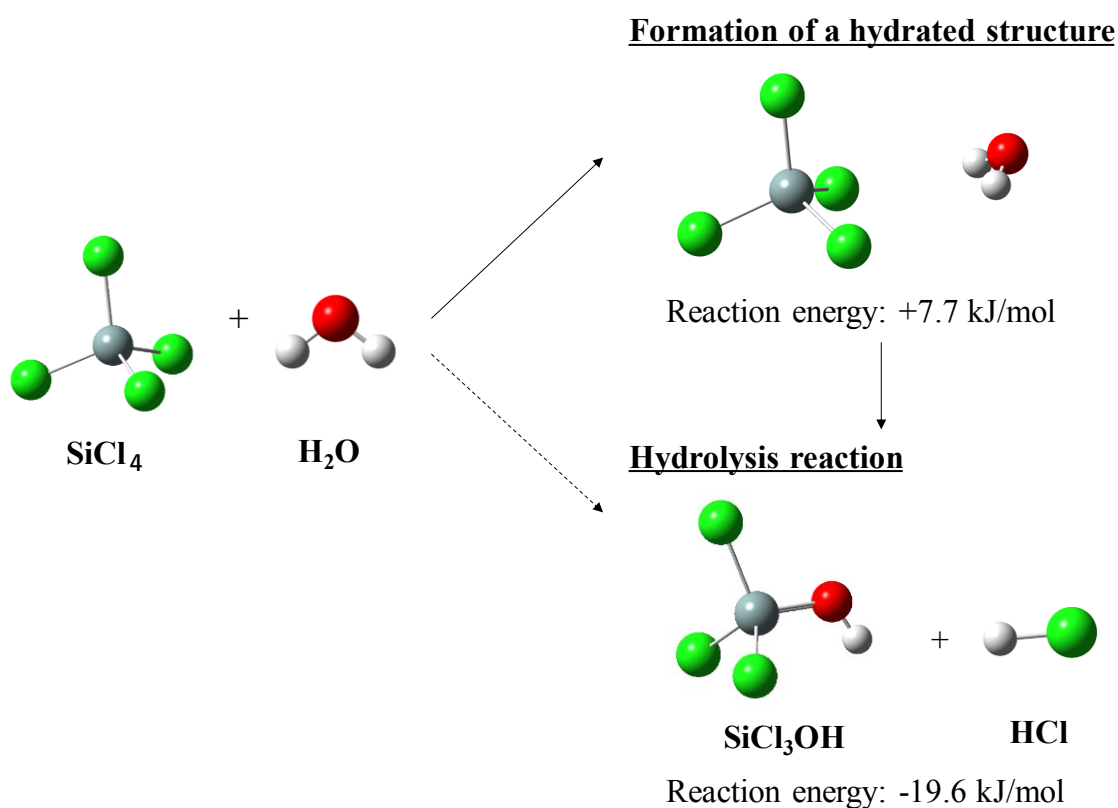


Fig. 4.10 The assumption of the reaction between SiCl_4 and H_2O

In this SiCl_3OH formation, the effect of solvent molecules on the formation of SiCl_3OH (the hydrolysis product) was investigated. The activation energy of the above reaction in a CH_3CN environment was $+45.7 \text{ kJ mol}^{-1}$, while that in a solvent-free environment was $+105.0 \text{ kJ mol}^{-1}$. The transition state structure is shown in Fig. 4.11. In addition, the solvation energy between the SiCl_3OH (the hydrolysis product) and CH_3CN molecules was -25.5 kJ/mol , meaning the stabilization of SiCl_3OH by the CH_3CN molecules, while SiCl_4 did not interacted with CH_3CN molecules (the solvation energy was calculated as $+11.7 \text{ kJ/mol}$). That optimized structure is shown in Fig. 4.12. These results indicate that the CH_3CN molecules stabilize the hydrolysis reaction, in which the hydroxy group in SiCl_3OH were interacted with CH_3CN molecules.

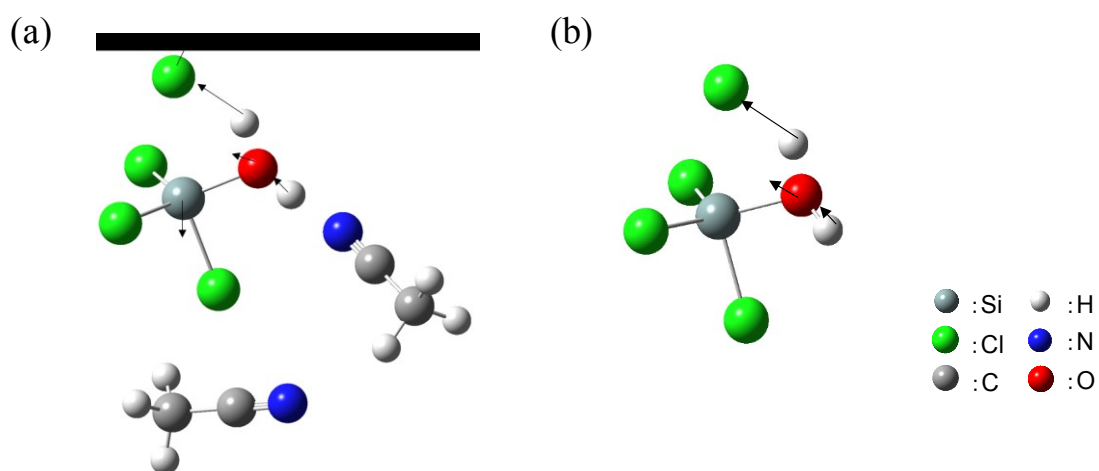


Fig. 4.11 The transition state during the hydrolysis reaction (a) with and (b) without the consideration of CH_3CN molecules

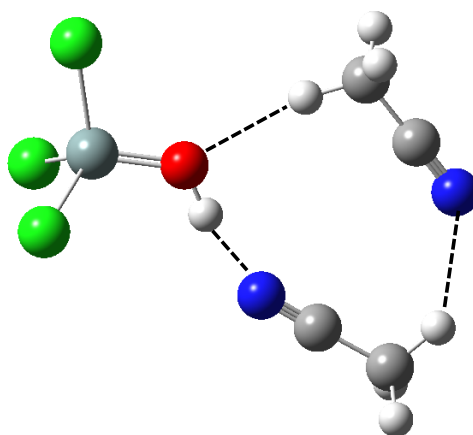


Fig. 4.12 The optimized structure of SiCl_3OH and CH_3CN
 (The black dot lines show the interaction between the hydroxy group of CH_3CN molecules and the hydrolysis product.)

Then, in order to consider whether SiCl_3OH adsorbs on the electrode surface during the electrodeposition or not, the structure of SiCl_3OH adsorbing on the surface was considered, in which the surface was considered as the Si cluster Si_9H_{14} . The optimized structure was shown as Fig. 4.13, and the adsorption energy was -493.0 kJ/mol. These

results suggest that the CH_3CN molecules would get close to the surface because the formed SiCl_3OH attracts them to be stabilized described above. This phenomenon would result in the incorporation of the solvents into the electrodeposited films during the electrodeposition, suggesting the increase of the carbon content in the films with the increase of the water content in the solvent.

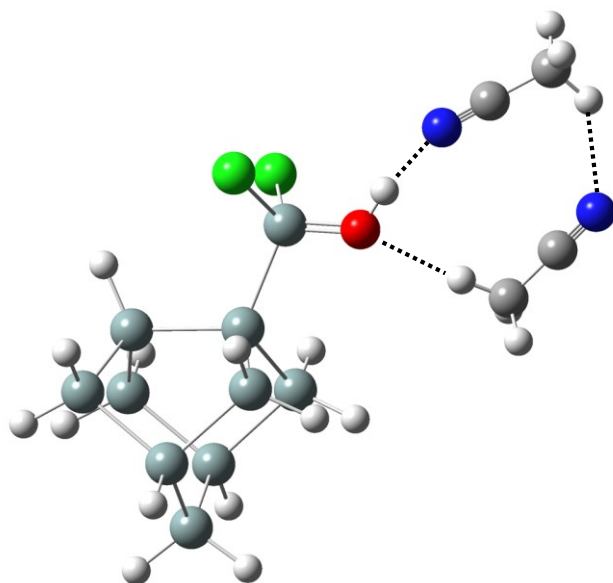


Fig. 4.13 The stable structure between the hydrolysis product of SiCl_4 and Si surface (It is assumed that a Cl^- ion of SiCl_3OH , which is the hydrolysis product of SiCl_4 , was released in order to bond with the Si surface. The black dot lines show the interaction between the CH_3CN molecules and the hydrolysis product.)

This hydrolysis reaction is considered to be continuously progressed after the formation of SiCl_3OH as follow's equation [12]. The energy diagram of each reaction is also shown in Fig. 4.14

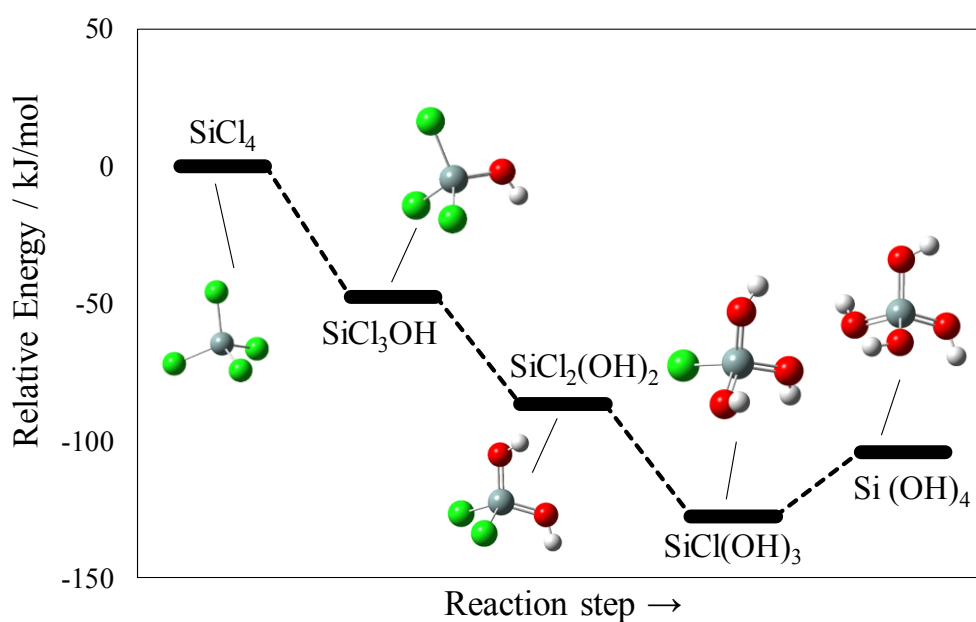
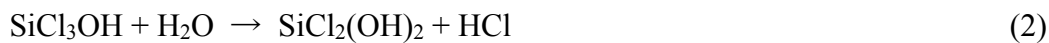


Fig. 4.14 Energy profiles in the hydrolysis reaction

From this energy profile, the continuous hydrolysis reaction will be occurred. Then, the structure of each hydrolysis product on the surface were assumed. The adsorption energy of $\text{SiCl}(\text{OH})_3$ and $\text{Si}(\text{OH})_4$ on the surface was -124.4 and -83.1 kJ/mol, respectively, in which the CH_3CN molecules interacted with the hydroxy group in each hydrolysis product.

4.3.2 Analysis of the reduction mechanism of SiCl_4

The reduction mechanism of SiCl_4 was analyzed because SiCl_4 was the dominant precursor in the Si electrodeposition, whereas the hydrolysis reaction was proceeded. Figure 4.15 shows a current transient and mass changes from the open circuit potential to -3.0 V vs Ag/Ag^+ .

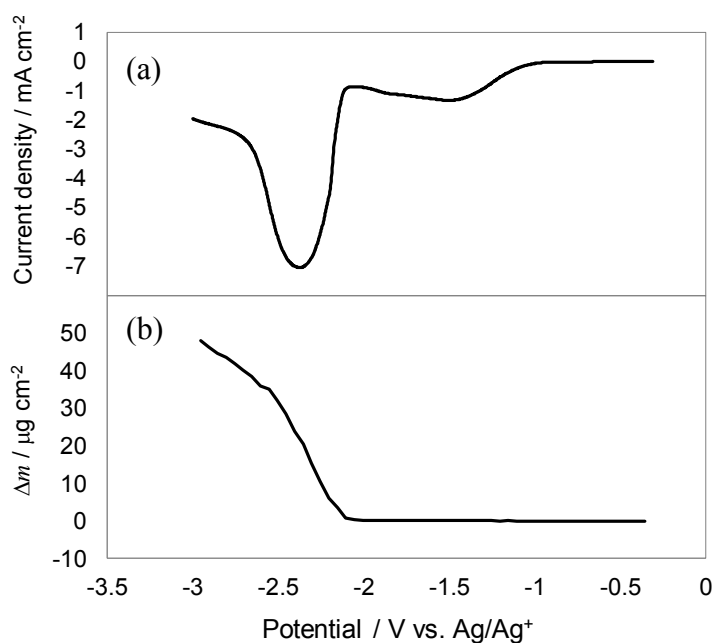


Fig. 4.15 (a) Linear sweep voltammogram, scan rate = 10 mVs^{-1} , (b) Mass changes during linear sweep voltammogram in the dehydrated CH_3CN bath

This linear sweep voltammetry (LSV) measurement identified several reduction peaks: -1.0 , -1.8 (very small changes), and -2.1 V vs Ag/Ag^+ . No mass changes were taken place at either -1.0 or -1.8 V vs Ag/Ag^+ , indicating that the electroactive species were reduced at these points but not deposited. On the other hand, mass changes accompanied the reduction peak at -2.1 V vs Ag/Ag^+ , which was attributed to the deposition of Si (whose existence was confirmed by XPS). These distinct peaks suggest that this Si

reduction process involves multiple elementary steps with stable intermediates before the deposition. In other words, before reaching -2.1 V vs. Ag/Ag^+ , electroactive species of SiCl_4 in this system receive electrons to form some type of intermediate. This multiple step was also suggested by J. Gobet et al. [3]. They electrodeposited Si from tetrahydrofuran with silicon halides, and reported that all the electrons were probably transferred in a multistep process. After sweeping to -2.1 V vs. Ag/Ag^+ in the LSV measurement, some films considered as the intermediates were observed to form. These films were rinsed off in the cleaning process of the samples after the LSV measurement, suggesting that they seemed not to adhere to the electrode surface. This phenomenon was corresponding to the result of the EQCM measurement which showed that there were no mass changes until -2.1 V vs. Ag/Ag^+ . The XPS analysis of those films, which are only vacuumed after the measurement to dry the residue organic solvents instead of the cleaning using the dehydrated CH_3CN , showed the existence of Si and Cl (Fig. 4.16), indicating that the compounds of Si and Cl were the intermediate species.

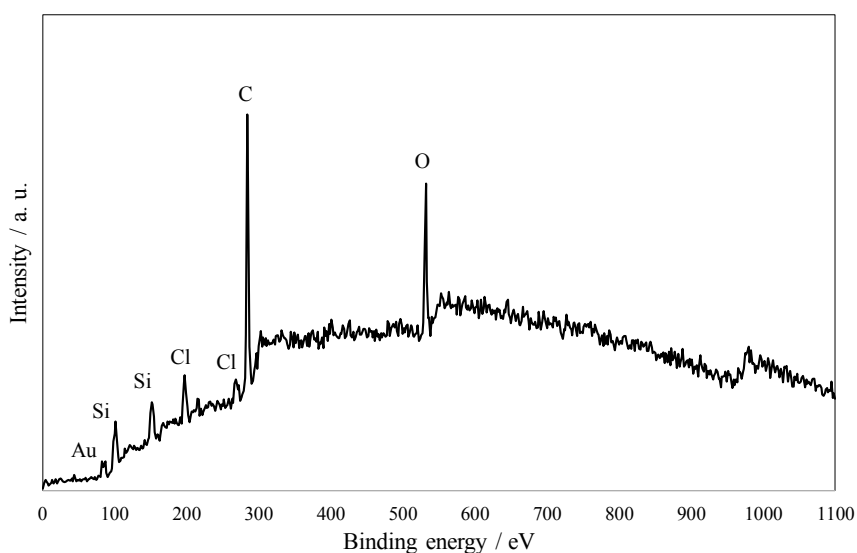


Fig. 4.16 The XPS result of the electrodeposited films after sweeping to -2.1 V in the linear sweep voltammetry in the dehydrated CH_3CN bath

In order to elucidate the kinds of intermediate species formed, the films electrodeposited at -2.1 V vs. Ag/Ag^+ for several minutes were analyzed by Raman spectroscopy (Fig. 4.17).

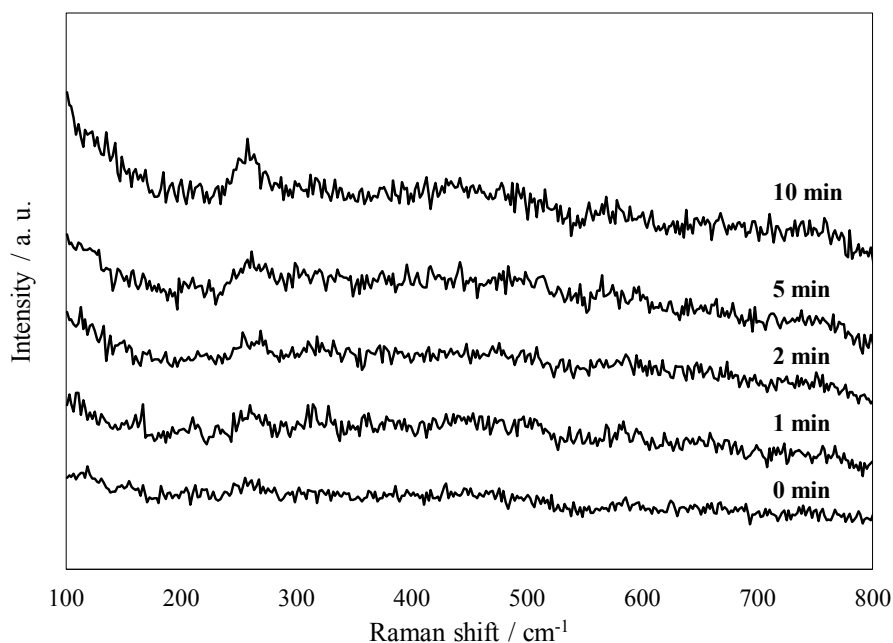


Fig. 4.17 The time dependence of Raman spectra of the films electrodeposited at -2.1 V in the dehydrated CH_3CN bath

With increasing deposition time, a peak appeared at around 230 cm^{-1} . Since the samples were carefully cleaned before the measurement, and there were no peaks at 0 min, this peak could not have been derived from the solvent. Instead, this peak was assigned to reduction products of the electroactive species such as SiCl_4 . Indeed, there are several reports about Si species with $-\text{SiCl}_3$ bonding that have spectral peaks at around 230 cm^{-1} [19-21] In this case, Si species with $-\text{SiCl}_3$ bonding such as Si dimer or multimer could be formed as intermediate states during the electrodeposition. A similar reduction behavior of dichlorosilanes to form Si dimer has been reported in the research of organic electrolytic synthesis, even though the functional groups of these dichlorosilanes are not $-\text{Cl}$. According to Wang et al [22], in the electroreduction of organo-substituted

dichlorosilanes in tetrahydrofuran, the $RR'SiCl_2$ species are reduced to $R_2R'_2Si_2Cl_2$ by radical coupling or nucleophilic substitution with the release of Cl^- , and other similar studies have also been reported [23-24].

The Raman spectra also showed that these intermediates of Si multimers are electrochemically reduced to form a-Si, as shown in Fig. 4.18. From these results, the following reduction steps are proposed. $SiCl_4$ is first reduced to produce intermediate states containing $-SiCl_3$, and this intermediate formation process continues to generate Si multimers, which are finally electrodeposited as a-Si on the substrate with the release of Cl^- ion

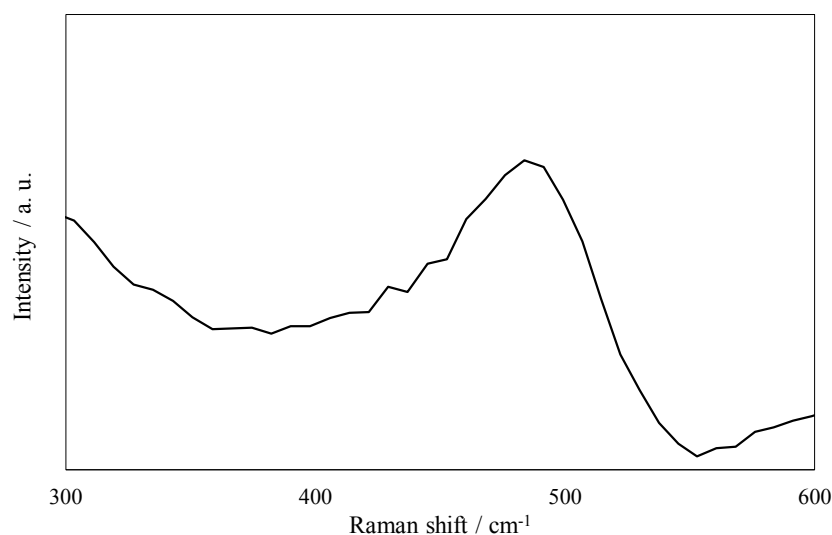


Fig. 4.18 Raman spectrum of the films electrodeposited at -2.3 V at 1000 $mC\ cm^{-2}$ in the dehydrated CH_3CN bath (The peak around $480\ cm^{-2}$ was appeared, meaning the electrodeposition of a-Si.)

It has also been reported that these electrodeposited Si films in organic solvents might be a semiconductor [8]. In order to check the nature of semiconductor, a halogen lamp was used to irradiate the sample during the electrodeposition, with reference to the photo-assisted electrodeposition of semiconductors. The current density changes with and without the light irradiation are shown in Fig. 4.19.

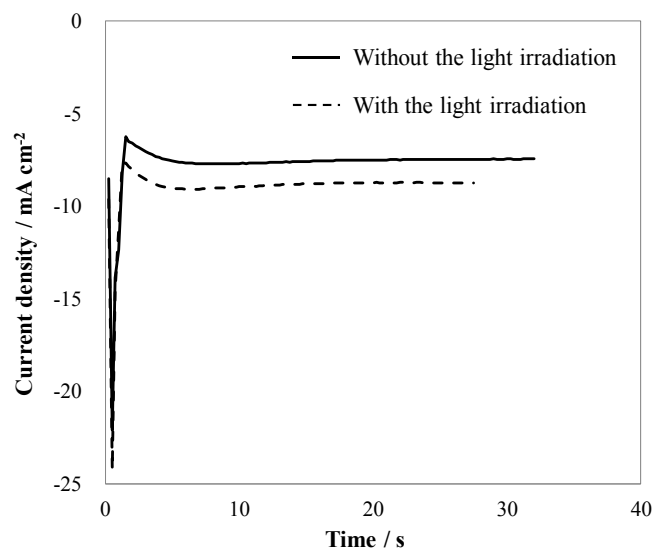


Fig. 4.19 The current density changes during the electrodeposition at $-2.3\text{ V vs. Ag/Ag}^+$ at 500 mC cm^{-2} in the dehydrated CH_3CN with and without the light irradiation

The current density during the electrodeposition with the light irradiation was larger than that without the light irradiation and it was observed the decrease of the crack formation during the electrodeposition. In addition, the cross-sectional view (Fig. 4.21) at the crack with the light irradiation condition seems to be more compact and thicker than that without light irradiation. These mechanisms with the light irradiation will be described in detail in Chapter 5. From these results, it should be mentioned here that the electrodeposited films seem to be semiconductors.

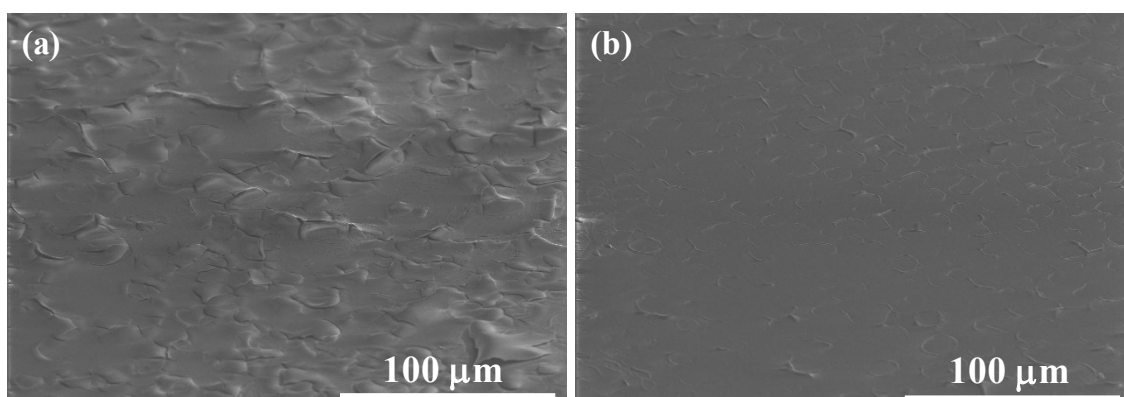


Fig. 4.20 The morphology of the film electrodeposited at $-2.3\text{ V vs. Ag/Ag}^+$ at 500 mC cm^{-2} in the dehydrated CH_3CN (a) without and (b) with the light irradiation

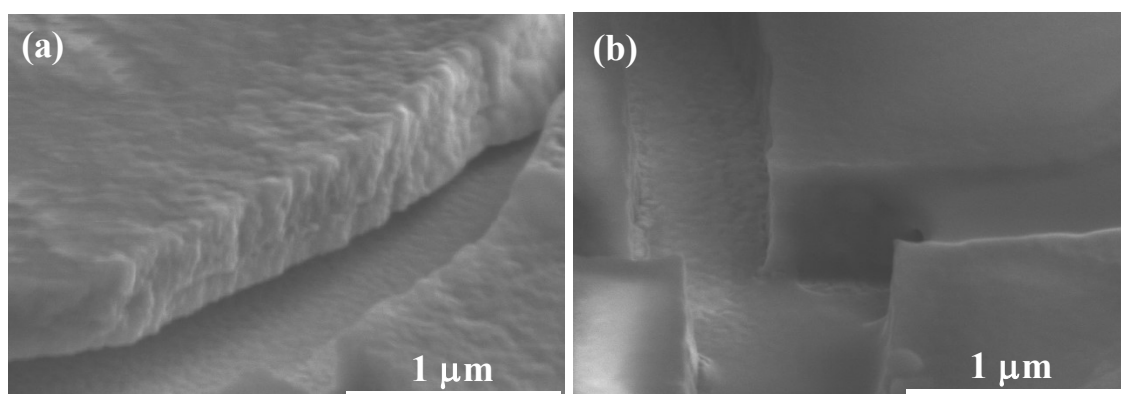


Fig. 4.21 The morphologies of the films electrodeposited at -2.3 V at 500 mC cm^{-2} in the dehydrated CH_3CN bath with and without the light irradiation

Conclusions

This chapter described the Si electrodeposition in organic solvents, and the influence of the solvent species and the water content on the film composition, and the reduction mechanism of SiCl_4 in the Si electrodeposition with organic solvents were mainly described.

It was revealed that the water content affected to the film composition, especially the carbon content, while there is small influence of solvent species. With the increase of the water content in the solvents, the carbon content in the films increased. The molecular level mechanism in this phenomenon was suggested that the solvent molecules of CH_3CN could get close to the electrode surface during the electrodeposition due to the strong interaction of solvents molecules with the hydrolysis product of the SiCl_4 under the water existence condition. In order to decrease the impurities inclusion into the films, the suppression of above mechanism can potentially be a way as well as the annealing treatment. It was also shown by the measurement using the rotating disk electrode to enhance the diffusion of SiCl_4 , which indicated the enhancement of the reduction of SiCl_4 would improve the film composition. In addition, the measurement of the light irradiation supported that mechanism.

As for the reduction mechanism of SiCl_4 , it was confirmed that there was the intermediate state formation step, in which Si species with SiCl_3 bonding were formed.

Form this chapter, the analysis methods for the reaction mechanism used in ionic liquid system can be applied to the other solvents, and the analysis method described in this chapter would be potentially be a way for the reaction mechanism analysis of other electrodeposition systems in organic solvents as well as the formation of films.

References

- [1] Y. Takeda, R. Konno, and O. Yamamoto, *J. Electrochem. Soc.*, **128**, 1221 (1981)
- [2] A. K. Agrawal and A. E. Austin, *J. Electrochem. Soc.*, **128**, 2292 (1981).
- [3] J. Gobet and H. Tannenberger, *J. Electrochem. Soc.*, **135**, 109 (1988).
- [4] Y. Nishimura and Y. Fukunaka, *Electrochim. Acta*, **53**, 111 (2007).
- [5] Y. Nishimura and Y. Fukunaka, *ECS Trans.*, **6**, 77 (2007).
- [6] R. Epur, M. Ramanathan, F. R. Beck, A. Manivannan, and P. N. Kumta, *Mater. Sci. Eng., B*, **177**, 1157 (2012).
- [7] D. Elwell, *J. Cryst. Growth*, **52**, 741 (1981)
- [8] T. Munisamy and A. J. Bard, *Electrochim. Acta*, **55**, 3797 (2010).
- [9] J.P. Nicholson, *J. Electrochem. Soc.*, **152**, C795 (2005).
- [10] M. Bechelany, J. Elias, P. Brodard, J. Michler, and L. Philippe, *Thin Solid Films*, **520**, 1895 (2012).
- [11] C. Vichery, V. Le Nader, C. Frantz, Y. Zhang, J. Michler, and L. Philippea, *Phys.Chem.Chem.Phys.*, **16**, 22222 (2014).
- [12] S. K. Ignatov, P. G. Sennikov, A. G. Razuvaev, L. A. Chuprov, O. Schrems, and B. S. Ault, *J. Phys. Chem. A*, **107**, 8705 (2003).
- [13] M. J. Frisch, G. W. Trucks, H. B. Schlegel, G. E. Scuseria, M. A. Robb, J. R. Cheeseman, G. Scalmani, V. Barone, B. Mennucci, G. A. Petersson, H. Nakatsuji, M. Caricato, X. Li, H. P. Hratchian, A. F. Izmaylov, J. Bloino, G. Zheng, J. L. Sonnenberg, M. Hada, M. Ehara, K. Toyota, R. Fukuda, J. Hasegawa, M. Ishida, T. Nakajima, Y. Honda, O. Kitao, H. Nakai, T. Vreven, J. A. Montgomery, Jr., J. E. Peralta, F. Ogliaro, M. Bearpark, J. J. Heyd, E. Brothers, K. N. Kudin, V. N. Staroverov, R. Kobayashi, J. Normand, K. Raghavachari, A. Rendell, J. C. Burant, S. S. Iyengar, J. Tomasi, M. Cossi, N. Rega, J. M. Millam, M. Klene, J. E. Knox, J. B. Cross, V. Bakken, C. Adamo, J. Jaramillo, R. Gomperts, R. E. Stratmann, O. Yazyev, A. J. Austin, R. Cammi, C. Pomelli, J. W. Ochterski, R. L. Martin, K. Morokuma, V. G. Zakrzewski, G. A. Voth, P. Salvador, J. J. Dannenberg, S. Dapprich, A. D. Daniels, Ö. Farkas, J. B. Foresman, J. V. Ortiz, J. Cioslowski, and D. J. Fox, Gaussian 09, Revision A.01, Gaussian, Inc., Wallingford, CT (2009).
- [14] A.D. Becke, *J. Chem. Phys.*, **98**, 5648 (1993).
- [15] C. Lee, W. Yang, and R.G. Parr, *Phys. Rev. B*, **37**, 785 (1988).

- [16] B. Mennucci, *WIREs Comput. Mol. Sci.*, **2**, 386 (2012).
- [17] Katsuei Ishida, Annual report, i09sf, *TAIYO YUDEN CO., LTD*, (2009)
- [18] C. Puglisi, L. Sturiale, and G. Montaudo, *Macromolecules*, **32**, 2194 (1999).
- [19] M. A. Qtaitat, A. B. Mohamad, T. A. Mohamed, D. J. Gerson, A. Q. McArver, M. S. Afifi, and J. R. Durig, *Spectrochim. Acta, Part A*, **50**, 621 (1994).
- [20] W. Malisch, H. Jehle, S. Möller, G. Thum, J. Reising, A. Gbureck, V. Nagel, C. Fickert, W. Kiefer, and M. Nieger, *Eur. J. Inorg. Chem.*, **1999**, 1597 (1999).
- [21] T. H. Johansen, K. Hassler, A. D. Richardson, G. Tekautz, and K. Hagen, *Spectrochim. Acta, Part A*, **61**, 1307 (2005).
- [22] X. Wang, Y. Yuan, and I. Cobasso, *J. Electrochem. Soc.*, **152**, 259 (2005).
- [23] M. Umezawa, M. Takeda, H. Ishikawa, T. Ishikawa, T. Koizumi, T. Fuchigami, and T. Nonaka, *Electrochim. Acta*, **36**, 621 (1991).
- [24] S. Kashimura, M. Ishifune, N. Yamashita, H-B. Bu, M. Takebayashi, S. Kitajima, D. Yoshiwara, Y. Kataoka, R. Nishida, S. Kawasaki, H. Murase, and T. Shono, *J. Org. Chem.*, **64**, 6615 (1999).
- [25] A. J. Bard and L. R. Faulkner, *Electrochemical Methods, Fundamentals and Applications* (John Wiley and Sons, NY), Chapter 18 (2001).
- [26] S. Yoshihara, K. Endo, E. Sato, and J. O'M. Bockris, *J. Electroanal. Chem.*, **372**, 91 (1994).
- [27] Y. L. Kawamura, T. Sakka, and Y. H. Ogata, *J. Electrochem. Soc.*, **152**, C701 (2005).
- [28] D. W. Redman, H. J. Kim, K. J. Stevenson, and M. J. Rose, *J. Mater. Chem. A*, **4**, 7027 (2016).

Chapter 5:

***Study for The Fabrication of Si Thin Film Solar
Cell Devices***

5.1 Introduction

In this chapter, the study for the fabrication of Si thin film solar cells as one example of the application of the electrodeposited Si thin films by electrodeposition is described. It is important to electrodeposit Si for considering the application as well as the reaction mechanism analysis discussed in the previous chapters.

As the author mentioned in previous chapters, electrodeposition can potentially be a way to fabricate thin film solar cells because it can help to fabricate the nanostructures in a large area without using high voltage and high vacuum equipment. In applying the electrodeposited thin films for solar cells, the impurities inclusion and the crack formation and/or porous structure [1-6] is problem, and it is necessary to electrodeposit doped thin films. As for the improvement of the morphology, there are some reports that the mixed electrolyte of ionic liquids and organic solvents [7], and the selectivity of the supporting electrolyte [8] would be helpful to obtain the relatively smooth surface. On the other hand, it is necessary to control the morphology by understanding the growth mechanism of Si thin films. For this, T. Munisamy et al. [2] has studied the initial growth of the electrodeposited Si in acetonitrile and tetrahydrofuran containing tetrabutylammonium chloride with SiCl_4 and SiHCl_3 . However, the above study did not furnish sufficient data for the precise control of Si electrodeposition. As for the doped films, J.P. Nicholson [9] has reported as one trial study the doped films in organic solvents would be possible to add the dopant such as PCl_5 and AlCl_3 , although the effects of dopant on electric properties have not been discussed. Further development of Si electrodeposition in ionic liquids for the fabrication of solar cells based on Si thin films requires the establishment of methods for controlling their growth and doping.

To address this issue, in this chapter, the influence of electrodeposition parameters on Si thin film morphology by analyzing the initial-stage growth of these films was investigated to control the growth process of Si thin films, and the effects of dopant and the electric properties of doped thin films were also focused on as the initial study to form doped thin films.

5.2 Experimental

The electrochemical cell used in this study is schematically illustrated in Fig. 5. 1. TMHATFSI, which is received from Stella Chemifa Corp) containing 0.5 M SiCl_4 was used as the ionic liquid, and electrodeposition was performed using a three-electrode system. Three substrates were used as working electrodes, namely Au film (100 nm-thick) on mica and Au film (200 nm-thick) on a Si (111) substrate with a Cr adhesion layer (10 nm-thick), both deposited by electron beam evaporation (ULVAC, EBX-6D), and a highly doped n-type Si substrate (100) with a resistivity of $\sim 1.9 \times 10^{-3} \Omega \text{ cm}^{-1}$. A Pt wire was used as the counter electrode, and a Ag/Ag^+ electrode was used as a reference. The Au film on mica was used to analyze early-stage electrodeposition due to exhibiting a very smooth surface ($R_a = 0.20 \text{ nm}$; Fig. 5.2) and thus being suitable for the observation of initially produced Si grains. Figure 5.2 also illustrates the roughness of Au films formed on Cr/Si and pure Si.

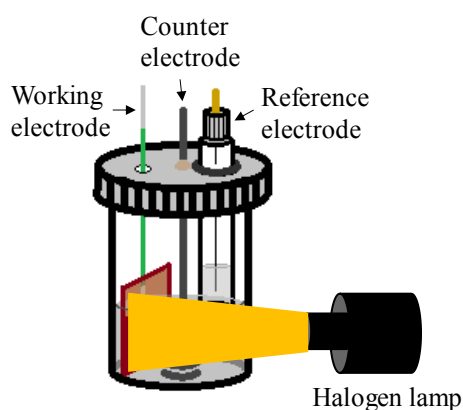


Fig. 5.1 Schematic illustration of the electrochemical cell, in which a halogen lamp was used only in the electrodeposition with the light irradiation

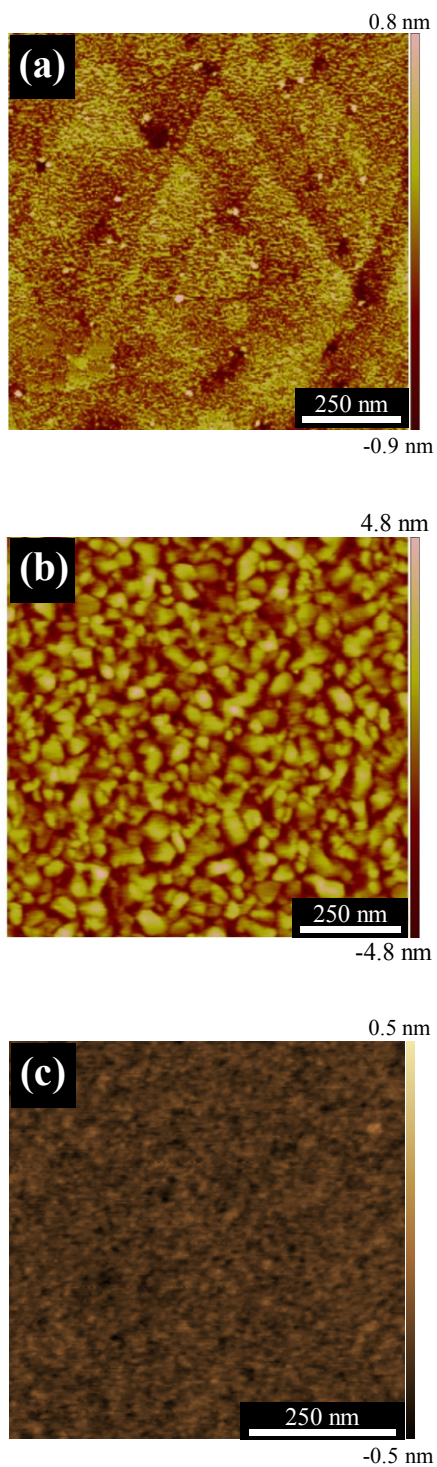


Fig. 5.2 AFM images of each substrate; (a) Au / mica ($R_a = 0.20$ nm), (b) Au / Cr / Si ($R_a = 2.2$ nm), and (c) Si ($R_a = 0.15$ nm)

In the formation of n-type thin films, 8.8×10^{-4} M AlCl_3 was used as p-type dopant, and as for p-type thin films, 8.8×10^{-7} M PCl_5 was used as n-type dopant, in which dopant was added to the ionic liquids of TMHATFSI with 0.5 M SiCl_4 .

All electrochemical measurements were performed at 40 °C in an Ar-filled glove box using a potentiostat/galvanostat (Hokuto Denko, HZ-7000). A quartz halogen lamp (30 W m^{-2}) was employed as a light source.

Sample morphology was characterized by high-resolution scanning electron microscopy (Hitachi High-Technologies, S5500). After exposure to air, as-deposited Si films were subjected to rapid 1 h annealing (ULVAC, MILA 3000) in Ar/ H_2 (90/10, v/v) at 700 °C. Seebeck coefficient and resistivity were measured by the two-probe method in a steady state using a self-made apparatus [10]. When measuring Seebeck coefficient, the effects of the substrate were eliminated which will be described in Results and Discussion section. Film compositions were determined by glow discharge optical emission spectrometry (GDOES; Rigaku, GDA 750).

5.3 Results and Discussion

5.3.1 The control of the film structure control

It has been shown that the electrodeposited films they became rougher and more porous with increasing electrodeposition time, i.e., with increasing film thickness. Figure 5.3 shows the electrodeposited films at 500 and 1500 mC cm^{-2} .

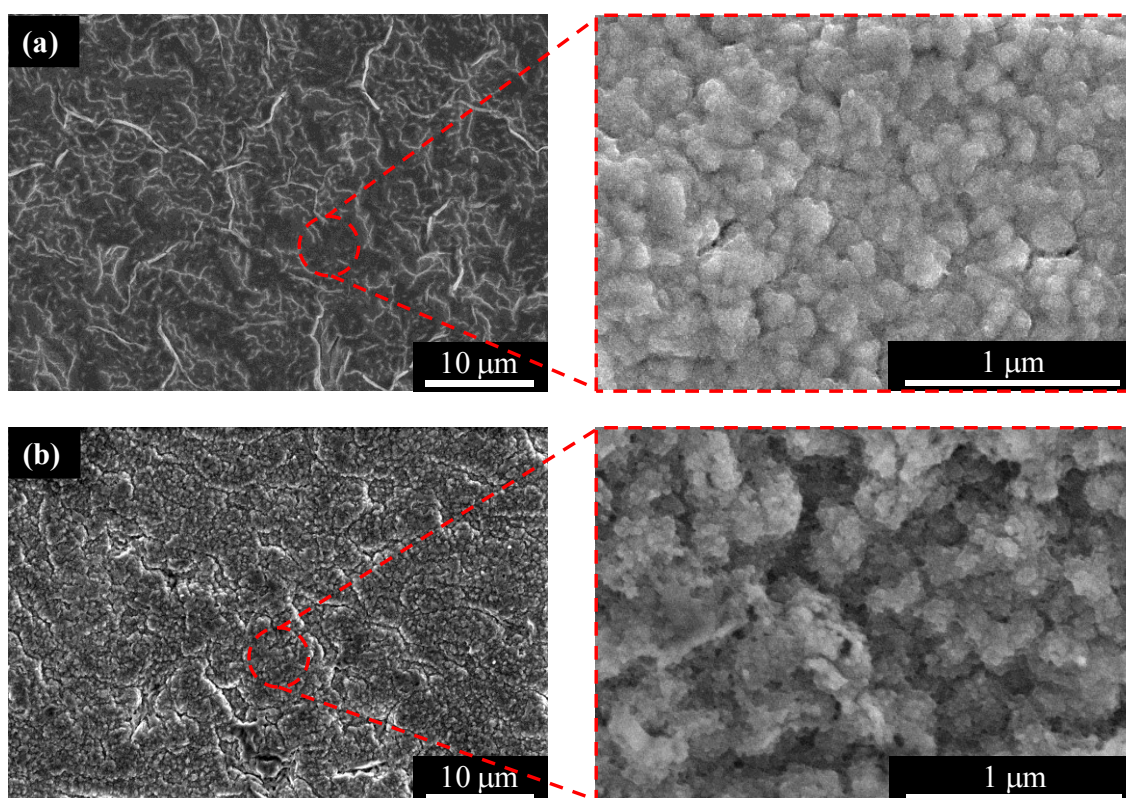


Fig. 5.3 SEM images of the films electrodeposited at $-2.3 \text{ V vs. Ag/Ag}^+$
(a) at 500 mC cm^{-2} , (b) at 1500 mC cm^{-2}

The thickness of the electrodeposited films is estimated approximately 150 and 450 nm at 500 and 1500 mC cm⁻², respectively by Faraday's law.

$$Ah\rho = \frac{M_{Si} Q}{zF} \quad (5.1)$$

where,

A = the electrodeposited area

h = the thickness of the electrodeposited Si

ρ = the density of Si

M_{Si} = the molar mass of Si

Q = the charge density

z = the number of the electron

F = the Faraday constant

In order to understand the growth process of Si, the very initial stage during Si electrodeposition was analyzed. Figure 5.4 shows the morphologies of the films electrodeposited at the very initial stage at -2.3 V vs. Ag/Ag⁺, in which Au formed on Mica was used. With the increase of the charge density from 0 to 10 mC cm⁻², it was observed the electrodeposited Si covers the electrode surface. However, it was confirmed that there were voids or areas where Si grains were not formed at the charge density of 50 mC cm⁻² (red dots circle in Fig. 5.4 (d)). These tendencies were same when the cleaning process before the electrodeposition was changed; the Au substrate are usually cleaned by O₂ plasma ashing to remove the impurities on the surface. As other cleaning processes, wet cleaning processes using acid solutions and/or ethanol with O₂ plasma ashing. Therefore, it could be concluded that Si was not electrodeposited in these areas, which was also confirmed by EDX analysis (Fig. 5.5).

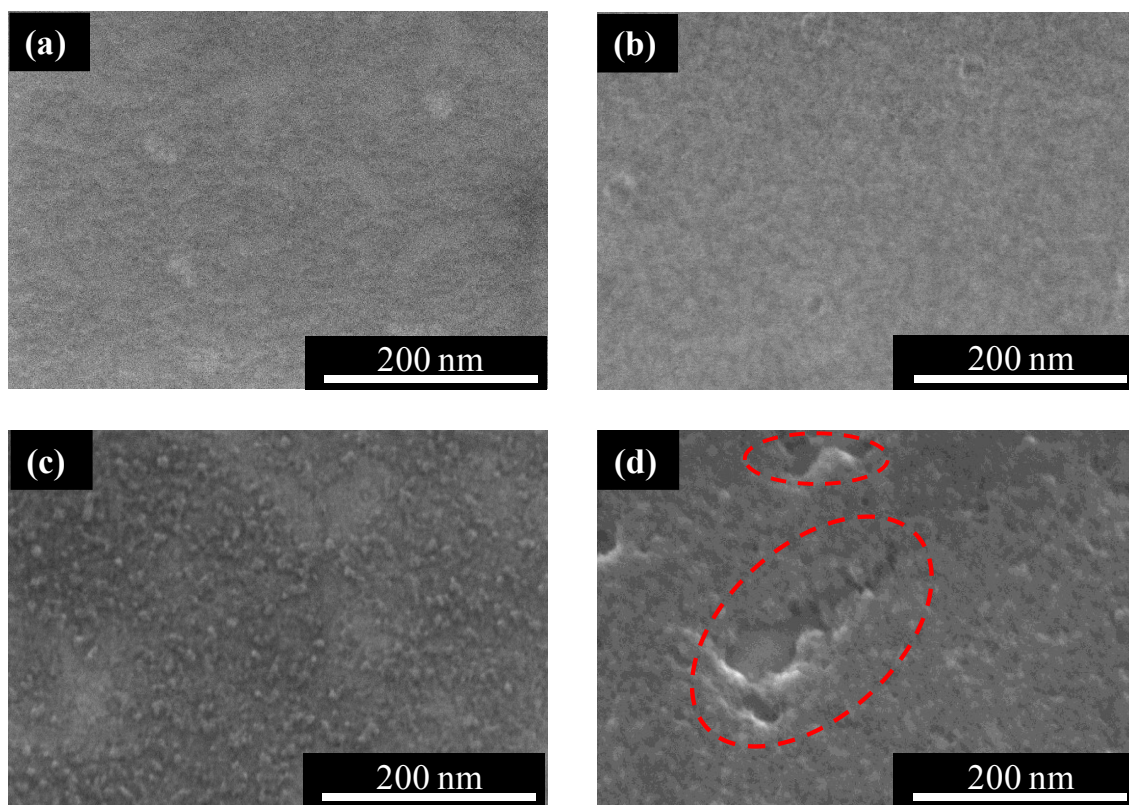


Fig. 5.4 SEM images of the films electrodeposited at $-2.3\text{ V vs. Ag/Ag}^+$ at the very initial stage (a) before electrodeposition, (b), (c), and (d) after electrodeposition; (b) at 5 mC cm^{-2} (approximately 1.5 nm), (c) at 10 mC cm^{-2} (approximately 3.0 nm), (d) at 50 mC cm^{-2} (approximately 15 nm)

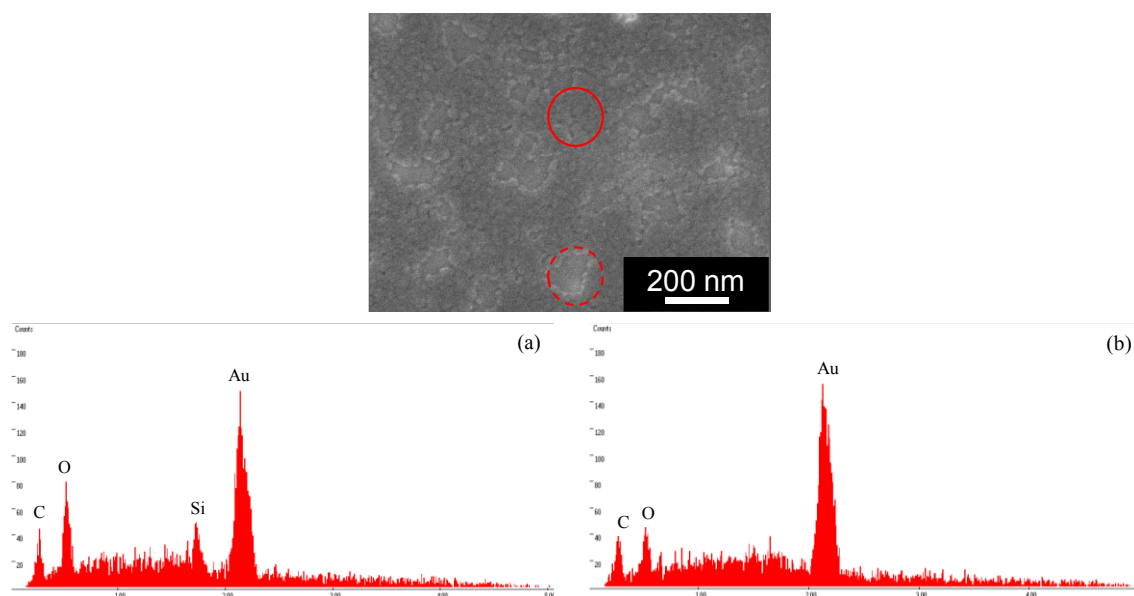


Fig. 5.5 EDX analysis results of the films electrodeposited at $-2.3\text{ V vs. Ag/Ag}^+$ at 50 mC^{-2} at the area (a) where Si is electrodeposited (red solid circle), and (b) where Si is not electrodeposited (red dot circle)

From these results, the nuclei of Si were grown in two dimensions when the potential of $-2.3\text{ V vs. Ag/Ag}^+$ was applied, and a lateral growth should be enhanced if SiCl_4 exists enough to react at the electrode surface. In this case, it was also confirmed the diffusion limited phase during the electrodeposition. The current transient during the electrodeposition is shown in Fig. 5.6. As you can see, the current has almost reached the limiting current density around 3 or 4 s. It means that, the ideal two-dimensional and lateral growth can not be occurred in this case. In general, this diffusion limited condition is known to afford rough surfaces. Here, it should be noted that T. Munisamy et al. [2] has reported that the electrodeposited Si should be semiconductor and behaves like an insulator, resulting in the current decay tendency during the electrodeposition. For this, the author also focuses on later.

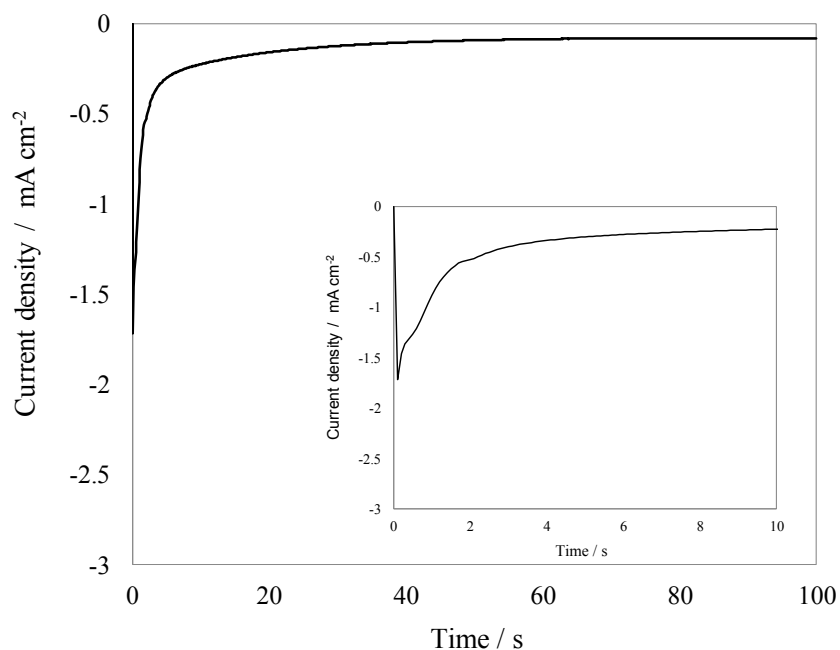


Fig. 5.6 Initial current density changes during the constant potential electrodeposition at $-2.3\text{ V vs. Ag/Ag}^+$ (The inner figure is the enlarged one between $0 \sim 10\text{ s.}$)

As discussed above, the two-dimensional growth was considered at $-2.3\text{ V vs. Ag/Ag}^+$. Therefore, in order to analyze the effect of overpotential at the initial stage, Si electrodeposition was investigated at $-3.0\text{ V vs. Ag/Ag}^+$, since large overpotentials typically result in increased numbers of nuclei and enhance three-dimensional growth. [11]. Figure 5.7 shows the morphologies of films electrodeposited on Au/mica at $-3.0\text{ V vs. Ag/Ag}^+$ at the initial stage.

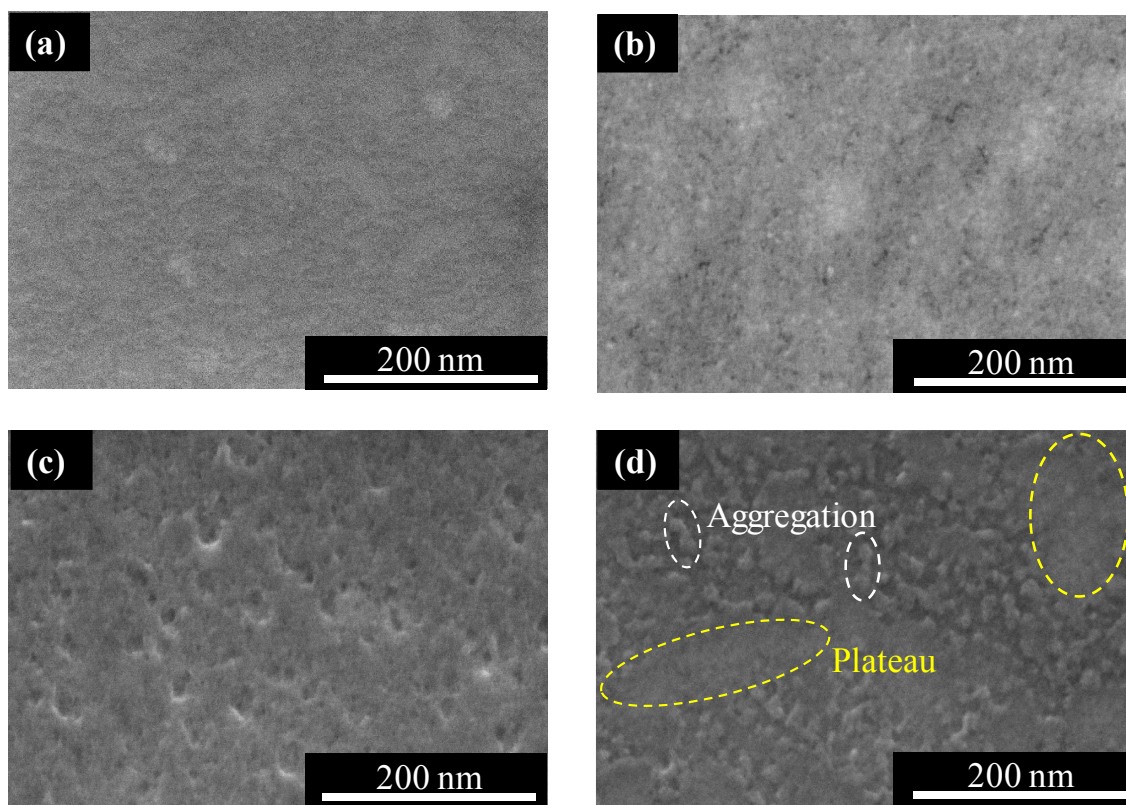


Fig. 5.7 SEM images of the films electrodeposited at $-3.0\text{ V vs. Ag/Ag}^+$ at the very initial stage (a) before electrodeposition, (b), (c), and (d) after electrodeposition; (b) at 5 mC cm^{-2} (approximately 1.5 nm), (c) at 10 mC cm^{-2} (approximately 3.0 nm), (d) at 50 mC cm^{-2} (approximately 15 nm)

As the charge density was increased from 0 to 10 mC cm^{-2} , the electrodeposited Si covered the electrode surface, although a porous structure was formed at 10 mC cm^{-2} . As electrodeposition was continued (at 50 mC cm^{-2}), two phases of growing process of aggregation and plateau appeared, with the plateau considered to be formed after aggregation. Thus, a relatively smooth surface would be obtained if the plateau covered the electrode surface. However, as described above, homogeneous growth was suppressed under the diffusion-limited conditions, with this limitation being more pronounced than in the case of $-2.3\text{ V vs. Ag/Ag}^+$ due to the applied potential being more negative. For considering forming the smooth surface, a periodic reverse (PR) electrodeposition was applied. As described above, the current has almost reached the limiting current density

around 3 or 4 s, thus, PR electrodeposition featured the application of a potential for 2 s to electrodeposit Si followed by a 3-s rest phase to recover the cation depletion layer. The recovery of the diffusion rate of SiCl_4 molecules to the electrode surface resulted in the concentration of SiCl_4 at the substrate surface being retained at a relatively high level. Notably, PR electrodeposition conditions were selected in consideration of an appropriate duty ratio it has reported that it would be better to set from 0.2 to 0.6 to retain the concentration of reductant at a relatively high level near the electrode surface during the electrodeposition [12-14]. Therefore, we set 3 s rest phase to recover the depletion layer. The results are shown in Fig. 5.8 and 5.9.

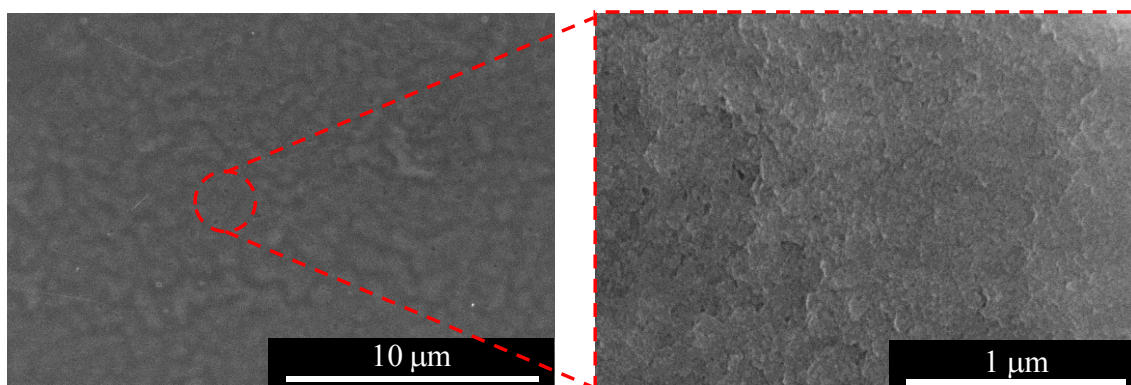


Fig. 5.8 SEM images of the films formed by PR electrodeposition at $-2.3 \text{ V vs. Ag/Ag}^+$ at 1500 mC cm^{-2}

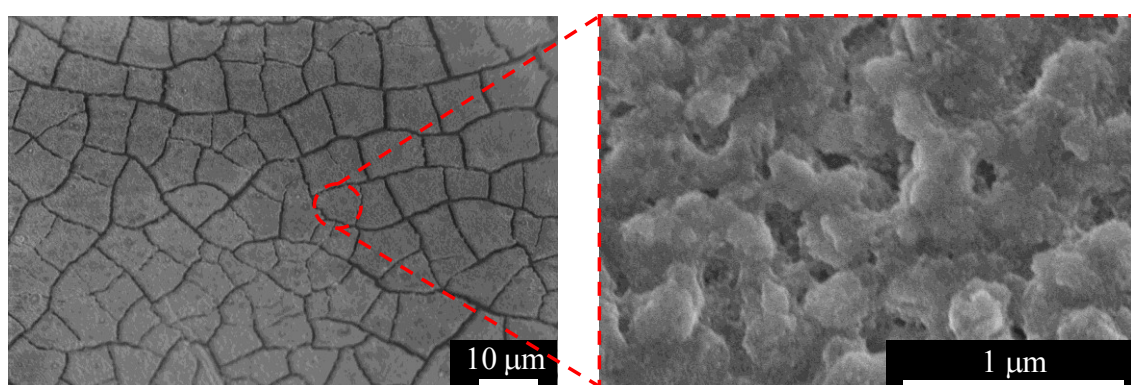


Fig. 5.9 SEM images of the films formed by PR electrodeposition at $-3.0 \text{ V vs. Ag/Ag}^+$ at 1500 mC cm^{-2} .

From these results, the relatively smooth surface was obtained by applying this PR electrodeposition, especially electrodeposited at $-2.3\text{ V vs. Ag/Ag}^+$. At the $-3.0\text{ V vs. Ag/Ag}^+$, a random nucleation for 2 s on the surface might result in the crack formation during electrodeposition.

Another concern is the semiconducting nature of electrodeposited Si thin films. Studies on photo-assisted electrodeposition of semiconductors indicate that light irradiation can produce photoexcited electrons that are consumed by the electrochemical reaction, whereas the growing semiconductor layers might restrict the reaction rate due to their low carrier concentration [15]. Therefore, to determine whether the electrodeposited Si is a semiconductor, PR electrodeposition was performed during light irradiation. Figure 5.10 shows the current density changes during each cycle of PR electrodeposition, revealing that in the absence of the light irradiation, the current density decreased upon cycling, whereas almost no such decrease was observed during the light irradiation. These mechanisms are described as follows.

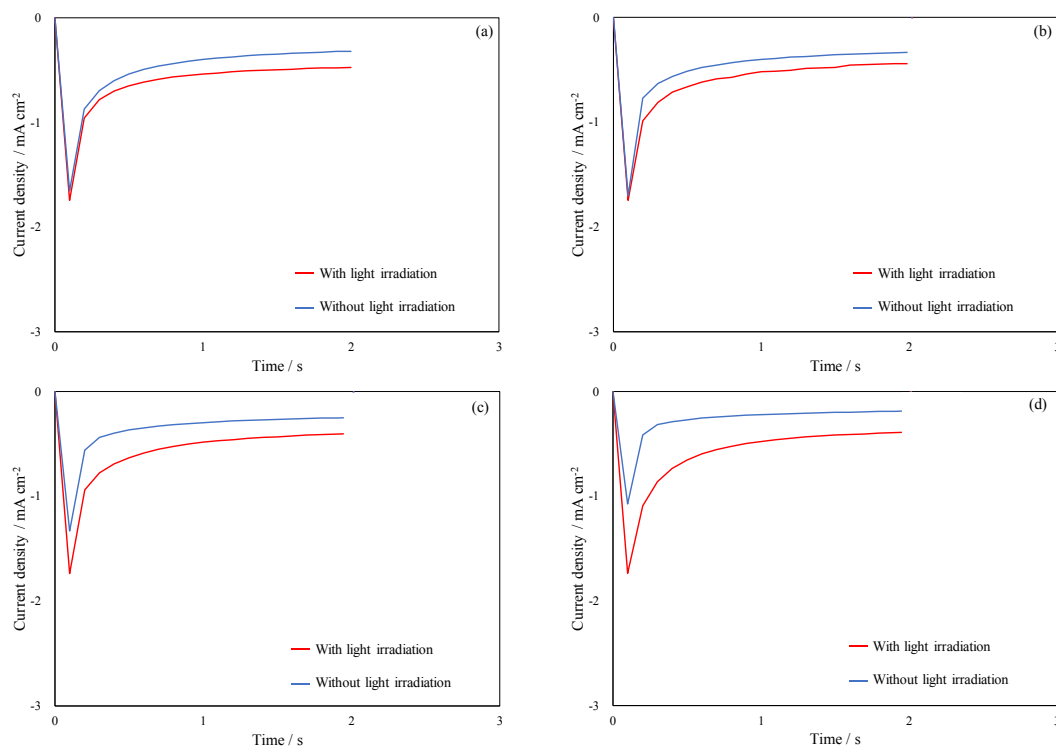


Fig. 5.10 Current density changes during the electrodeposition time at -2.3 V vs. Ag/Ag^+ at (a) 10^{th} , (b) 100^{th} , (c) 1000^{th} , and (d) 2000^{th} cycle in the PR electrodeposition with and without the light irradiation

In order to consider these phenomena, band structures should firstly be described. The general band bending structures in a junction between a semiconductor and solution can be illustrated in Fig. 5.11. After applying the cathodic potential, the bands are bent upward in spite of the nature of semiconductor [15]. Following this knowledge, the band bending during the electrodeposition under the condition in the absence of the light irradiation can be illustrated in Fig. 5.12 [15-19]. At the initial stage, metal of Au contacted to the solution, therefore, there are no band bending (Fig. 5.12 (a)) because there are a lot of free electrons in metals which can accumulate at the surface and move toward the solution side. When the electrodeposited Si is accumulated on the metal substrate, the junction formation between semiconductor and solution should be considered. At the stage during the electrodeposition of very thin Si films, the band bending structure was formed because the interface was consisted of the semiconductor

and solution. However, the electrons could accumulate at the surface when very thin films were electrodeposited, resulting in the behavior of an inert metal electrode (Fig. 5.12 (b) [15]). This tendency would not change depending on the nature of the electrodeposited Si thin films, although the current density should change because electrons are major carrier in n-type semiconductor, while electrons are minor carrier in p-type semiconductor. After the accumulation of the electrodeposited Si, the number of electrons which accumulate at the surface (i_{diff}) decrease (Fig. 5.12 (c)) due to the resistivity of Si even if n-type Si would be electrodeposited, resulting in the decrease of current density.

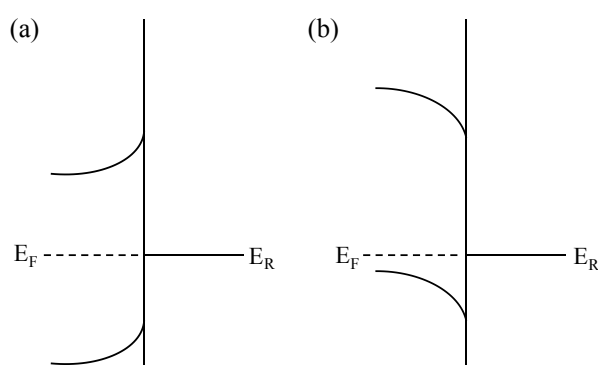


Fig. 5.11 Formation of the junction between (a) n-type, (b) p-type semiconductors and a solution; left side is semiconductor and right side is solution

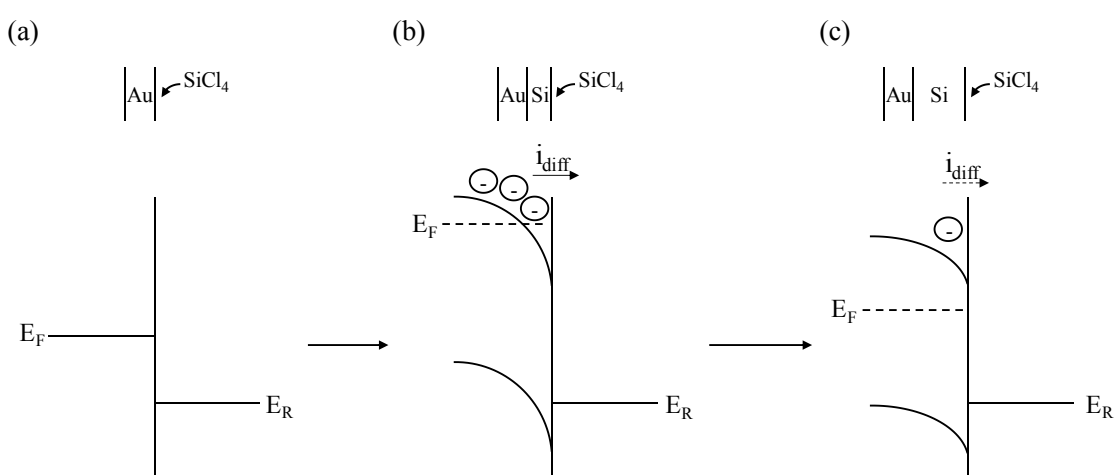


Fig. 5.12 Formation of the junction between the metal, semiconductor and solution during the electrodeposition; left sides are metal and semiconductor and right side is solution

This current density change can also be understood by Eq. (5.2) [15], indicating that the decrease of the current density with decreasing the concentration of electrons at the interface. This phenomenon was observed in the absence of the light irradiation in this case, therefore, the current density decreased upon cycling.

$$i = nFk'_b n_{sc} C_O(x = 0) \quad (5.2)$$

where,

n_{sc} : the concentration of electrons at the interface

k'_b : heterogeneous rate constant

During the light irradiation, the band bending structure is considered to change as shown in Fig. 5.13. The difference between in the absence of the light irradiation and during the light irradiation would be the creation of electron-hole pair as shown in Fig. 5.13 (b). Photo excited electrons in the bulk and at the interface help not to decrease the number of electrons to accumulate at the interface (Fig. 5.13 (c)), resulting in not decreasing the current density during the electrodeposition. In addition, it is known that photo generated holes decrease the flat band potential (E_{fb}) [18], meaning the positively shift of the open circuit potential [19]. It also indicates that the overpotential becomes large with the positively shift of the open circuit potential when a same cathodic potential is applied, which might cause a densification of the electrodeposited films. It could be also indicated by the accumulation of electrons at the interface because the accumulation of electrons causes the increase of over potential. The knowledge in the photo-assisted electrodeposition on semiconductors would help this mechanism. It has been reported that the grain size and precipitated particle density could be controllable with the light irradiation, in which the nucleation process could be the dominant [20-22]. Abovementioned phenomena were observed during the light irradiation in this case, therefore, the current density did not decrease upon cycling, and it increases in same cycle number compared with that in the absence of the light irradiation. The effect of

overpotential might be shown in Fig. 5.14. The morphology seems to become relatively smoother compared with the absence of the light irradiation, though there are not significant change.

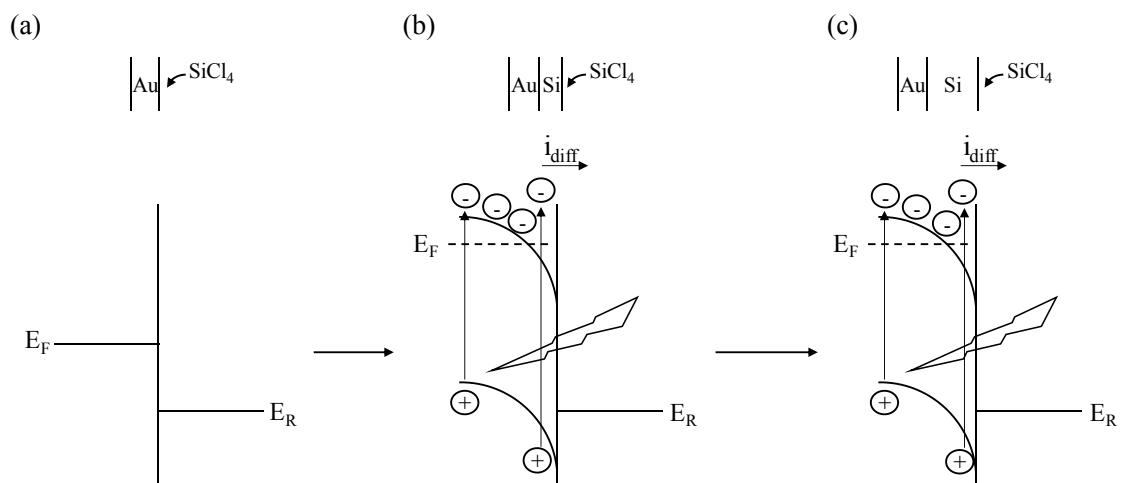


Fig. 5.13 Formation of the junction between the metal, semiconductor and solution during the electrodeposition with the light irradiation; left side is metal and semiconductor and right side is solution

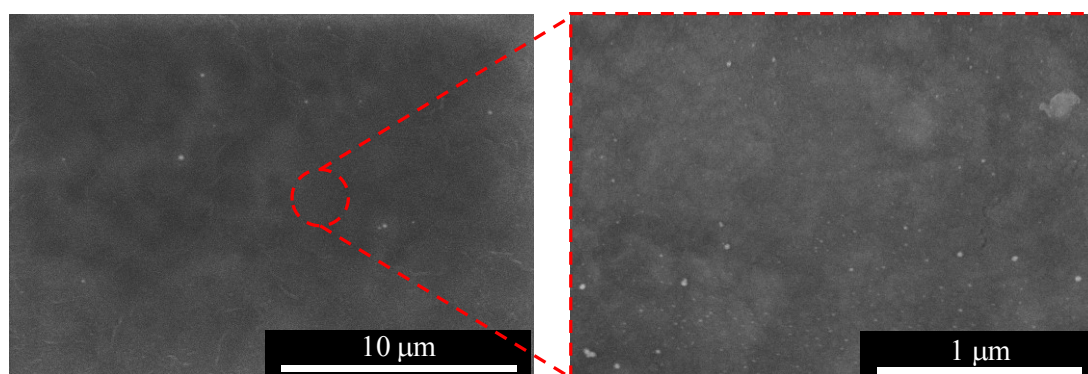


Fig. 5.14 SEM images of the films formed by the PR electrodeposition with the light irradiation

The cross-sectional view of the films electrodeposited by each process are also shown in Fig. 5.15. The increase of film thickness also indicated that the abovementioned mechanism. The films formed by the constant potential electrodeposition was more porous and thicker than the films under PR electrodeposition. It corresponds to the compactness of the films by applying the PR electrodeposition. Therefore, it is suggested that the electrodeposited films would be a semiconductor (not perfectly) to suppress the cathodic reaction during the electrodeposition without the light irradiation.

Form these results, it was confirmed that the current decay during the Si electrodeposition was due to both the diffusion-limited condition and the nature of the semiconductor characteristic of the electrodeposited films.

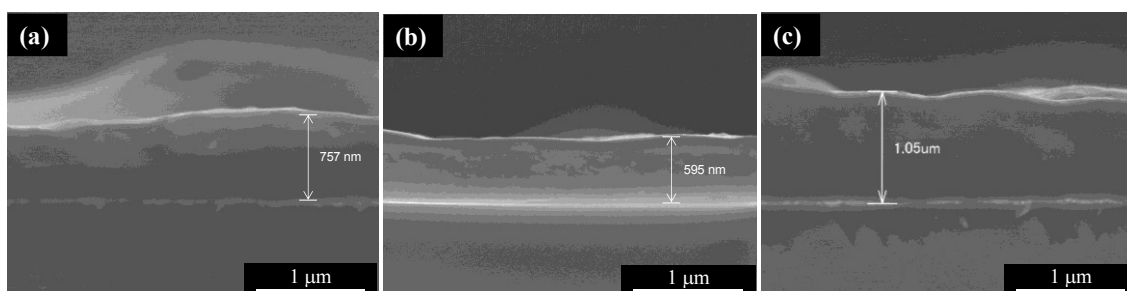


Fig. 5.15 Cross-sectional SEM images of the films formed by (a) the constant potential electrodeposition, (b) the PR electrodeposition in the absence of the light irradiation, (c) the PR electrodeposition with the light irradiation

5.3.2 Doping on the electrodeposited films

As the formation of p-type thin films, there are possibility to dope Al as a dopant because the electrodeposition of Al has been reported in non-aqueous solutions by many researchers [9, 15]. Then, in this thesis work, it is thought that AlCl_3 could be helpful to electrodeposit p-type dopant, and in this formation of p-type thin films, a working substrate of Si was used for considering annealing treatment. In the evaluation of the electric property of the electrodeposited films, it would be better to measure the films with low impurities and a relatively smooth surface. As described in chapter 2, the annealing treatment can decrease impurities in films, however, it was shown that the crack was formed after the annealing treatment in using Au substrate due to the diffusion of Au during the annealing. These optical images are shown in Fig. 5.16.

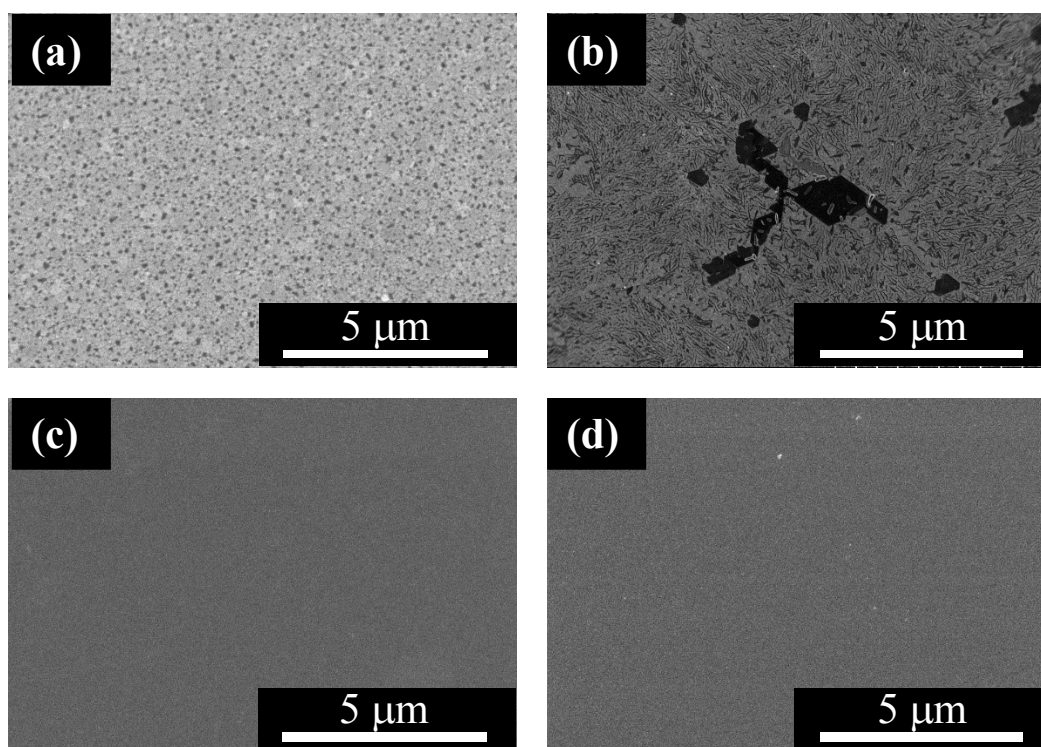


Fig. 5.16 SEM images of each substrate (a), (c) before and (b), (d) after the annealing treatment; (a), (b) Au substrate, (c), (d) Si substrate

In order to understand the possibility of Al electrodeposition in TMHATFSI, the electrochemical behavior was investigated. Figure 5.17 shows the cyclic voltammogram in TMHATFSI with 1.0 M AlCl_3 .

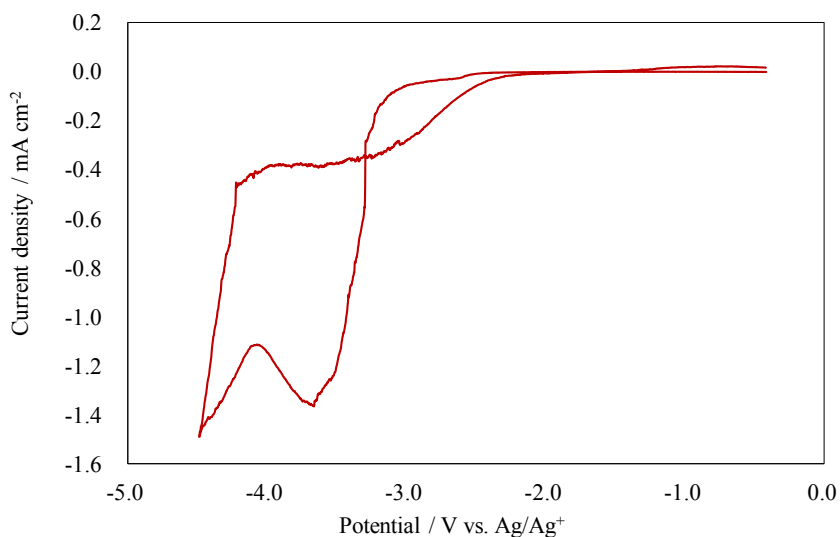


Fig. 5.17 Cyclic voltammogram in 1.0 M AlCl_3 / TMHATFSI on Si substrate

It seems that the increase of the current density around -3.0 V vs. Ag/Ag^+ derived from the cathodic reaction of AlCl_3 , while the second peak would derive from the decomposition of ionic liquids. Then, the electrochemical behavior in mixed electrolyte of SiCl_4 and AlCl_3 was investigated. Figure 5.18 shows the cyclic voltammogram in TMHATFSI with only 0.5 M SiCl_4 and 8.8×10^{-4} M AlCl_3 and 0.5 M SiCl_4 .

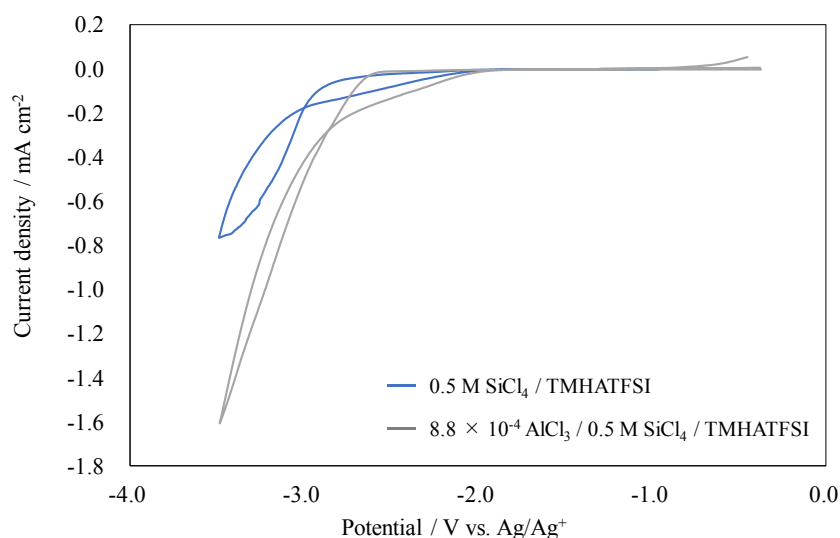


Fig. 5.18 Cyclic voltammogram in 0.5 M SiCl_4 / TMHATFSI and 8.8×10^{-4} M AlCl_3 and 0.5 M SiCl_4 / TMHATFSI

With the addition of AlCl_3 , the current density of the Si electrodeposition increase, suggesting the resistivity of the electrodeposited films became low. Therefore, it could be considered that doped films are formed.

In order to evaluate the electric property of the electrodeposited films, the Seebeck coefficient and resistivity was measured for the films after the annealing treatment, in which the electrodeposition was conducted at -3.0 V vs. Ag/Ag^+ . In the measurement of the Seebeck coefficient, the effect driving from the substrate itself was eliminated by the following Eq. (5.3), which can help to understand the Seebeck coefficient of the electrodeposited films themselves. In addition, the smooth films are surely obtained after annealing treatment as shown in Fig. 5.19.

$$S = \frac{R_h S_e + R_e S_h}{R_e + R_h} \quad (5.3)$$

where,

S = the measured Seebeck coefficient

R_h = the resistance of the Si substrate

R_e = the resistance of the electrodeposited films

S_h = the Seebeck coefficient of the Si substrate

S_e = the Seebeck coefficient of the electrodeposited films

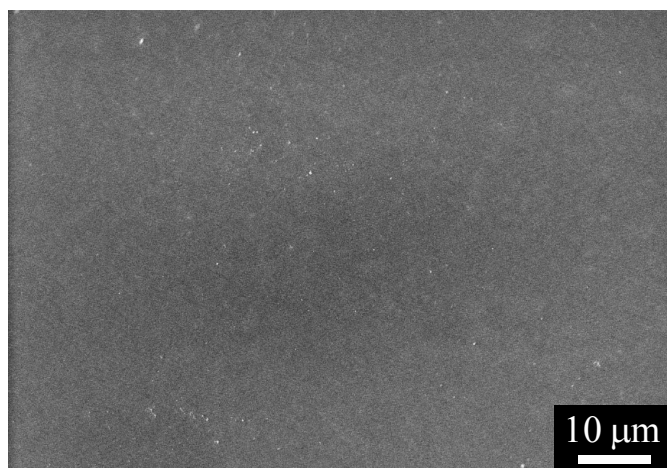


Fig. 5.19 SEM images of the electrodeposited films at -3.0 V vs. Ag/Ag⁺
(The condition of the annealing treatment was at 700 °C for 1h with the heating up time
of 1680 °C/min.)

As a result, the films with the Seebeck coefficient of 700 ~ 900 $\mu\text{V K}^{-1}$ and the resistivity of $6 \sim 576 \times 10^2 \Omega \text{ cm}$ was successfully electrodeposited. Therefore, it was suggested that the film with p-type characteristic could be formed by electrodeposition.

As described above and Chapter 2, the annealing treat can decrease impurities in films. This annealing treatment also be helpful to obtain the crystalline films. The crystallinity was measured by Raman spectra of the Si thin films electrodeposited at -2.3 V vs. Ag/Ag⁺ before and after annealing are shown in Fig. 5. 20 (a). A broad peak detected

at around 480 cm^{-1} changed to a sharp peak at 520 cm^{-1} after annealing. The sharper peak suggests that Si in the deposited films is crystallized by annealing. This spectrum was also analyzed using Origin (Fig. 5.20 (b)). The pink line shows the original data measured by Raman spectroscopy, and the black and red lines show the existence of peaks in the measured spectrum. Further, the blue line shows the fitting results. This analysis confirms the existence of the peak around 520 cm^{-1} . As you can see, it is possible to fabricate crystalline Si thin films, which could also enlarge the application field of the electrodeposited films.

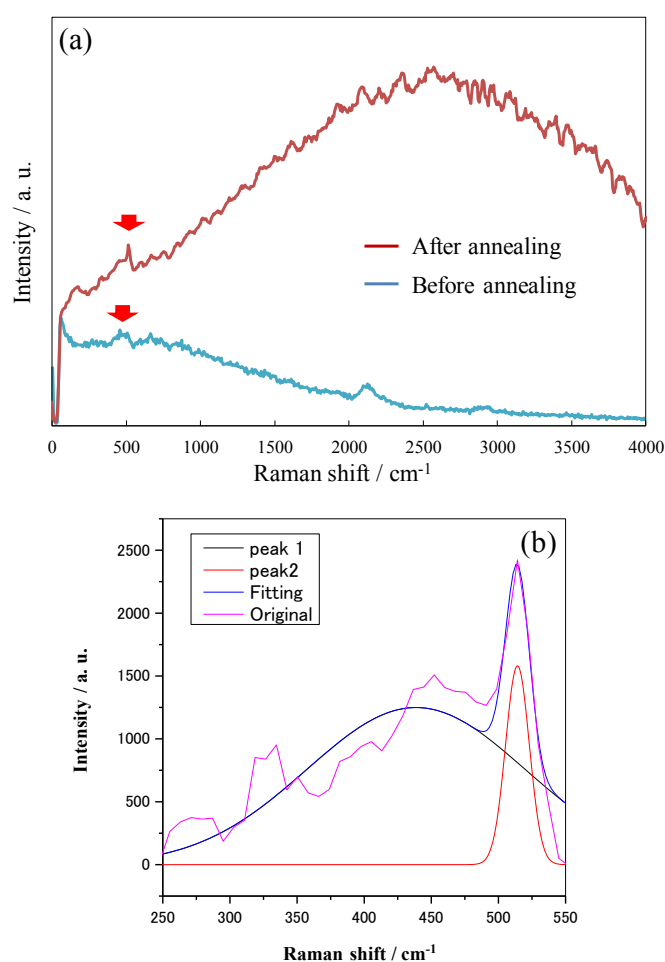


Fig. 5.20 (a) Raman spectra of the Si thin films electrodeposited at -2.3 V vs. Ag/Ag^+ before and after annealing (at $700\text{ }^\circ\text{C}$ for 1 h) (b) Analyzed result of the peak around 520 cm^{-1}

Table 5.1 shows the Seebeck coefficient and resistivity measurements of the Al-doped Si thin films after annealing treatment. The films showed the Seebeck coefficient ranges (600 - 900 $\mu\text{V K}^{-1}$) and the resistivity (400 - 800 $\Omega \text{ cm}$). The positive value of the Seebeck coefficient suggests that films electrodeposited in TMHATFSI containing 0.5 M SiCl_4 and 8.8×10^{-4} M AlCl_3 exhibited p-type characteristics. Figure 5.21 presents film compositions measured by GDOES, showing that the content of Al equaled ~ 600 ppm, with the considerably higher oxygen content ascribed to air exposure. Here, Al content is too high for the application in comparison with the study in molten salts [23], therefore, the p-type characteristics of doped films need to be determined from their photoresponses. Nevertheless, this study revealed that the addition of AlCl_3 to the electrolyte promotes the electrodeposition of p-type Si films.

Table 5.1 The results of the Seebeck coefficient and resistivity measurement of Al-doped Si thin films

Potential / V vs. Ag/Ag^+	Dopant (AlCl_3) concentration / M	Seebeck coefficient / $\mu\text{V K}^{-1}$	Resistivity / $\Omega \text{ cm}$
-3.0	8.8×10^{-4}	600 - 900	400 - 800

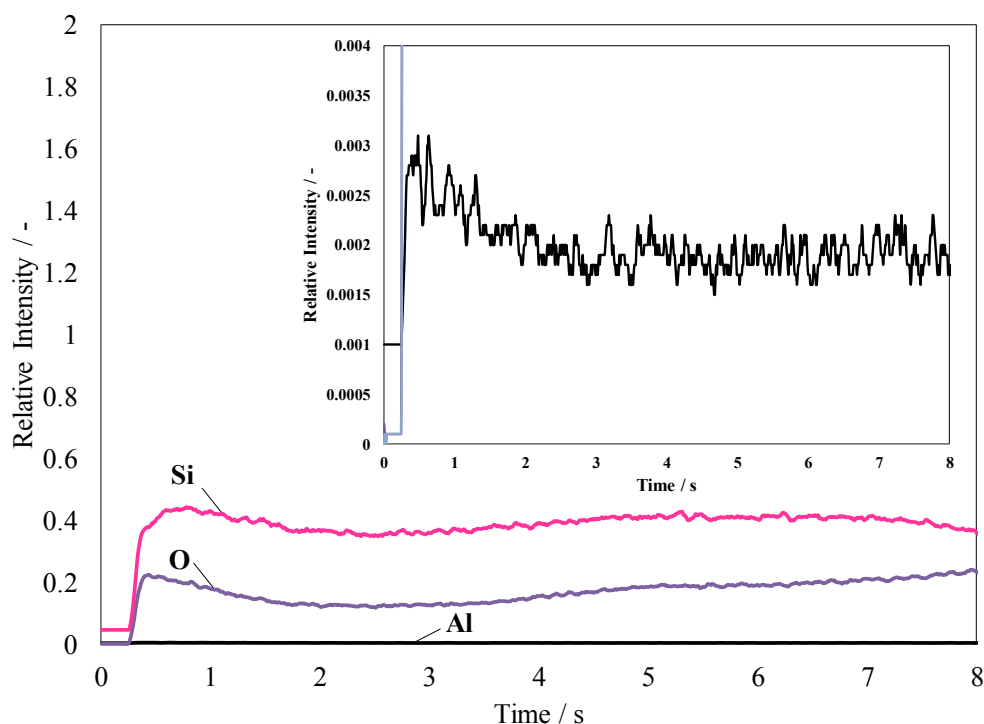


Fig. 5.21 (Color Online) The film composition of doped Si thin films electrodeposited at -3.0 V vs. Ag/Ag^+ in TMHATFSI with 0.5 M SiCl_4 and 8.8×10^{-4} M AlCl_3 (The inner figure shows the Al content.)

The same tendency was observed in the measurement of the Seebeck coefficient and resistivity of the films electrodeposited at -3.0 V vs. Ag/Ag^+ in CH_3CN , meaning the possibility to form the p-type Si thin films in organic solvents.

As for the n-type Si thin films electrodeposition, first, in order to understand the possibility of P electrodeposition in TMHATFSI, the electrochemical behavior was investigated. Figure 5.22 shows the cyclic voltammogram in TMHATFSI with $1/30$ M PCl_5 . Several peaks were observed, and the electrodeposition at -2.0 V vs. Ag/Ag^+ was conducted. The EDX result showed the existence of P, while there are no peak relating to Cl, meaning that the successful electrodeposition of P in TMHSTFASI. Figure 5.23 shows the cyclic voltammogram in TMHATFSI with only 0.5 M SiCl_4 , and 0.5 M SiCl_4 with 8.8×10^{-7} M PCl_5 .

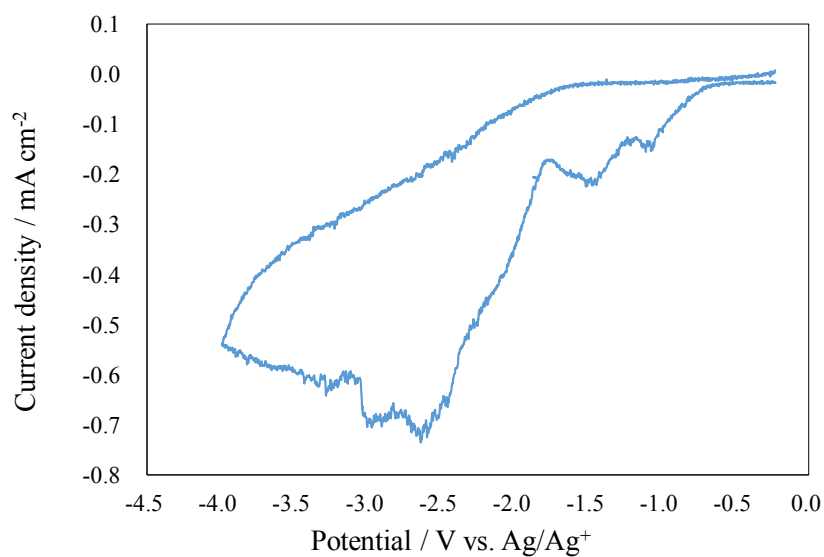


Fig. 5.22 Cyclic voltammogram in 1/30 M PCl₅ / TMHATFSI on Si substrate

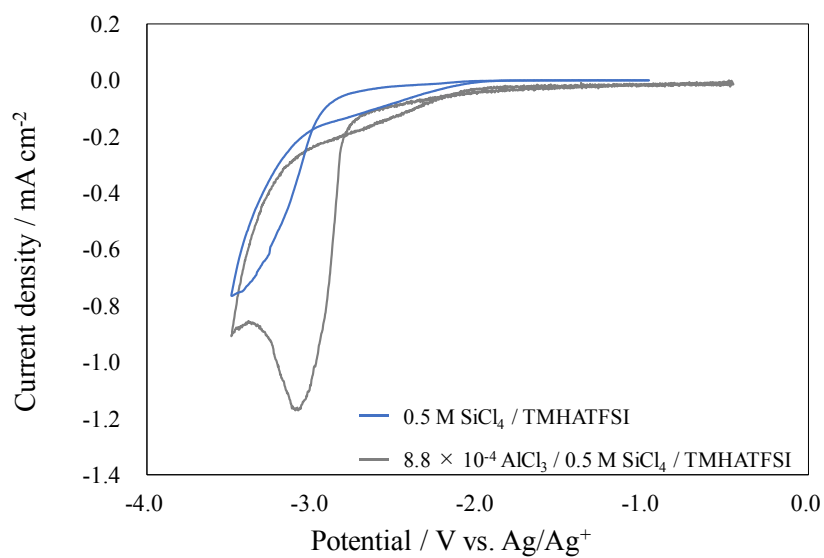


Fig. 5.23 Cyclic voltammogram in 0.5 M SiCl₄ / TMHATFSI and 0.5 M SiCl₄ and 8.8 × 10⁻⁷ M PCl₅ / TMHATFSI

With the addition of PCl_5 , the current density of the Si electrodeposition increase, suggesting the resistivity of the electrodeposited films became low. Therefore, it could be considered that doped films are formed. In order to evaluate the electric property of the electrodeposited films, the Seebeck coefficient and resistivity was measured for the films after the annealing treatment, in which the electrodeposition was conducted at $-3.0 \text{ V vs. Ag/Ag}^+$. In this measurement of the Seebeck coefficient, the effect driving from the substrate itself was also eliminated by Eq. (5.3). Table 5.2 shows the Seebeck coefficient and resistivity measurements of the P-doped Si thin films after annealing treatment. The films showed the Seebeck coefficient ($-90 - -190 \mu\text{V K}^{-1}$) with the resistivity ($50 - 80 \Omega \text{ cm}$). The negative value of the Seebeck coefficient indicates the n-type semiconductor, suggesting that films electrodeposited in TMHATFSI with 0.5 M SiCl_4 and $8.8 \times 10^{-7} \text{ M PCl}_5$ exhibited n-type characteristics.

Table 5.2 The results of the Seebeck coefficient and resistivity measurement of P-doped Si thin films

Potential / V vs. Ag/Ag^+	Dopant (PCl_5) concentration / M	Seebeck coefficient / $\mu\text{V K}^{-1}$	Resistivity / $\Omega \text{ cm}$
-3.0	8.8×10^{-7}	-90 ~ -190	50 ~ 80

Conclusions

By analyzing the influence of the electrodeposition parameter on the morphology, the relatively smooth films were obtained by applying PR electrodeposition in ionic liquids, in which the applied potential and the diffusion of the reductant of SiCl_4 to the electrode surface played a key role. It was also suggested that the electrodeposited films were semiconductor and behaved like an insulator. For this, the photoexcited electrons by the light irradiation during the electrodeposition was helpful to enhance the Si electrodeposition.

As the formation of the doped thin films, the addition of AlCl_3 and PCl_5 to the electrolyte could potentially be a way to form films with p-type and n-type characteristic by electrodeposition in both ionic liquids and organic solvents.

References

- [1] J. Gobet and H. Tannenberger, *J. Electrochem. Soc.*, **135**, 109 (1988).
- [2] T. Munisamy and A. J. Bard, *Electrochim. Acta*, **55**, 3797 (2010).
- [3] M. Bechelany, J. Elias, P. Brodard, J. Michler, and L. Philippe, *Thin Solid Films*, **520**, 1895 (2012).
- [4] C. Vichery, V. Le Nader, C. Frantz, Y. Zhang, J. Michler, and L. Philippea, *Phys.Chem.Chem.Phys.*, **16**, 22222 (2014).
- [5] G. Pulletikurthi, A. Lahiri, T. Carstens, N. Borisenko, S. Zein El Abedin, and F. Endres, *J. Solid State Electrochem.*, **17**, 2823 (2013).
- [6] Y. Nishimura, Y. Fukunaka, T. Nishida, T. Nohira, and R. Hagiwara, *Electrochem. Solid-State Lett.*, **11** (9), D75 (2008)
- [7] A.K. Agrawal, A.E. Austin, *J. Electrochem. Soc.*, **128**, 2292 (1981).
- [8] Q. Liao and C. L. Hussey, *J. Chem. Eng. Data*, **41**, 1126 (1996).
- [9] J.P. Nicholson, *J. Electrochem. Soc.*, **152**, C795 (2005).
- [10] K. Uda, Y. Seki, M. Saito, Y. Sonobe, Y-C. Hsieh, H. Takahashi, I. Terasaki, and T. Homma, *Electrochim. Acta*, **153**, 215 (2015).
- [11] Shiro Haruyama, *Hyomengijyutusyanokagaku* (Maeuzen, Tokyo, 2005) 2nd ed., Chapter 9.
- [12] A. Ispas and A. Bund, *Trans. Inst. Met. Finish.*, **90**, 298 (2012).
- [13] J. Tang, and K. Azumi, *Electrochim. Acta*, **56**, 1130 (2011).
- [14] S. Shresth, M. Nagi, and E. J. Biddinge, *J. Electrochem. Soc.*, **163**, D74 (2016).
- [15] A. J. Bard and L. R. Faulkner, *Electrochemical Methods* (WILEY, New York, 2001) 2nd ed., Chapter 18.
- [16] N. Sato, *Tetsutohagane*, **9**, 1423 (1990).
- [17] Y. Matsuda and C. Iwakura, *Denkikagakugairon* (Maruzen, Japan, 2014) 2nd ed., Chapter 8.
- [18] M. Fujihira and K. Uosaki, *Denkikagaku* (Tokyokagakudojin, Japan, 2016), Chpater 6.
- [19] Y. Ogata, *Hyomengijutsu*, **57**, 181 (2006).

- [20] S. Yoshihara, K. Endo, E. Sato, and J. O'M. Bockris, *J. Electroanal. Chem.*, **372**, 91 (1994).
- [21] Y. L. Kawamura, T. Sakka, and Y. H. Ogata, *J. Electrochem. Soc.*, **152**, C701 (2005).
- [22] D. W. Redman, H. J. Kim, K. J. Stevenson, and M. J. Rose, *J. Mater. Chem. A*, **4**, 7027 (2016).
- [23] X. Yang, L. Ji, X. Zou, T. Lim, J. Zhao, E.T. Yu, and A. J. Bard, *Angew. Chem. Int. Ed.*, **56**, 15078 (2017).

Chapter 6:

General Conclusion

The fabrication of Si by electrodeposition in ionic liquids has been attracted as an alternative approach for several applications. There are the backgrounds of that the electrodeposition has advantages in fabricating nanostructures with nm order in a large area without using high voltage and high vacuum environment, and the characteristic and recent availability of ionic liquids. Although there are several studies of Si electrodeposition in ionic liquids, it still has challenging in the decrease of impurities in the Si structures which is especially needed for solar cell applications and the elucidation of reaction mechanism. The reason of these difficulties seems to be strongly related to the insufficient clarification of the reaction system in utilizing the ionic liquids in the electrodeposition, while there are many studies of the electrodeposition in ionic liquids. It is also considered that, especially in the Si electrodeposition, the impurities inclusion might relate to the uncertainty of the reaction mechanism. Therefore, the main objective of this thesis work is to elucidate the electrodeposition reaction of Si in ionic liquids focusing on the molecular level understanding at the solid-liquid interface. Following this thesis work, it is also studied in order to elucidate the cause of the impurities inclusion, to establish the reaction analysis system in other non-aqueous solvents, and the formation of thin films in terms of the application, especially for solar cell applications.

In order to achieve these objectives, several interfacial techniques were used such as electrochemical quartz crystal microbalance method, X-ray reflectivity, and density functional calculation etc. These combinations of experimental measurement and theoretical analysis was powerful tools to elucidate the mechanism.

In this chapter, elucidated results in this thesis work are summarized, and the possibility of Si electrodeposition in the future is described.

In chapter 2, the overall reaction mechanism of the Si electrodeposition in ionic liquids were discussed.

In order to understand the growth behavior of Si thin films at several conditions, the effect of the applied potential and the electrodeposition temperature was investigated. From these discussions, it was suggested that the ionic liquids were incorporated as the impurities. It was also indicated by the annealing treatment because the impurities of mainly carbon content decreased after the treatment. As the Si thin films, amorphous thin

films with Si–Si bonding were obtained. As the reduction mechanism of SiCl₄, the combination of EQCM and XPS results showed suggested the apparent Si electrodeposition with a net four-electron reduction from SiCl₄ of $\text{SiCl}_4 + 4 e^- \rightarrow \text{Si} + 4 \text{Cl}^-$, in which the current efficiency was calculated as 94.6 and 93.4 % at -2.0 and -2.5 V vs. Pt QRE, respectively at the very initial stage.

In chapter 3, the detailed interfacial reaction mechanisms starting with the elementary steps of the SiCl₄ reduction process in Si electrodeposition with ionic liquids as the solvent were discussed. Based on chapter 2, in order to elucidate the detailed reduction behavior of SiCl₄, it is continuously needed to understand the mechanism for how these reactions proceed or what kind of intermediate are produced by focusing on the molecular level behavior at the solid-liquid interface.

In order to elucidate such interfacial reaction mechanism, several precise interfacial analyses of EQCM, XRR measurement and DFT calculation were used. As the detailed interfacial reaction mechanism of the SiCl₄ in ionic liquids reduction process from molecular point of view, the following process is proposed: a SiCl₄ molecule reduces with the release of a Cl⁻ ion, followed by the reaction between the residual SiCl₃⁻ and another nearby SiCl₄ to produce the intermediate states containing Si₂Cl₆. This intermediate formation takes place successively, generating a polymer-like species, which is finally deposited as Si on the substrate. Dividing these process, EQCM measurement firstly showed the multiple steps reduction during the electrodeposition. XRR measurement secondly revealed that the details of the multiple steps in which Si multimer such as Si₂Cl₆ were formed, and those multimer seemed to be electrodeposited as Si. DFT calculation finally indicated the reduction pathway that Si multimer was formed by the reaction of SiCl₃⁻ and another nearby SiCl₄, and their polymer-like reaction.

In chapter 4, the electrodeposition of Si in organic solvents were described. Organic solvents are also the promising solvent for the electrodeposition of Si at low temperatures which allow a faster electrodeposition at room temperature and could turn out to be useful for practical applications, so that several studies of the Si electrodeposition have also been conducted. For this, the influence of solvent species (an oxidized and a non-oxidized

solvents), and the water content in solvents on the electrodeposition process was investigated, and the reduction mechanism of SiCl_4 that how the reactions proceed or what kind of intermediate are produced during the electrodeposition was analyzed as well as the investigation of the application of the reaction mechanism analysis system in ionic liquids to other non-aqueous solvents.

It was revealed that the water content affected to the film composition, especially the carbon content, while there is small influence of solvent species. With the increase of the water content in the solvents, the carbon content in the films increased. The molecular level mechanism in this phenomenon was suggested that the solvent molecules of CH_3CN could get close to the electrode surface during the electrodeposition due to the strong interaction of solvents molecules with the hydrolysis product of the SiCl_4 under the water existence condition. As for the reduction mechanism of SiCl_4 , it was confirmed that there was the intermediate state formation step, in which Si species with $-\text{SiCl}_3$ bonding were formed.

In chapter 5, the study for the fabrication of Si thin film solar cells as one example of the application of the electrodeposited Si thin films by electrodeposition was described. For the further developing the Si electrodeposition, it is important to fabricate the Si thin film for applications. For this, the film structure control and the doping on the films were investigated.

In order to prevent the crack formation and porous structure, the PR electrodeposition and the light irradiation during the electrodeposition was engaged. It was suggested that the diffusion of the reductant of SiCl_4 to the electrode surface played a key role and the light irradiation in this thesis work was enough to retain the electron accumulation to the interface. In order to form the doped thin films, AlCl_3 and pCl_5 was added to the electrolyte, and these techniques could potentially be a way to form films with p-type and n-type characteristic.

This thesis work could provide the electrodeposition reaction mechanism of Si in ionic liquids as well as the film formation control though there are few study focusing on and revealing the detailed reaction mechanism of Si electrodeposition in especially ionic

liquids. Based on these studies, the Si electrodeposition could be further developed for several applications, and also it could be possible to indicate ways to analysis other electrochemical reaction of metal or semiconductor in non-aqueous solvents and their developing and possibilities in the future.

List of Achievements

1. Original Articles

“Electrochemical quartz crystal microbalance, X-ray photoelectron spectroscopy, and Raman spectroscopy analysis of SiCl_4 reduction in ionic liquids”

Yasuhiro Tsuyuki, Tram Anh Pham Huynh, Jason Komadina, Yasuhiro Fukunaka, Takayuki Homma

Electrochimica Acta, **183**, 49-55 (2015)

“Analysis of Cathodic Reaction Process of SiCl_4 during Si Electrodeposition in Ionic Liquids”

Yasuhiro Tsuyuki, Tatsuki Fujimura, Masahiro Kunimoto, Yasuhiro Fukunaka, Piero Pianetta, Takayuki Homma

Journal of The Electrochemical Society, **164** (14), D994-D998 (2017)

2. Presentation

[International Conference]

“Electrolyte-Electrode Interfacial Study for Si Electrodeposition in Ionic Liquid”

Jason Komadina, Yoko Ishibashi, Yasuhiro Tsuyuki, Yin He Zhang, Yasuhiro Fukunaka, Piero Pianetta, Takayuki Homma

224th ECS Meeting, San Francisco, U.S.A, 2013. 10

“The Study of Electrodeposition of Si in Tmhatfsi-SiCl₄ Analyzed by EQCM Method”

Yasuhiro Tsuyuki, Tram Anh Pham Huynh, Jason Komadina, Yasuhiro Fukunaka, Takayuki Homma

226th Meeting of The Electrochemical Society, Cancun, Mexico, 2014. 10

“EQCM and XPS Analysis of SiCl₄ Reduction in Ionic Liquids”

Yasuhiro Tsuyuki, Tram Anh Pham Huynh, Jason Komadina, Yasuhiro Fukunaka, Takayuki Homma

10th International Symposium on Electrochemical Micro & Nanosystem Technologies, Okinawa, Japan, 2014. 11

“Growth Process of Electrodeposited Si Thin Films in Ionic Liquid for Solar Cell Applications”

Yasuhiro Tsuyuki, Tram Anh Pham Huynh, Jason Komadina, Yasuhiro Fukunaka, Takayuki Homma

The 6th World Conference on Photovoltaic Energy Conversion, Kyoto, Japan, 2014. 11

“Electrodeposition of Si Thin Films in Ionic Liquids for Solar Cell Applications”

Yasuhiro Tsuyuki, Minami Tsuzuki, Yasuhiro Fukunaka, Takayuki Homma

3rd DGIST-WASEDA Workshop on electrochemistry, Tokyo, Japan, 2015. 12

“Reduction Mechanism Analysis of SiCl_4 during Si Electrodeposition in Ionic Liquids”
Yasuhiro Tsuyuki, Tatsuki Fujimura, Masahiro Kunimoto, Yasuhiro Fukunaka, Piero Pianetta, Takayuki Homma
Nucleation and Growth Research Conference 2016, Kyoto, Japan, 2016. 9

“The Effect of Bath Condition on The Composition of Si thin Films Electrodeposited in Non-aqueous Solvents”
Yasuhiro Tsuyuki, Minami Tsuzuki, Yasuhiro Fukunaka, Takayuki Homma
PRiME 2016, Hawaii, U.S.A., 2016. 10

“Analysis of Cathodic Reaction Process of SiCl_4 in Ionic Liquids”
Yasuhiro Tsuyuki, Tatsuki Fujimura, Masahiro Kunimoto, Yasuhiro Fukunaka, Piero Pianetta, Takayuki Homma,
231st ECS Meeting, New Orleans, U.S.A., 2017. 5

“Theoretical Analysis of SiCl_4 Reaction Mechanism for Si Electrodeposition Process in Tmha-Tfsi As Ionic Liquids”
Tatsuki Fujimura, Yasuhiro Tsuyuki, Masahiro Kunimoto, Yasuhiro Fukunaka, Takayuki Homma
231st ECS Meeting, New Orleans, U.S.A., 2017. 5

“Electrodeposition of Si Thin Films in Ionic Liquid with Growth Control from Initial Stages”
Hidenori Takai, Yasuhiro Tsuyuki, Tatsuki Fujimura, Masahiro Kunimoto, Yasuhiro Fukunaka, Piero Pianetta, Takayuki Homma
27th International Photovoltaic Science and Engineering Conference, Shiga, Japan, 2017. 11

[Domestic Conference]

“Analysis of Growth Process of Si Thin Films Electrodeposited from Ionic Liquids”
Yasuhiro Tsuyuki, Yoko Ishibashi, Takahiro Akiyoshi, Jason Komadina, Yasuhiro Fukunaka, Takayuki Homma
80th Meeting of Electrochemical society of Japan, Sendai, Japan, 2013. 3

“Fabrication of Electrodeposited Si Thin Films in Organic Solvents and Its Composition Analysis”

Minami Tsuzuki, Yasuhiro Tsuyuki, Tram Anh Pham Huynh, Yasuhiro Fukunaka, Takayuki Homma

2015 Fall Meeting of Electrochemical society of Japan, Saitama, Japan, 2015.9

“The Effect of Bath Condition on Si Electrodeposited in Organic Solvents”

Minami Tsuzuki, Yasuhiro Tsuyuki, Hidenori Takai, Yasuhiro Fukunaka, Takayuki Homma

133th Meeting of the Surface Finishing Society of Japan, Tokyo, Japan, 2016. 3

“The Effect of Heat Treatment on Electrodeposited Si Thin Films in Ionic liquids”

Hidenori Takai, Yasuhiro Tsuyuki, Minami Tsuzuki, Yasuhiro Fukunaka, Takayuki Homma

133th Meeting of the Surface Finishing Society of Japan, Tokyo, Japan, 2016. 3

“Theoretical Analysis of SiCl_4 Reaction Pathway in Si Electrodeposition Process using Ionic Liquids”

Tatsuki Fujimura, Takehiro Naito Yasuhiro Tsuyuki, Masahiro Kunimoto, Yasuhiro Fukunaka, Takayuki Homma

83th Meeting of Electrochemical society of Japan, Osaka, Japan, 2016. 3

“Electrodeposition of P-type Si Thin Films in Organic Solvents”

Shoko Iwata, Yasuhiro Tsuyuki, Minami Tsuzuki, Yasuhiro Fukunaka, Takayuki Homma

84th Meeting of Electrochemical society of Japan, Tokyo, Japan, 2017. 3

“Theoretical Analysis of The Interaction between Reduction Species and Organic Solvents in Si Electrodeposition Process”

Ayumu Sanada, Masahiro Kunimoto, Yasuhiro Tsuyuki, Yasuhiro Fukunaka, Hiromi Nakai, Takayuki Homma

2017 Fall Meeting of Electrochemical society of Japan, Nagasaki, Japan, 2017.9

3. Award

Best Poster Award, Nucleation and Growth Research Conference 2016, 2016.9

Acknowledgement

I would like to express my sincere appreciation to Professor Dr. Takayuki Homma. I have learned from him that the science knowledge and the mind for researching as well as what to do as human being in society. He has taken his time for me to teach those things since I have belonged the laboratory as the undergraduate member. His taught has usually been encourage to me, and he has also given me a lot of opportunities for developing scientific viewpoints. I would like to continue to keep having his taught as a researcher and human being in the future. I would also like to express my appreciation to Professor Dr. Kenichi Oyaizu, Professor Dr. Yoshinori Nishikitani, Professor Dr. Toshiyuki Momma, Dr. Kenichi Uemura (NIPPON STEEL & SUMIKIN MATERIALS Co.) for reviewing this thesis. Their ideas relating to the composition of this thesis work, helpful suggestions and encouragements keep me doing hard.

I am very grateful to Professor Dr. Yasuhiro Fukunaka, Dr. Masahiro Kunimoto for kind helps and suggestions to this thesis work. In the research discussions with them, their insightful suggestions and basic knowledge helped me to consider this thesis work deeply and get various viewpoints. I also thank to Professor Dr. Masahiro Yanagisawa, Professor Dr. Mikiko Saito. Their kind teaching in measurement helped me to develop my skill as a researcher.

In the course of leading program, I would like to express my appreciation to Professor Dr. Hiroyuki Nishide, Professor Dr. Toru Asahi for giving me a lot of opportunities that could not be experienced if I were not in leading program. In addition, their passions always encourage me to keep doing hard.

In the work of XRR measurement, I would like to appreciate to Professor Dr. Piero Pianetta (Stanford Univ. and SLAC National Accelerator Laboratory), Dr. Apurva Mehta (SLAC National Accelerator Laboratory), Trevor Petach (Stanford Univ.) for their kind advices and helps in the measurement. Especially, I would like to express my appreciation to Dr. Piero Pianetta for his kind acceptance and setting of my internship in Stanford Univ. and SLAC National Accelerator Laboratory.

In the research relating to the electrodeposition of Si, I would like to thank to Mr.

Tetsuo Nishida (Stella Chemifa Co.), Dr. Jason Komadina, Mr. Takahiro Akiyoshi, Ms. Yoko Ishibashi, Ms. Minami Tsuzuki, Mr. Hidenori Takai, Ms. Shoko Iwata, Mr. Shuei Watanuki for their kind help and contribution. The discussions with them has been given me several viewpoints to develop my thesis work.

I also thank to Dr. Nobufumi Matsuo, Dr. Siggie Wodarz, Mr. Tomohiro Otani, Mr. Yelchur Venkata Akash for giving me the encouragement in my doctoral course.

Lastly, I would like to express my grateful to my parents and sister for their always kind helps, believing me and letting me study in Tokyo alone. I could not keep working my thesis research hard without their supports.

Yasuhiro Tsuyuki